STUDIES OF THE TRAVEL TIMES, PERIODS, AND ENERGY OF SEISMIC WAVES SKP AND RELATED PHASES

Thesis by

Robert Donald Forester

In Partial Fulfillment of the Requirements

for the Degree of

Doctor of Philosophy

California Institute of Technology

Pasadena, California

1953

ACKNOWLEDGEMENTS

I am grateful to Dr. Beno Gutenberg for suggesting the investigation of SKP and related phases. Dr. Gutenberg offered inspiration and guidance in the preparation of the thesis, and carefully reviewed the interpretation of the final results.

Dr. Charles Richter and Mr. John Nordquist helped to familiarize me with the facilities of the Seismological Laboratory, and were of considerable assistance in my search for pertinent records and data.

Dr. Charles Richter and Dr. Hugo Benioff kindly discussed with me some of the complex problems of seismology.

Appreciation is extended to Rev. F. J. Donohoe, Assistant Director of the Seismological Observatory at Weston, Robert W. Knox, Acting Director of the U. S. Coast and Geodetic Survey, and Dr. L. Don Leet, Director of the Harvard Seismological Laboratory for furnishing me with additional seismograms for the study of SKP and related phases.

I am indebted to my wife for calculating the data for the theoretical travel time curves on a Monroe Calculator.

ABSTRACT

The travel times, periods, and amplitudes of SKP core waves have been investigated for shocks of normal, 60 km, and 100 km depths.

For shallow shocks, multiple SKP phases are observed as long as 54 seconds after the initial SKP motion on short period instruments, and as long as 87 seconds on long period instruments. Amplitude data indicate that each multiple phase has a focal point similar to that of the initial SKP phase. The focal point for waves having periods of 1 to 5 seconds occurs at $131\frac{1}{2}^{\circ}$, and that for waves having periods of 5 to 10 seconds is broadly defined between 130 and 131°. Short period SKP phases extend from 129 to at least 140°; and long period SKP phases, from 125 to 145°. The long period waves are believed to be diffracted from the caustic in accordance with Airy's hypothesis. Multiple reflections and refractions in the outer layers of the mantle seems more plausible as an explanation of multiplicity than dispersion.

In order to analyze the energy content of the SKP phases, a system was developed for determining the magnifications of the ground motion of seismometers from their records of earthquakes.

As an experiment, theoretical travel times for PKP, SKP, and SKS were computed by integration along the travel

paths. For this purpose, the velocity distribution within the earth was broken into segments which were represented by continuous functions. The resultant travel times are not valid for rays of grazing incidence to the core. The times computed for PKP and SKP are intermediate between the smoothed times given for them by Jeffreys and the times for them based upon recent observed data. The theoretical travel times for SKP provided a basis for the analysis of the energy content of the SKP phases.

For all types of SKP phases, the energy content of short period waves is a small fraction of that of long period waves. For vertical instruments, the agreement between theoretical and observed values of energy is good. For horizontal instruments, the observation of too little energy is not satisfactorily explained.

SKP", the SKP phase associated with the inner core, is observed between 114° and 125°. It records with periods of 1 to 3 seconds on both long and short period instruments. The observations of SKP" present additional support for the hypothesis of a large, but continuous increase of velocity at the transitional boundary of the inner core.

Evidence for a difference between the travel paths of short and long period waves is less apparent for SKP than for PKP.

CONTENTS

(Observed SKP travel times for shocks of normal depth are in pocket on back cover.)

INTRODUCTION

PKS is a body seismic wave composed of three parts, namely, "P", "K", and "S". "P" is a longitudinal wave which travels through the mantle, from the shock hypocenter to the core. "K" is a longitudinal wave which travels through the core. "S" is a transverse wave which travels through the mantle, from the core to the observing station. For SKP, a shear wave leaves the hypocenter and a longitudinal wave arrives at the observing station. Hence, the path relationship of SKP to PKS is reversed. For a shock of zero focal depth, PKS and SKP should have identical travel times. For increasing focal depths, the interval by which SKP leads PKS should increase.

The path relationships of PKS are shown in fig. 1. In fig. 2, travel times for PKS computed by Jeffreys (1939c) can be compared with those synthesized by the method of Wadati and Masuda (1934) from travel times given by Jeffreys (1939a) for PcS and from travel times given by Gutenberg (1951a) for K. In the two figures, "a", "b", "c", and "d" designate corresponding ray paths and travel times.

At an epicentral distance of about 131°, PKS rays converge to a focus. This is a result of the fact that the longitudinal velocity drops from about 13.7 to about 8.0 km/sec at the core boundary. The focal ray path, "b",

is analogous to a light ray being transmitted at the angle of minimum deviation through a prism. Unlike PKP, the two focal branches of the PKS travel time curve are not easily distinguished from each other. This is a result of the fact that near the focus, the upper branch follows the lower, main focal branch by a very short time, and at larger epicentral distances the upper branch probably records with much smaller amplitudes than does the main branch.

The difference between the two travel time curves in fig. 2 results primarily from the difference in core velocities computed by Jeffreys (1939c) and Gutenberg (1951a). (See fig. 3.) The slope of the upper focal branch, "a-b", is similar for the two travel time curves. The focal distance of 130° computed by Jeffreys checks within a degree or so of the new curve. The distance at which the "P" component of PKS grazes the outer core is 148° for Jeffreys's curve and 143° for the new curve. Which of these two values is more nearly correct is difficult to verify because of the low amplitudes associated with rays which have a travel time curve whose slope approaches that of a straight line. The epicentral distance calculated for the grazing ray is sensitive to the velocity gradient assumed to exist just outside the core.

The apparent surface velocity (the reciprocal slope of the travel time curve) of the main focal branch, "b-c",

is larger for Jeffrey's curve than for the new curve, because Jeffreys computes higher velocities for the outer core than does Gutenberg.

The existence of an "inner" core was postulated by Miss Lehmann (1936). She contended that the amplitudes of P" were much too large to be ascribed to diffraction associated with the caustic of PKP, but that they could result from the effects produced at the boundary of a high velocity "inner" core. This hypothesis has been corroborated by Jeffreys and by Gutenberg and Richter; however, they differ in their interpretation of the nature of the inner core boundary. Jeffreys (1939c) assumed, for convenience, that true reflection occurs at the inner core, and calculated that the velocity must decrease abruptly by 3/4 km/sec at a depth of 4970 km.

Making no assumption as to whether or not the reversed travel time segment, "c-d", results from reflection or refraction, Gutenberg and Richter (1938 and 1939a), using the method of Herglotz-Weichert-Bateman as extended by Slichter (1932), calculated that the velocity increases at the inner core boundary. In his latest revision of core velocities, Gutenberg (1951a) calculates that the velocity at the inner core increases continuously by 1.1 km/sec from a depth of 5100 km to 5300 km. His revision is based mainly upon the new travel time data for P"

presented by Denson (1950).

The main focal branch of PKS, "b-c", extends from 130 to 140° for Jeffrey's curve and from 131 to 149° for the new curve. "c" represents the ray which grazes the inner core. The epicentral distance for "c" is less for the curve of Jeffreys than the new curve, partly because Jeffreys calculates 130 km less depth to the inner core than does Gutenberg; and partly because Jeffreys has calculated core velocities which have higher gradients than those of Gutenberg. High velocity gradients produce greater ray curvature, and accordingly reduce the central angle subtended by a ray in the core.

For PKP, Denson (1952) presents evidence that the short period waves and the long period waves are separated from each other, and concludes that they must travel over different paths through the core. He found that the short period focal point occurs at 147°, and that the long period focal point is broadly defined near 143°. For the lower focal branch of PKP, the energy of short period waves attenuates beyond the focus; whereas, long period waves persist with large amplitudes as far as 157°. At 157° he believes that the PKP travel time curve reverses as a result of refraction produced by the transition zone of the inner core boundary. He also observed that for P", the energy of short period waves is large between 120 and 125°, and for distances

less than 120°, P'' is observed only as short period motion.

On the basis of Denson's findings, Gutenberg (1951a) postulates that the reversed segment of the travel time curve of P'' between 157 and 120° is refracted by the inner core, and that focal points exist at 157 and 120°. He ascribes observations of P'' between 105 and 120° mainly to reflections from the inner core.

The purpose of the present investigation is to study the travel times, periods, and energy of SKP and related phases, and to determine if the features observed for SKP are consonant with those observed by Denson for PKP. Associated with SKP, there should be an inner core phase, SKP'', which is analogous to P'', the inner core phase associated with PKP. Observations of SKP'' should furnish corroborative, and perhaps additional, information about the nature of the transition zone at the boundary of the inner core.

MATERIALS AND PROCEDURES

Seismograms recorded at Pasadena, at some of its auxiliary stations (Tinemaha, Haiwee, Riverside, Mount Wilson, and China Lake), and at Huancayo comprised the main source of data for the study of SKP and related phases. Some data were obtained from seismograms recorded at Tucson, Weston, and Harvard.

The original travel times given for SKP by Gutenberg and Richter (1934) were based largely upon the data obtained from the Sumatra shocks of 1931. Copies of the original seismograms, which were received from all parts of the world, provided some material for the present study of SKP.

Most of the seismograms from Pasadena, all those from its auxiliary stations, and all those from Tucson, Weston, and Harvard were recorded by either short or long period Benioff variable-reluctance seismometers. A few early Pasadena seismograms were recorded by experimental seismometers. The seismograms from Huancayo were recorded by a vertical, long period Benioff and by a pair of horizontal, long period Wenner instruments. The seismograms of the Sumatra shocks of 1931 were recorded by a wide variety of long period instruments.

Because of the relative scarcity of good data for SKP,

records of widely varying quality were investigated. Readings were taken from seismograms recorded as early as 1928 at Pasadena and as early as 1932 at Huancayo. With the exception of several Sumatra shocks recorded in the fall of 1951, no shocks recorded after 1950 were investigated. The shocks examined ranged in magnitude from 6 to 8.5 on the Richter scale. Shocks of very large magnitudes were frequently rejected on account of their complexity.

A range of epicentral distances from 105° to 155° was examined. The distribution of data with epicentral distance was uneven. For the study of SKP, a serious lack of data existed at 135°. Most of the examined shocks which were recorded at Pasadena, its auxiliary stations, and at Tucson originated in the Sunda Arc. A few originated in the Indian Ocean and Southern Antilles. At Pasadena, Sumatra shocks yielded a large number of data for the study of the SKP focal point. The examined shocks which were recorded at Huancayo originated in the western half of the Pacific island belt. About 90 shocks originating from shallow depths and 105 shocks originating from intermediate depths were examined. Data from shocks originating at depths greater than 200 km were not used because of the difficulty in separating PP, $_{p}$PP, and $_{s}$PP from SKP.

Origin times and geographical coordinates were taken

primarily from Gutenberg and Richter (1949), and the rest were taken from either the International Seismological Summary or from the private files of Dr. Gutenberg. Epicentral distances were computed by use of the geocentric latitudes and station coordinates published in the International Seismological Summary. Epicentral distances to the auxiliary stations were computed by applying small corrections to the epicentral distances obtained for Pasadena.

The origin times at each station were adjusted on the basis of their quality and the deviation of the travel times of P" and PP from the values given by Gutenberg and Richter (1934 and 1936). Negative corrections as large as 10 seconds were necessary for many of the shocks of magnitudes larger than 7½. Very large corrections were not accepted until they could be justified on the basis of the residuals given in the International Seismological Summary for P-O and other prominent comparisons. The times, periods, and amplitudes of all phases occuring within 1½ minutes after the initial SKP motion were measured. All "picks" were graded on the basis of their distinctness and prominence. Most "picks" of very low quality were rejected for the final travel time and "A" value plots. Because of a lack of information regarding the instrumental constants, some seismograms, such as those recorded by the

Huancayo long period Benioff vertical instruments, could be used only for travel times. Because of very large origin time corrections or because of complex motion, some seismograms were used only for the study of energy.

CALIBRATION OF THE SEISMOMETERS WITH SEISMIC DATA

Martner (1950), Mooney (1951), and Denson (1952) each studied the energy of seismic body waves reaching the earth's surface by ascertaining the ratio of the energy in the phase of interest to that of a well established phase, such as, P or PP. The advantage of the energy ratio method is that it is essentially independent of the distribution of energy imparted to transverse and longitudinal waves if the two phases used for the energy ratio leave the hypocenter with the same mode of vibration. Other advantages are that earthquake magnitudes and absolute instrumental magnifications need not be known. It cannot be used to investigate asymmetric variation of seismic energy with azimuth. The energy ratio method involves more error arising from the measurements of amplitudes and periods than the direct method, for twice as many measurements are used for the ratio method than the direct method.

Because PP is often too small for measurement or else inseparable from SKP motion, it does not make a good standard for comparison with SKP. P'' is usually large and distinct enough, but its energy has not been accurately enough determined to be used as a standard. Since there was no phase suitable for a standard, the absolute magnification of the

instruments had to be determined in order to study the energy content of SKP and related phases. Changes in the gain settings of the Pasadena and auxiliary station instruments had not been recorded, for they were used primarily for studies of travel times rather than energy. Consequently, the only way to determine the magnification of these instruments for any period in the past was to make use of the recorded seismic data. Seismic data were also used to determine magnifications of the instruments at Huancayo and Tucson.

For the calibration of the seismometers by use of seismic data, the amplitudes and periods of P, PP, and S were measured for shocks of magnitudes from 7.0 to 7.7. The epicentral distance for P ranged from 30° to 90°; for PP, from 85° to 130°; and for S, from 30° to 100°. Readings were not taken at epicentral distances where the "A" values given by Gutenberg (1945a) change abruptly.

The equation used to determine the magnification was adapted from equations developed by Gutenberg (1945a):

$$\log R_o = A_o - M + \log\left|\frac{W}{T}\right| + G + K(M - 7) \qquad (1)$$

R_o = absolute magnification.

A_o = energy parameter. Values of this parameter for P, PP, and S at various epicentral distances are listed by Gutenberg (1945a).

M = earthquake magnitude as given by Gutenberg and Richter (1949).

W = trace amplitude.

T = period.

G = station ground factor as given in table I of Gutenberg (1945b).

$K(M-7)$ = a residual factor given by Gutenberg (1945a) for the magnitude determination of earthquakes from seismic body waves. $K = 0.1$ for $6.5 \leq M \leq 7.5$, 0.0 for $M < 6.5$, and 0.25 for $M > 7.5$.

Actually, the effect of the station ground factor, "G", is nullified if the magnification curves computed from earthquake data are used to determine "A" values. If the ground factor is omitted in equa. 1, the magnifications obtained will be relative rather than absolute.

The ratios of the magnification determined by earthquakes to the magnification read from reference frequency response curves were computed. Dr. Markus Båth determined the absolute magnification of the short and the long period, Benioff vertical seismometers at Pasadena in 1951. His values were used, respectively, as reference curves for all the short and the long period Benioff seismometers to be calibrated, both vertical and horizontal.

Records of the indicial response tests for the Huancayo, horizontal Wenner seismometers indicate that the pendulum and galvanometer periods are significantly longer than the values listed for them by Wenner (1929) for instruments of

his design. For a reference curve for the Huancayo instruments, a frequency response curve based upon the actual pendulum and galvanometer periods was computed. The peak magnification of this curve was set equal to that tabulated by Wenner (1929).

The logarithms of the magnification ratios were plotted for each instrument on a separate graph. The log ratios were plotted as ordinates and the dates of the earthquakes for which the ratios pertained were plotted as abscissae. Fig. 4 shows such a plot for the Benioff, short period, vertical instrument. The use of logarithms gives a statistically normal distribution of points. The very low values from 1944 to 1948 indicate that the sensitivity was definitely lower during that period. The only other instrument which appeared to have had a large change in sensitivity was the Haiwee, short period, Benioff vertical instrument.

The mean value of the log ratios was taken for each period in which the graphs indicated no change in sensitivity. The antilog of this value, designated as the "sensitivity factor", appears in the last column of table 1.

The standard deviation of the log ratios was generally about 0.3. This indicates that the standard deviation factor for the sensitivity (see table 1) was about 2. For a standard deviation in the log ratio of 0.3, the Student's "t" distribution of statistics indicates that at least 30

log ratios must be averaged if there is to be 95% confidence that the true mean will not differ by more than 0.1 from the sample mean, or in other words 30 readings are necessary to be 95% certain that the sensitivity is not in error by more than 25%. An abnormally high value for the standard deviation factor would suggest that the sensitivity had been changed within the time interval for which the mean value of the log ratios had been determined.

Since the sensitivity of the N-S component was suspected to differ appreciably from that of the E-W component for each pair of horizontal instruments, the components were calibrated separately.

Figs. 5, 6, and 7 indicate that the procedure of dividing the amplitude of a P or PP wave by the cosine of the azimuthal difference between the direction of wave propagation and the seismometer response axis produces over-correction. Both figures show that the log ratios increase with an increase of the azimuthal difference, θ. Thus the energy recorded for P and PP is sizable even when the recording instrument is transverse to the direction of propagation. This may result from the fact that there is SH motion mixed with P motion or that appreciable P energy has been horizontally refracted by lateral discontinuities in the earth's crust.

To eliminate such over-correction, the amplitudes were

RESULTS OF THE CALIBRATION OF SEISMOMETERS BY MEANS OF EARTHQUAKE DATA

Location	Type of Instrument	Calibration Dates	Number of Observations	Ground Factor	Standard Deviation Factor	Pendulum Period	Galvanometer Period	Observed Mean Period	Magnification at Mean Period	Sensitivity Factor
Pasadena	Short Period Benioff Vertical	Apr.1,36 - Feb.1,44 Feb.28,44 - July 17,46 Aug.2,46 - July 8,47 July 9,47 - Jan.1,51	55 29 19 54	0.2 0.2 0.2 0.2	2.3 2.1 1.8 1.9	0.99? 0.99? 0.99? 0.99?	0.19? 0.19? 0.19? 0.19	1.38 1.13 1.33 1.32	3,970 ±24% 3,530 ±31% 2,020 ±29% *3,330 ±19%	0.429 0.270 0.202 0.330
Mt. Wilson	"	Oct.5,36 - Sept.27,49	87	0.2	2.1	1.0?	0.19	1.28	3,560 ±17%	0.335
Tinemaha	"	June 13,36 - Sept.27,49	64	0.2	2.3	1.0?	0.17	0.95	2,497 ±21%	0.150
Riverside	"	June 30,36 - Sept.27,49	58	0.2	2.5	1.0?	0.17	1.07	1,880 ±24%	0.133
Haiwee	"	Jan.25,39 - Sept.27,49	38	0.0	1.9	1.0?	0.17?	0.91	1,337 ±23%	0.078
Tucson	"	May 33,38 - Oct.23,50	44	0.0	2.1	1.03	0.236	1.62	2,110 ±24%	0.310
Pasadena	Short Period Benioff N-S Horizontal	May 23,38 - Dec.2,50	46	0.2	2.0	1.0?	0.19?	1.15	4,590 ±22%	0.363
Pasadena	Short Period Benioff E-W Horizontal	Dec.23,37 - Dec.2,50	46	0.2	1.8	1.0?	0.19?	1.18	4,100 ±19%	0.336
Pasadena	Long Period Benioff Vertical	June 10,38 - Dec.2,50	62	0.2	2.0	0.99	1.12	3.36	*903 ±10%	0.970
Pasadena	Long Period Benioff N-S Horizontal	Feb.21,37 - Dec.2,50	46	0.2	1.8	0.99?	0.95	3.18	955 ±18%	0.970
Pasadena	Long Period Benioff E-W Horizontal	Dec.23,37 - Dec.2,50	46	0.2	2.2	0.99?	0.78	3.55	1,142 ±26%	1.276
Huancayo	Long Period Wenner N-S Horizontal	Oct.2,32 - Nov.28,42	48	0.0	2.0	8.5	11.8	6.25	900 ±21%	0.894
Huancayo	Long Period Wenner E-W Horizontal	Oct.2,32 - Nov.28,42	44	0.0	2.0	9.3	12.8	6.27	1,000 ±33%	0.999

* Dr. Bath's Value

Table 1.

divided by a parabolic function, $1-\theta^2 K$, where θ equals the azimuthal difference, and K is a constant determined from the ratio of the square root of the energy appearing on an instrument oriented transverse to the direction of propagation to that appearing on an in-line instrument. Since there were only a few cases where a pair of horizontal instruments were so oriented, it was necessary to extrapolate the values for the recorded energy to what they would have been for such an orientation. The extrapolation thus produces, in effect, a rotation of the horizontal instruments. In order to extrapolate, values for K were initially assumed, and subsequently refined by a process of successive approximation. Energy values which required more than 30° of extrapolation were not used, for the ability to refine an assumed value for K is maximum when the horizontal components are transverse and in-line, and nil when they are oriented at angles of 45° with respect to the direction of wave propagation.

Since an energy ratio comparison for a pair of horizontal instruments depends upon the relative sensitivity of the instruments to each other, as well as K, the entire calibration procedure had to be repeated until the values determined for the sensitivity ratio and K remained stationary.

In fig. 8, the upper three curves are plots of the

horizontal correction factor $1- \theta^2 K$, where K serves as a parameter. Each curve indicates what the amplitude of a wave recorded as unity on the in-line component would be for various azimuthal differences. For $\theta = 90^\circ$, the short period Benioff instrument has an amplitude equal to 0.8 that of its in-line value; the long period Benioff, 0.63; and the very long period Wenner, 0.45. This indicates that the longer the periods which determine the instrumental response, the "purer" is the motion recorded for P and PP.

Since shear waves consist of both SH and SV components, their analysis is more complex; and, accordingly they were not used to calibrate the horizontal instruments.

The gain ratios of both the long and short period instruments appeared to be independent of the type of phase used for calibration. This attests the relative accuracy of the Gutenberg "A" values for P, PP, and S to each other.

The lowermost curve in fig. 8 is a plot of the commonly used correction factor, $\cos \theta$. If this factor were used for azimuthal differences ranging between 0 and 45°, and the value for $\cos 45^\circ$, 0.707, were used for azimuthal differences ranging between 45 and 90°, the resultant error would not be overly large. This was the procedure adopted for the analysis of SKP and related phases when data were available from only a single horizontal component. Wherever possible, however, the amplitudes were combined by vectorial

addition of both components.

The fact that for shallow shocks, SKP and PKS motion have nearly the same travel time, and the fact that $_{s}$SKP and $_{s}$PKS and also $_{p}$SKP and $_{p}$PKS should have exactly the same travel times would tend to complicate azimuthal studies of SKP and related phases.

In table 1, the arithmetic mean for the periods of the observed waves and their respective magnifications are listed for each instrument. The magnification for the Pasadena, short period, vertical instrument for the period from July 9, 1947 to January 1, 1951 was taken directly from Båth's curve for the instrument, for his calibration is believed to be valid for this period. The magnification for the Pasadena, long period, vertical instrument was taken directly from his curve for that instrument; the curve being assumed valid for it since its inception. The "sensitivity factor" for the short period instrument is listed as 0.330 and that for the long period instrument as 0.970. Values of unity would indicate perfect agreement with the reference curves. The long period "sensitivity factor" agrees with a value of unity well within the limits of experimental error. However, the short period "sensitivity factor" is much too small to be ascribed to experimental error, and probably indicates that less energy was recorded by short than by long period instruments. Accordingly, the "A" values listed by Gutenberg do not seem to

be independent of the wave period.

Figs. 9 to 14 show plots of the log of the magnification ratio versus the period of the phase used for calibration. With the exception of the apparently random plot for the Wenner instruments, the graphs indicate that the value of the log ratio increases with increasing period. Unless the shapes of the reference curves were in error, this increase suggests a rise of energy* recorded for longer period waves on Benioff instruments. This rise probably ceases for periods as long as those recorded on the Wenner instruments. Since the Riverside instrument has a galvanometer period somewhat shorter than that of the Pasadena instrument used to determine the short period reference curve, the Riverside instrument would be expected to show a drop of energy with increasing period. Because the reverse is true, the slope of the plot for the Riverside instrument has added significance.

For each instrument, the magnification of the mean period was determined by multiplying its value on the reference curve by the "sensitivity factor". However, because the "sensitivity factor" of the instrument which

*Strictly speaking, unless the total duration of a phase is considered, the computed magnification ratios depend upon relative "power" rather than relative energy.

furnished the short period reference curve was too small by a factor of three, the magnifications obtained for the other short period instruments were increased by a factor of three.

The Huancayo instruments indicate a "sensitivity factor" close to unity. Since for the periods of the waves investigated, there was only a small difference between the magnification of the reference curve used and that given by Wenner (1929), the Huancayo instruments have been, in effect, operating at magnifications close to those specified by Wenner for instruments of his design.

Complete magnification curves were determined for each instrument by use of the magnification of the mean period listed in table 1 and the response factor for critically damped electromagnetic instruments:

$$\text{Response} = \frac{T}{\left(1 + \frac{T^2}{T_o^2}\right)\left(1 + \frac{T^2}{T_g^2}\right)} \qquad (2)$$

T = period of wave motion

T_o = period of the pendulum

T_g = period of the galvanometer

Earthquake data were also used to determine the magnifications used for early Pasadena seismograms, for the seismograms of the 1931 Sumatra earthquakes obtained from

many parts of the world, and for the seismograms received from the United States Coast and Geodetic Survey, Harvard, and Weston. Because of the limited amount of data available for such calibration, the magnifications obtained were not nearly as accurate as those given in table 1. In some cases, the "A" values of Gutenberg (1945b) for shocks of intermediate focal depth, and those of Denson (1950) for P" were used. Reference curves were constructed by substitution of the appropriate instrumental constants in equa. 2. The magnificationsobtained for short period instruments were multiplied by a factor of three to allow for the assumed dependence of "A" values upon the period. The magnifications obtained were not absolute because the station ground factors were unknown; however, as mentioned before, this does not preclude the use of such magnifications for "A" value studies.

Numerous causes can be advanced to explain the large standard deviation factors observed for the gain ratios shown in table 1. Such causes are not independent of each other:

1. "A" values are not independent of frequency.
2. The basic assumptions upon which the magnitude scale depends are approximate empirical relations. (See Gutenberg and Richter 1942, and Gutenberg 1945a.)
3. Energy emanates from the hypocenter of an earthquake asymmetrically with azimuth.

4. The amplitudes of waves incident to the surface are dependent upon its "acoustic impedance", that is, the product of the velocity of propagation and the density of the transmitting medium. Unless Poisson's ratio remains constant, the amplitudes of P and S waves will be differently affected by the uppermost crustal materials. The ratio of ground displacement to the amplitude of an incident wave is a function of the wave type, Poisson's ratio, and the angle of incidence to the surface (see Gutenberg 1944). It is also possible that the angle of incidence depends somewhat upon frequency.

The use, therefore, of a fixed station ground factor to account for all these variables results in error due to oversimplification.

5. Equa. 2 is derived for steady state solutions. It can be shown from Fourier integral analysis that the sideband energy of a pulse consisting of two cycles of a simple sine wave is very small. Unless the observed pulse is unusually short, or else the frequency response curve is quite steep, the use of steady state frequency response curves for pulses comprising rather simple sine waves will cause little error.

However, Berlage (1932) shows that considerable error can result from attempts to measure the fundamental frequency of damped oscillatory pulses when the measurement of the period is taken as the time between successive alternate peaks. He analyzes a pulse defined by

$$Ate^{-\alpha t} \sin \omega t$$

where "A" is an amplitude constant, "t" is the time, "α" is a damping constant, and "ω" is the frequency. He shows that the time measured between successive alternate peaks recorded by a seismometer functioning as an accelerometer can indicate a period which is too small by a factor of two.

6. Sometimes the maximum amplitude within a phase does not signify maximum energy. In fig. 15, a slope of 45° to the right indicates that energy is constant for waves of a constant amplitude, but differing frequencies. This slope for the short period Benioff instrument is much steeper than 45°. Consequently, for waves of a given amplitude, those with the longer periods contain more energy. For the Huancayo instrument, the shorter periods would carry more energy, for all but very long periods.

OBSERVED DATA

Travel Times and Periods

(Shallow Shocks)

Figs. 16, 17, and 18 (in pocket on back cover) give the unsmoothed data used to analyze the SKP travel times. Six rather definite phases appear on both the long and the short period vertical and horizontal instruments. These six phases agree closely with the times given for them by Gutenberg and Richter (1934). Two additional phases are sometimes well recorded at later times on the long period instruments.

On the short period vertical instruments, the first and generally the principal phase, $_1$SKP, occurs 1 second earlier than the times listed for it by Gutenberg and Richter (1934). On the long period vertical instruments, its travel time at the focus agrees with that given by Gutenberg and Richter; but it occurs about 3 seconds earlier at 140°. On the horizontal instruments, the travel times occur 1 to 2 seconds later than the values given by Gutenberg and Richter. This probably results from the fact that PKS motion, which records with larger amplitudes on the horizontal instruments than SKP, has a travel time slightly longer than SKP, even for shallow focus earthquakes. Generally, $_1$SKP is impulsive; in some shocks however, especially those of large magnitude,

it is clearly emergent. (See fig. 19.) Usually, P", PP, and, SKP are either all emergent or all impulsive.

$_2$SKP occurs 7 to 8 seconds after $_1$SKP. On the long period instruments, $_2$SKP is usually masked by the motion of $_1$SKP, which is usually larger than $_2$SKP.

$_3$SKP occurs about 16 seconds, and sometimes as early as 12 seconds after $_1$SKP. On the short period vertical instruments, it is often followed 5 seconds later by another phase of similar amplitude, $_{3b}$SKP. $_3$SKP may have amplitudes as large as those of $_1$SKP. The periods of $_3$SKP are usually longer than those of $_1$SKP. $_3$SKP is strongly related to prominent secondary phases associated with P" and PP. The time interval between the secondary phase and the principal phase for P" and for PP is smaller than that between $_3$SKP and $_1$SKP. $_3$SKP probably represents a phase reflected from the surface. Fig. 20 shows a clear example of $_3$SKP. It appears to be out of phase with $_1$SKP, and is suspected to be $_s$SKP.

$_4$SKP occurs 27 seconds later than $_1$SKP. On the short period vertical instruments, it is followed 7 seconds later by another phase of similar amplitude, $_{4b}$SKP. $_4$SKP generally has large amplitudes on the long period horizontal instruments.

$_5$SKP occurs about 43 seconds after $_1$SKP. It is usually distinct on all the instruments.

$_6$SKP occurs about 54 seconds after $_1$SKP, and appears most distinct on the long period horizontal instruments.

$_7$SKP occurs about 70 seconds and $_8$SKP occurs about 87 seconds after $_1$SKP. Generally, these two phases appear clearly only on long period instruments.

It is rare that all of the above-mentioned phases can be clearly discerned on one record, or even a group of records of one earthquake. SKP motion of the same earthquake recorded at stations as close together as Pasadena and Mount Wilson sometimes show poor duplication. On the other hand, SKP motion recorded on long period instruments as far apart as Pasadena and Tucson may show an excellent duplication. The greater resemblance between the motion recorded by long period than by short period instruments probably results from less dispersion of the longer period waves by local crustal inhomogeneities.

The scatter of the data for the travel time plots shown in figs. 16 to 18 probably results from the effects of crustal inhomogeneity, uncertainties in shock location and origin time, and complexities associated with the propagation of rupture at the hypocenter. Because of the wide scatter to some of the data, and gaps in data at several epicentral distances, the travel times for the phases shown in figs. 16 to 18 should not be considered as conclusive.

SKP cannot be definitely followed beyond epicentral distance of 145°. This may be due partly to the interference by late PP phases which commence to intersect the $_1$SKP travel time curve at 143°; and due, possibly, to an interruption in the SKP travel time curve produced by refraction at the inner core. On the short period instruments, SKP cannot be followed at distances much less than 129°. On the long period instruments, SKP can be followed as far back as 125°. (See fig. 18.) The travel time curves of all SKP phases appear to be parallel to each other.

The variation in amplitude among the SKP phases is considerable. However, there is some tendency for the later phases to have relatively larger amplitudes as the distance from the focus increases. This may indicate an en echelon pattern noted by Denson (1950) for the multiple phases of PKP.

In figs. 21 and 22, the relative amplitudes of well-identified phases of two New Britain shocks can be compared. The amplitude ratio of $_5$SKP to $_1$SKP is much larger for the shock of February 28, 1934 (fig. 21) than for the shock of March 21, 1943 (fig. 22).

Although there were many widely different types of SKP motion, many seismograms recorded several years apart showed a striking duplication. This was true for both the Sumatra and the New Britain shocks.

In order that the multiple phases observed for the New Britain shocks coincide with those observed for the Sumatra shocks, the New Britain shocks consistently required negative travel time corrections of 5 to 10 seconds.

Evidence for the upper focal branch, SKP_2, exists in the fact that the multiple phases which appear to be unitary near the focus often appear as couplets at distances between 135 and 138°. Each couplet consists of two pulses which are separated by an interval of 2 to 5 seconds. (See fig. 23.) The later part of each couplet has the same period, but lesser amplitude than the first part. Because of the small duration of the couplets, the two focal branches can be discerned only on short period instruments.

For shocks of normal depth of focus, figs. 36 to 39 give the periods observed for each phase of SKP as a function of epicentral distance. It was not definitely established that the readings for epicentral distances greater than 145° actually represent true SKP phases. Symbols* on the figures distinguish between the magnitudes of the shocks, and between data obtained from long and very long period instruments. Seismometers, such as the Benioff long period instruments, having pendulum periods of about 1 second and having galvanometer periods greater than 10

*An explanation of the symbols used in figs. 36 to 53 appears on page 103.

seconds are defined as "long period" instruments. Seismometers, such as the Huancayo Wenner instruments, having pendulum periods equal to several seconds, and having galvanometer periods greater than 10 seconds are defined as "very long period" instruments.

Because no consistent difference could be detected between the data obtained from similar vertical and horizontal instruments, the components of the instruments from which the data were recorded are not distinguished in the figures. Very long period data were taken mostly from the Huancayo, horizontal Wenner seismograms, and short period data were taken mostly from short period, vertical Benioff seismograms.

On all instruments, the periods of $_1$SKP are noticeably shorter than the later phases. There is only a slight increase in period from $_2$SKP to $_8$SKP. The periods increase markedly with an increasing magnitude of the shock and with increasing periods for the instrumental constants of the recording seismometers. The periods increase slightly with epicentral distance.

The spectral energy of the recorded shocks varied widely. In some cases, shocks were recorded well only on short period instruments and, in other cases, well only on long period instruments. Most shocks, however, showed a wide band of spectral energy, for they recorded well on

both short and long period instruments. Undoubtedly, some of the wide variation observed for the periods results from Doppler effects produced by the propagation of rupture.

On some of the long period instruments, SKP phases were superimposed upon very long period waves of 25 to 30 seconds. (See figs. 21a and 21b.) The Pasadena seismogram (fig. 21a) indicates that the very long period motion commences separately at the onsets of PP and SKP. On the Tucson seismogram (fig. 21b), very long period motion associated with PP has probably merged with that of SKP. Perhaps, this very long period motion represents body waves produced concomitantly with surface waves by shallow focus earthquakes. Another possible explanation was revealed in a theory propounded in a seminar given at the California Institute of Technology in 1951 by Dr. W. W. Garvin. According to Dr. Garvin, the arrival of an impulse at the earth's surface should cause the surface to reverberate in a manner which is characteristically related to the velocity gradient. The period of these oscillations is equal to $4\pi/k$, where "k" is the velocity gradient. For a period of 30 seconds, the gradient indicated would be 0.4/second, a value which is not unreasonable for the upper several kilometers of the earth's crust.

(Shocks of Intermediate Focal Depth)

Figs. 31 to 35 show unsmoothed travel time data derived from shocks of a wide range in focal depth. Shocks ranging in depth from 40 to 75 km comprise the data used for the 60 km focal depth plots; those ranging from 80 to 145 km comprise the data for the 100 km focal depth plots. Shocks ranging in focal depth from 160 to 260 km were examined, but did not provide sufficient data for a 200 km focal depth plot. The time corrections for SKP, PKS, $_{p}$PKS, and $_{s}$SKP necessitated by this procedure were interpolated from tables given by Gutenberg and Richter (1934 and 1936). The travel time data for the reflected phases were frequently rejected when the quality of the depth determination assigned by Gutenberg and Richter (1934) was extremely low. This was a result of the difficulty of making time corrections to phases which cannot be definitely distinguished from each other unless the focal depth of the shock is known rather accurately. Travel times for PP shown in figs. 31 and 33, and for $_{p}$PP and $_{s}$PP shown in figs. 31 to 35, are based upon data given by Gutenberg and Richter (1934 and 1936). Due to the interference of reflected PP phases, the initial SKP motion is not easily discerned at epicentral distances greater than 140° for shocks for 60 km focal depth, and is

not easily discerned at epicentral distances greater than 136° for focal depths of 100 km. On the short period instruments, SKP is not observed at epicentral distances less than 129°. On long period instruments, SKP is usually impulsive; however, it is frequently preceded by very short period emergent motion. On the short period vertical instruments for the 60 km plot, the travel times for SKP are 3 seconds later at the focus and 1½ seconds earlier at 138° than the travel times indicated by Gutenberg and Richter (1934 and 1936); those for the 100 km plot are 3 seconds later at the focal point. SKP has large amplitudes on the vertical instruments and small amplitudes on the horizontal instruments. PKS has large amplitudes on the horizontal instruments, and it appears at distances as short as 125° on the Huancayo records. The interval between PKS and SKP is about 2 seconds shorter than that indicated by Gutenberg and Richter.

$_{p}$PKS has high amplitudes on the horizontal instruments. Its time-twin, $_{p}$SKP, is usually prominent on the vertical instruments. On the vertical instruments, $_{s}$SKP often has amplitudes exceeding those of SKP. $_{s}$PKS, which is the time-twin of $_{s}$SKP, usually has large amplitudes on the horizontal instruments. As a rule, strong PKS motion is followed by strong $_{p}$PKS motion, and strong SKP motion is followed by strong $_{s}$SKP motion. The reversal in phase between $_{s}$SKP and

SKP is usually evident when the phases are distinct. (See figs. 25, 26a and 26b.)

For many of the shocks of intermediate focal depth, both SKP and $_{s}$SKP are followed from 12 to 15 seconds later by a definite pulse of smaller amplitude. (See figs. 26a, 26b, and 27.) These secondary pulses could possibly result from some form of double reflection in the crust beneath the recording station. Such a double reflection might be produced by the Mohorovičić discontinuity. Possibly, they might result from the refraction of some longitudinal energy into transverse energy over the last two hundred kilometers of the SKP and $_{s}$SKP travel paths. Perhaps, these secondary pulses correspond to the prominent phase, $_{3}$SKP, noted for shallow shocks. The data were insufficient to note whether or not they were reversed in phase with respect to SKP and $_{s}$SKP, or to note whether or not corresponding secondary phases occur after P^{m} and PP.

Figs. 40 to 43 show periods observed for SKP, PKS, and for the various reflected phases for shocks of 60 and 100 km focal depth plotted as a function of epicentral distance. Only data from vertical instruments were used for SKP, and only data from horizontal instruments were used for PKS. Since no difference for the data of the reflected phases obtained from vertical and horizontal instruments could be detected, the components of the instruments from which data

were obtained are not designated in the figures.

The periods increase slightly with epicentral distance. The periods of the intermediate shocks do not increase as markedly with an increase of shock magnitude as do the shallow shocks. The periods observed for the phases increase with increasing periods for the instrumental constants even more markedly for intermediate than for shallow shocks.

Since PKS starts out as a longitudinal wave, and SKP starts out as a transverse wave, the periods of PKS waves would be expected to be shorter than those of SKP waves much as the periods of P waves are shorter than those of S waves. However, no appreciable difference between the periods of PKS and SKP waves was observed.

On short period instruments, the periods observed for SKP are slightly shorter than those observed for $_{s}$SKP for both the 60 and 100 km plots. On the long period instruments, the periods observed for PKS are slightly shorter than those observed for $_{p}$PKS for both the 60 and 100 km plots. On the short period instruments, the periods of $_{p}$SKP are slightly shorter than those of $_{s}$SKP for the 60 km plot. Although there is very little difference between periods observed for the normal and 60 km plots, the periods of the various phases for the 100 km plot seem definitely shorter than those of the corresponding ones on the 60 km plot.

Energy

(Shallow Shocks)

The equation used to investigate the observed energies was

$$A_o = M - \log \left| \frac{W}{R_o T} \right| - K(M - 7) - G \qquad (3)$$

It is based upon theory presented by Gutenberg (1945a). It depends upon the definition of magnitude and its empirical relation to energy, and upon the assumption that the duration of a phase increases with epicentral distance proportionally to the period. The terms of the equation have been previously defined for its transposed form, equa. 1.

Figs. 44 to 47 give values for A_o as a function of the distance, Δ, for various phases and recording instruments. Symbols distinguish between short, long, and very long period instruments, and between horizontal and vertical components.

The paucity of data between distances of 133 and 134° weakens the exact determination of the focal point. Both long and short period data indicate that the focal point occurs at 131½°. Very long period data from horizontal instruments indicate a broad focal point between 130 and 131°. The rise of energy at the focal point is more marked for the short than the long period data. On the short period records, little focal energy could be detected at

distances less than 129°. On the very long period Huancayo records, large focal energy persists 5 or 6° behind the focal point. This may indicate that long period energy is diffracted several degrees from the caustic in accordance with Airy's hypothesis. The appearance of a definite focus of energy for each of the later phases corroborates the hypothesis that they are associated with the principal SKP motion.

A gradual drop in energy with increasing distance from the focal point is evident on all plots as far as 145°. On the vertical instruments, the energy increases beyond 145°. This may result from the fact that some late PP phases have been mistaken for SKP phases. Theoretically, PP energy rises to a focus as the antipode is approached; whereas, SKP energy should drop to zero.

For all phases, and for the entire range of epicentral distance, the energy recorded on the short period instruments is definitely less than that recorded on the corresponding long period instruments.

Over most of the epicentral range for SKP, no consistent dependence of A_o upon magnitude was observed. Near the focal point, however, values of A_o for horizontal instruments are larger for shocks of greater magnitude. A dependence of A_o at the focal point on magnitude may result from the fact that large shocks generally produce

waves of longer duration than do small shocks. The effect of a longer duration would be to spread the peak focal energy out over a wide interval of time and reduce its prominence by a process of averaging.

$_1$SKP contains the largest energy, however, $_3$SKP is nearly as strong as $_1$SKP. The drop in energy for the successively later phases is more marked for the short, than the long period records.

(Shocks of Intermediate Focal Depths)

In figs. 48 to 53, values for A_o are given for SKP, PKS, $_p$SKP, $_p$PKS, $_s$SKP, and $_s$PKS, for focal depths of 60 and 100 km. The data are too sparse for more than a few limited conclusions.

On the 60 km, short period vertical plots for SKP and $_s$SKP, the focal point lies between 131 and 131½°. On all plots, the focal point indicated for the short periods is more prominent than that indicated for the long periods. The long period data for PKS, $_p$SKP, and $_s$SKP do not appear to indicate a focus; this may be due to error resulting from too small a sampling.

All plots indicate that the energy of the short period waves is less than that of the long period waves. However, this is less apparent on the 100 km plots than on the 60 km plots.

Both the 60 and 100 km data indicate several times less energy for SKP on the horizontal than on the vertical instruments.

The short period data for the 60 km plots, and the short and long period data for the 100 km plots indicate that PKS records with larger energy on horizontal than on vertical instruments. For short period, vertical instruments, the 60 km plots indicate that the energy of $_{s}$SKP is as large as that of SKP.

The long period, horizontal data for the 100 km plots indicate that the energy of $_{p}$PKS is less than that of PKS.

All plots indicate that near the focal point, smaller shocks record with smaller values for A_o on all types of instruments. At larger epicentral distances, the dependence of A_o on shock magnitude is random. At the focal point, the dependence of A_o on shock magnitude is even more pronounced for shocks of intermediate than shallow depth, because for shocks of shallow depth such a dependence could be observed only on the horizontal instruments.

SKP"

The data for SKP", which was observed sporadically between epicentral distances of 111 and 125°, are listed in table 2.

OBSERVED DATA FOR SKP" FROM PASADENA, ITS AUXILIARY STATIONS, AND FROM TUCSON

Date of Shock	Origin Time G.C.T.	Epicenter	Focal Depth	Magnitude	Range of Epicentral Distances	$\frac{dt}{d\Delta}$	A_o	Periods Observed on Long Period Instruments	Periods Observed on Short Period Instruments	Comments
January 2, 1936	17:26:42	9½S,119½E	Normal	6 3/4	122°		7.8		1.1 sec.	Pasadena (Δ = 122°): Large pulse followed by a series of smaller pulses several seconds apart.
September 7, 1936	12:17:26	58S,30W	160 km.	6 3/4	117.3		6.8		1.4	Pasadena (Δ = 117.3°): Two pulses 1.6 seconds apart having same period, but first pulse is larger than second pulse.
September 8, 1937	00:40:01	57S,27W	130	7.2	118.5 - 120.3	~2.1 sec/deg	7.7 - 8.6	1.7 sec.	0.8 - 1.1	Riverside (Δ = 118.0°): Twin pulses 1.8 seconds apart. Pasadena (Δ = 118.5°): Twin pulses 3.5 seconds apart.
October 20, 1938	02:19:27	9S,123E	90	7.3	118.8 - 125.2	2.1	7.2 - 7.8	2.0	0.6 - 2.1	Mount Wilson (Δ = 118.8°): Twin pulses 2.0 seconds apart. Riverside (Δ = 119.5°): Twin pulses 2.2 seconds apart. Tucson (Δ = 125.2°): Possible twin pulses 6.2 seconds apart.
November 7, 1942	07:32:09	8½S,123E	100	6 3/4	118.5 - 124.9	2.4	7.4 - 7.8		1.0 - 1.4	Mount Wilson (Δ = 118.4°): Two pulses 2.5 seconds apart having same amplitude, but period of first pulse is slightly shorter than period of second pulse. Tucson (Δ = 124.9°): Two pulses 5½ seconds apart having same amplitude, but period of first pulse slightly longer than period of second pulse.
March 9, 1943	09:48:55	60S,27W	Normal	7.3	114.4 - 119.4	2.0	7.9 - 8.8	1.5	0.7 - 1.1	Pasadena (Δ = 119.4°): Twin pulses 2.0 seconds apart. Tucson (Δ = 114.4°): Possible twin pulses 1.8 seconds apart.
March 22, 1944	00:43:18	8½S,123½E	220	7.5	118.1 - 124.5	1.5	8.0 - 8.4	2.8	0.9 - 1.8	Pasadena (Δ = 118.1°): Two pulses 3.8 seconds apart having same amplitude and period, but reversed in phase. Tucson: Twin pulses 4.2 seconds apart.
February 9, 1948	14:54:22	0,122½E	160	7.2	114.0 - 114.7		7.9 - 8.0	1.0	0.8 - 1.1	Pasadena (Δ = 114.0°): Twin pulses 3.4 seconds apart.

Table 2.

The fact that SKP" records with short periods on both long and short period instruments indicates that it has a narrow spectrum of energy. The periods recorded for SKP" on the short period, vertical Benioff instrument at Tucson (see fig. 30b) were slightly longer than those recorded on the same type of instrument at Pasadena (see fig. 30a). Part of the observed difference might be attributed to the fact that the galvanometer period for the Tucson instrument is slightly longer than that of the Pasadena instrument.

A striking feature of SKP" is its frequent appearance as a set of twin pulses separated by an interval of 1.6 to 3.9 seconds for distances less than 120° (see figs. 28, 29 and 30a) and, perhaps, by an interval of 3.9 to 6.2 seconds near distances of 125° (see fig. 30b). Such twins may signify the two branches of a focal point. Intervals of 5.5 and 6.2 seconds between the pulses recorded at distances of about 125° at Tucson seem definitely too large to signify two focal branches; probably, they signify ordinary multiple phases. Even an interval of 1.6 to 3.9 seconds observed for distances less than 120° seems too large to agree with the new travel time curve for SKP" shown in fig. 2. If the twin pulses do signify the two branches of a focus, the focal point would have to occur at a distance several degrees shorter than the distance of

$115\frac{1}{2}^{\circ}$ indicated for it by the new curve.

Prominent twin pulses for P" were not noted for the shocks listed in table 2. This is to be expected because the focal point for P" may exist between 120 and 125°. Accordingly, no separate focal branches should be observed at a distance smaller than the focal distance, and the separation of the focal branches at a distance 1 or 2 degrees greater than the focal distance should be too small to be observed.

The large number of multiple phases listed for P" by Gutenberg (1934) were not observed for SKP". This may be due to the fact that later SKP" phases are too small to be distinguished amongst the microseisms.

The slope of the new travel time curve for SKP" in fig. 2 ranges from 1.9 sec/deg at $\Delta = 115\frac{1}{2}^{\circ}$ to 1.6 sec/deg at $\Delta = 125^{\circ}$. The slope actually observed for the SKP" travel time curve ranges from 1.5 sec/deg to 2.4 sec/deg. The data for the observed slopes were too sparse to note whether or not the slopes decrease with epicentral distance. The observed slopes are definitely too low to associate SKP" with the principal SKP motion, which has a travel time slope of 3.9 sec/deg near the focal point.

The new travel times for SKP" shown in fig. 2 were computed for shocks of zero depth. These times were adjusted to apply to shocks at various depths by use of the

deep focus travel times for SKP at $\Delta = 145^{\circ}$ given by Gutenberg and Richter (1936). The interval between the SKP travel time for zero depth and that for the depth of interest was subtracted from the SKP" travel times for zero depth.* The observed travel times checked the travel times of SKP" adjusted for focal depths to within a few seconds. No consistent deviation between the observed and computed times was noted.

The energy observed for SKP" is low relative to that for SKP motion. The data were too sparse to note a consistent change of A_o over the epicentral range investigated.

On Multiplicity

The multiple phases of SKP can be better explained as resulting from reflections and refractions in the upper layers of the mantle than as resulting from dispersion.

---

*The error in using deep focus travel times of SKP at $\Delta = 145^{\circ}$ to adjust the travel times of SKP" to various focal depths is negligible because the apparent surface velocity for SKP at $\Delta = 145^{\circ}$ differs only slightly from those for SKP" over the epicentral range investigated.

Dispersion does not seem to be a dominant cause for multiple phases because:

1. The travel time curves for the multiple phases are essentially parallel to each other; and hence, the group velocity cannot differ much from the wave velocities.

2. The multiple phases appear on both long and short period instruments with no consistent time differences. Thus their travel times seem to be independent of the frequency.

3. The phases sometimes occur as sharp pulses; and hence must have considerable sideband energies. Dispersed pulses should have a simple envelope (such as that defined by a Gaussian wave packet) containing waves which have a narrow range of frequencies.

Reflections and refractions may be a dominant cause for multiplicity because:

1. $_3$SKP, a prominent phase observed for shallow shocks, may be a wave reflected from the surface. This is supported by the fact that the phase of $_3$SKP usually appears reversed to that of $_1$SKP, and by the fact that the time interval between $_3$SKP and $_1$SKP is about that which should be observed between reflected and direct shallow focus SKP waves.

2. There is some evidence for a relation among the multiple phases of P^m, PP, and SKP.

3. For intermediate shocks, SKP and $_3$SKP appear to be followed by a similar succession of pulses. This suggests that SKP and $_3$SKP undergo similar reflections or refractions in their transit through the crustal layers beneath the observing station.

4. The number of multiple phases appears to decrease with increasing focal depth. This might result from the fact that fewer layers for producing reflections or refractions exist at depth. However, some multiplicity would still arise from the passage of the SKP energy through the crustal layers beneath the observing station.

5. Evidence for a low velocity layer at a depth of 80 km is presented by Gutenberg and Richter (1939b) and Gutenberg (1948). Possibly, this layer is discrete enough to produce reflections or refractions. Jeffreys (1936 and 1937) and Gutenberg (1948) present evidence for a large increase of velocity at a depth of several hundred kilometers. It is highly conjectural whether or not this increase is abrupt enough for the production of reflections and refractions.

Dispersion is probably at least a secondary factor associated with multiplicity, for SKP energy appears to shift to the later phases with increasing distance from the focal point.

During the first minute of SKP motion, two more phases were noted for the short than the long period waves. (See figs. 16 to 18.) This may result from certain layers in the crust being too thin to reflect or refract long period waves.

The general diminution of energy for successively later SKP phases is more pronounced for short than long period waves. (See figs. 19 to 23.) This may result from a greater absorption and scattering of short period energy by the crustal layers. Absorption might also account for the general increase in wave periods observed for successively later SKP phases.

On Emergence

The fact that emergence, when present, is usually common for SKP, P^{m}, and PP may lend support to the hypothesis of dispersion at the source advanced by Fu (1945). If the emergence of SKP resulted from the conversion of transverse energy into longitudinal energy over a short interval of the initial travel path, the emergence of SKP should bear no relation to that of waves which are wholly longitudinal, such as P^{m} or PP.

For SKP, emergence in which short period motion preceded long period motion was more common than that in which long period motion preceded short period motion. Thus the evidence for normal dispersion is more prevalent than that for anomalous dispersion. Sometimes, emergence in which there was no change of frequency was observed.

Dix (1952, p. 238) notes that for materials like silty clay, velocity decreases with stress, with the result that waves of small amplitudes travel with higher velocity than waves of large amplitudes. Perhaps, some crustal materials behave to large stresses as does silty clay. This might explain the emergence so prevalently associated with shocks of large magnitude.

THEORETICAL DATA

Travel Times

In order to investigate the shape of the SKP travel time curve, estimate the surface amplitude expected for SKP at various epicentral distances, and in order to compare the relations between the foci of SKP and PKP, accurate travel time data are required. The observed travel time curve of PKP has been well established, but, due to insufficient data, that of SKP has not been accurately determined. Consequently, theoretical travel times should be used for the analysis of SKP. Wherever possible, the theoretical travel times should be modified to agree with the observed data.

The theoretical travel times presented in fig. 2 were not considered adequate for the analysis of SKP. The smooth curve of Jeffreys, although precisely determined, does not agree well with the observed data for SKP. The most prominent discrepancy is that Jeffrey's curve indicates that SKP_1 terminates at a distance of 140°; whereas, SKP_1 is believed to have been observed at distances as large as 145°. The new curve indicates a terminal distance for SKP_1 of 149°, a figure which may be too large. The new curve is not precise enough for an accurate determination of the curvature of the travel time curve, a factor

which is crucial in the analysis of the energy content of SKP.

The travel times finally used were computed directly by integration along the travel paths. Use was made of the velocities for the mantle and the core given by Gutenberg and Richter. (See fig. 54.) These velocities are listed, respectively, in tables 69 and 73 of Gutenberg (1951b). The large gradients of these velocities indicate that large errors would result if constant velocities, and hence straight ray paths, were assumed for the three components of SKP, namely, S, K, and P. Instead, the velocity curves were broken into six segments, designated by letters A through F. Segments A and B (longitudinal velocities in the mantle), segment C (longitudinal velocities in the core), and segments E and F (transverse velocities in the mantle) were expressed by the parabolic function

$$V = \frac{r^2}{2\rho p} + c \qquad (4)$$

where r = radius from the center of the earth.

ρ = curvature of the ray. Since the rays are circles, their curvatures are constant.

p = ray parameter

c = constant

Since the velocity discontinuity at the inner core boundary appears to be gradational, travel times were computed mostly for those waves which travel through the outer core. The segment D (velocity of the inner core) was assumed to be constant, and was used to calculate the travel times of only those waves which pass directly through the earth. Segments A, B, and C were used to compute the travel times of PKP, and segments E, F, and C were used to compute those of SKS. SKS travel times were calculated only as an additional check on how well the parabolic representation of the velocities would give a theoretical travel time curve agreeing with the observed one.

The boundary conditions imposed on equa. 4 in order to evaluate the parameters $2\beta p$ and c are shown in table 3. As shown in fig. 54, the agreement between the parabolic representation of the velocities and the data of Gutenberg and Richter is close.

Table 3.

Boundary Conditions for the Calculation of the Theoretical Travel Time Curves

Segment	r_1	r_2	v_1	v_2
A } P	5,500 km	6,370 km	11.2 km/sec	7.5 km/sec
B } P	3,450	5,500	13.8	11.2
C } K	1,370	3,450	10.35	8.0
D } K	0	1,370	11.35	11.35
E } S	5,400	6,370	6.40	4.00
F } S	3,450	5,400	7.30	6.40

The velocities are assumed to be independent of the wavelength. This assumption is quite reasonable, for Gutenberg (1945b) reveals that the absorption of core waves is quite low.

As indicated by Fu (1947), the assumption of the applicability of ray theory to seismic waves is valid as long as the velocity change along a wavelength is not overly large. This assumption is valid, perhaps, for all but the longer period body waves in the crustal layers of the earth.

(Derivation of the Epicentral Distance as a Function of the Ray Parameter)

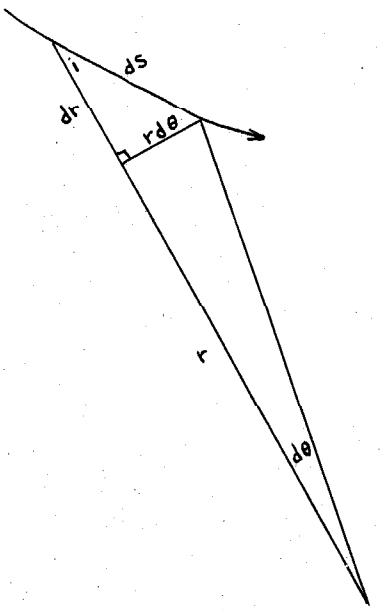

Diagram 1.

By expressing an increment of the wave path in polar coordinates (see diagram 1.), it can be shown that

$$\frac{r d\theta}{dr} = \frac{\sin i}{\sqrt{1-\sin^2 i}} \qquad (5)$$

If sin i is eliminated in equa. 5 by use of the expression for the

ray parameter, $P = \frac{r \sin i}{V}$, and the resulting equation integrated, there results

$$\theta = P \int_{r_1}^{r_2} \frac{dr}{r \sqrt{\frac{r^2}{V^2} - P^2}} \qquad (6)$$

where r_1 = inner radius

r_2 = outer radius

Solving equa. 7 with Dwight's intergral tables gives

$$2\theta = \arcsin \left[\frac{\frac{-2P^2}{(2\rho P)^2} r_2^2 + 1 - \frac{2P^2C}{(2\rho P)}}{\sqrt{1 - \frac{4P^2C}{(2\rho P)}}} \right] + \arcsin \left[\frac{\left(1 - \frac{2P^2C}{(2\rho P)}\right) r_2^2 - 2P^2C}{r_2^2 \sqrt{1 - \frac{4P^2C}{(2\rho P)}}} \right] \qquad (7)$$

$$- \arcsin \left[\frac{\frac{-2P^2}{(2\rho P)^2} r_1^2 + 1 - \frac{2P^2C}{(2\rho P)}}{\sqrt{1 - \frac{4P^2C}{(2\rho P)}}} \right] - \arcsin \left[\frac{\left(1 - \frac{2P^2C}{(2\rho P)}\right) r_1^2 - 2P^2C}{r_1^2 \sqrt{1 - \frac{4P^2C}{(2\rho P)}}} \right]$$

If the boundary conditions in table 3 are substituted into equa. 4, two simultaneous linear equations result which can be solved for $2\rho p$ and c

$$-2\beta P = \frac{r_2^2 - r_1^2}{V_1 - V_2} \qquad (8) \qquad\qquad C = \frac{V_2 r_1^2 - V_1 r_2^2}{r_1^2 - r_2^2} \qquad (9)$$

When equas. 8 and 9 are substituted into equa. 7, the resulting equation expresses θ as a function of the ray parameter, p. The second and last terms of equa. 7 vanish when the ray path does not penetrate as deep as the inner radius, r_1.

(Derivation of the Time as a Function of the Ray Parameter)

The time is

$$t = \int \frac{ds}{V} \qquad (10)$$

By use of the trigonometric relations shown in diagram 1 and the expression for Snell's law, $P = \frac{r \sin i}{V}$, it can be shown that

$$\left(\frac{dr}{ds}\right)^2 + \left(\frac{VP}{r}\right)^2 = 1 \qquad (11)$$

If equa. 11 is solved for ds and substituted into equa. 10, the variable of integration becomes dr.

$$t = \int_{r_1}^{r_2} \frac{dr}{v\sqrt{1-\left(\frac{vp}{r}\right)^2}} \tag{12}$$

The variable of integration in equa. 12 can be changed to dv by use of equa. 4.

$$t = \rho p \int_{v_1}^{v_2} \frac{dv}{v\sqrt{-v^2p^2 + v2\rho p - c2\rho p}} \tag{13}$$

where v_1 = inner velocity

v_2 = outer velocity

Solving equa. 13 with Dwight's integral tables gives

$$t = \frac{1}{2}\sqrt{\frac{-2\rho p}{c}}\, \ln \left| \frac{2c - v_2 + 2\sqrt{c}\sqrt{\frac{p^2v_2^2}{2\rho p} - v_2 + c}}{2c - v_1 + 2\sqrt{c}\sqrt{\frac{p^2v_1^2}{2\rho p} - v_1 + c}} \times \frac{v_1}{v_2} \right| \tag{14}$$

Substitution of equas. 8 and 9 into equa. 14 gives the time as a function of the ray parameter, p.

If the ray path does not penetrate as deep as the inner radius, r_1, a more complicated expression for the time results:

$$t = \tfrac{1}{2}\sqrt{\frac{-2\rho P}{C}}\ \ln\left|\frac{\frac{\sqrt{-2\rho PC}}{V_2}\ \frac{1}{2}\sqrt{\frac{-2\rho P}{C}}\ +\ \sqrt{-P^2+\frac{2\rho P}{V_2}-\frac{2\rho PC}{V_2^2}}}{\frac{2P^2\sqrt{-\frac{C}{2\rho P}}}{\sqrt{1-\frac{4P^2C}{(2\rho P)}}}\ -\ \frac{1}{2}\sqrt{\frac{-2\rho P}{C}}}\right| \qquad (15)$$

The solving of equas. 7, 14, and 15 for numerical answers is not as laborious as these equations might indicate, for they possess a high degree of symmetry and many terms are repeated.

The segments of epicentral distance and time for each specified value of the ray parameter were combined so as to give the theoretical travel times shown in table 4.

Listed in table 5 are a few key comparisons between the smoothed travel times for the core phases given by Jeffreys (1939c) and the theoretical travel times. The focal point data for PKP and PKS are in excellent agreement. The largest discrepancies occur for the waves which graze the outer core.

THEORETICAL TRAVEL TIMES

1/V	Δ PKP	t PKP	Δ PKS	t PKS	Δ SKS	t SKS
0.000 SEC/DEG	180.000°	1201.06 SEC	180.000°	1416.09 SEC	180.000°	1631.13 SEC
2.310	149.345	1186.60	142.776	1393.77	136.207	1600.94
2.319	149.264	1186.41	142.663	1393.50	136.061	1600.58
2.383	148.688	1185.06	141.838	1391.56	134.988	1598.06
2.446	148.136	1183.73	141.051	1389.61	133.926	1595.50
2.510	147.610	1182.42	140.241	1387.66	132.873	1592.89
2.574	147.109	1181.14	139.470	1385.69	131.831	1590.24
2.638	146.637	1179.92	138.719	1383.74	130.801	1587.55
2.701	146.193	1178.74	137.987	1381.78	129.780	1584.83
2.765	145.781	1177.60	137.276	1379.83	128.771	1582.07
2.828	145.400	1176.54	136.586	1377.91	127.772	1579.28
2.892	145.052	1175.55	135.918	1376.00	126.784	1576.45
2.955	144.740	1174.63	135.274	1374.11	125.808	1573.60
3.018	144.466	1173.82	134.654	1372.27	124.841	1570.72
3.082	144.231	1173.10	134.059	1370.45	123.886	1567.80
3.145	144.040	1172.50	133.491	1368.68	122.942	1564.86
3.208	143.894	1172.05	132.951	1366.97	122.009	1561.90
3.271	143.797	1171.72	132.442	1365.31	121.087	1558.90
3.334	143.757	1171.58	131.966	1363.74	120.176	1555.90
3.397	143.765	1171.63	131.520	1362.25	119.275	1552.87
3.460	143.841	1171.89	131.113	1360.85	118.385	1549.82
3.523	143.985	1172.38	130.746	1359.56	117.507	1546.74
3.586	144.205	1173.17	130.422	1358.41	116.638	1543.66
3.649	144.510	1174.28	130.146	1357.42	115.781	1540.56
3.711	144.913	1175.76	129.924	1356.59	114.934	1537.42
3.774	145.426	1177.68	129.762	1356.00	114.098	1534.31
3.836	146.067	1180.10	129.669	1355.62	113.272	1531.15
3.899	146.859	1183.18	129.658	1355.60	112.457	1528.01
3.961	147.834	1187.02	129.743	1355.93	111.651	1524.85
4.023	149.037	1191.82	129.947	1356.75	110.856	1521.68
4.086	150.535	1197.89	130.303	1358.20	110.071	1518.50
4.148	152.434	1205.72	130.866	1360.52	109.298	1515.31
4.210	154.932	1216.16	131.734	1364.14	108.536	1512.11
4.272	158.459	1231.12	133.119	1370.00	107.780	1508.91
4.334	164.504	1257.29	135.769	1381.49	107.034	1505.69
4.363	174.199	1299.38	140.442	1401.79	106.686	1504.20

Table 4.

TRAVEL TIME COMPARISONS OF CORE PHASES

Phase	Smoothed Travel Times of Jeffrey's (1939)		Theoretical Travel Times	
	Epicentral Distance	Time	Epicentral Distance	Time
PKP through center of earth	180°	1212.2 sec.	180°	1201.1 sec.
PKS through center of earth	180	1422.9	180	1416.1
SKS through center of earth	180	1633.5	180	1631.1
PKP focus	143	1173.5	143.8	1171.6
PKS focus	130	1356.2	129.6	1355.6
PKP grazing outer core	180	1330.6	174.2	1299.4
PKS grazing outer core	148	1435.0	140.4	1401.8
SKS maximum angle of incidence to outer core	62	1213.7	63.7	1232.3
PKP grazing inner core	147	1184.1	149.3	1186.6
PKS grazing inner core	140	1385.7	142.8	1393.8
SKS grazing inner core	133	1587.3	136.2	1600.9

Table 5.

The distance of the PKP_2 ray which grazes the outer core was computed as 174.2°. Jeffreys gives a figure of 180° for this distance. Jeffreys figure is more valid because Gutenberg (1934) has observed PKP_2 at a maximum distance of 180°.

The distance at which PKS_2 grazes the outer core was computed at 140.4°. Jeffreys gives a figure of 148° for this distance. Neither figure compares favorably with that of 143° indicated for this distance by the new curve in fig. 2.

The paths computed for rays which graze the core are highly sensitive to the velocity assumed to exist outside the core boundary. The function used to represent the longitudinal velocity near the core did not follow the sharp decrease in velocity gradient near the core boundary indicated by Gutenberg and Richter. (See fig. 54.) This may account for the fact that the theoretical distances computed for the PKP and PKS rays which graze the outer core were too small.

In figs. 55 to 57, the travel time curves for the core phases given by Jeffreys can be compared with those which were computed theoretically. The theoretical travel times for PKP are several seconds later than the smoothed travel times of Jeffreys; those for PKS, about equal to those of Jeffreys; and those for SKS, several

seconds earlier than those of Jeffreys. Actually, the theoretical travel times for PKP, PKS, and SKS would all be expected to be a few seconds earlier than the smoothed travel times of Jeffreys, because the theoretical curves were computed with velocity functions for the mantle which did not incorporate the low velocities which prevail in the crust.

For PKP and SKS, the slopes of the theoretical curves match those of Jeffreys rather well; for PKS, they diverge noticeably.

For PKP, the theoretical curve agrees better with the observed data of Denson (1952) than does the curve of Jeffreys. The focal point for the theoretical curve occurs at 143.8°, and that for the curve of Jeffreys at 143°. Denson, from the consideration of amplitude data, concludes that the focal distance for long period waves occurs at 143°, and that for short period waves at 147°. The distance of the PKP_1 ray which grazes the inner core is 149.3° for the theoretical curve, and 147° for the curve of Jeffreys. Denson believes this distance to be near 157°.

For PKS, the main focal branch of the theoretical curve agrees somewhat better with the observed data than does the curve of Jeffreys. The focal point of PKS occurs at 129.6° for the theoretical curve and at 130° for the curve of Jeffreys. The observed focal point occurs at

$131\frac{1}{2}^{\circ}$ for waves with periods of 1 to 5 seconds and between 130 and 131° for waves with periods of 5 to 10 seconds. The distance of the PKS_1 ray which grazes the inner core is 142.8° for the theoretical curve, 140° for the curve of Jeffreys, and 149° for the new curve in fig. 2. Long period PKS waves have been observed with certainty at a maximum distance of 145°. In fig. 58, the travel time slope for PKS as a function of the epicentral distance is shown for the theoretical curve, the curve of Jeffreys, and the new curve. The slopes of PKS_1 for the theoretical curve are higher than those of Jeffreys's curve and lower than those for the new curve. The slopes of PKS_2 are lower for the theoretical curve than those for either the curve of Jeffreys or the new curve.

The observed data for PKS indicate slopes more in agreement with the theoretical curve. The best check on the slope of the PKS travel time curve is afforded by data observed between distances of 130 and 138°. The mean slope of the first $6\frac{1}{2}^{\circ}$ of the theoretical curve for PKS_1 is 3.25 sec/deg. The mean slope observed for the interval from $131\frac{1}{2}$ to 138° is about 3.5 sec/deg for shallow shocks and 3.2 or 3.3 sec/deg for shocks of a focal depth of 60 km. The mean slope observed for the shallow shocks may be too large, for a comparison of the individual data for shocks recorded at both Pasadena and Tucson for epicentral distances

of 130 to 138° yield slopes ranging from 2.9 to 3.6 sec/deg with a mean close to the theoretical mean. Too much significance cannot be attached to the results of the Pasadena-Tucson recordings unless it can be demonstrated that the crustal layers beneath each station affect PKS phases in an identical manner. The use of the travel time data for shocks of 60 km depth to check theoretical travel times of shallow shocks is valid, for it can be shown from methods indicated by Gutenberg (1936, p. 341) that the focal point and the slope of the travel time curve for shallow focus earthquakes differ by negligible amounts from those for earthquakes with a focal depth of 60 km.

Fig. 59 gives the second derivative of the theoretical travel time curve of PKS as a function of epicentral distance. The use of the observed travel times to estimate the quantity, $di/d\Delta$, which is the change in the angle of emission of a ray from the hypocenter with respect to the change produced in epicentral distance, depends heavily upon the accurate determination of the second derivative of the travel time curve. (See Gutenberg and Richter, 1935, p. 300.) In fig. 59, the small values for the second derivative indicate how accurately observed travel times for PKS must be if they are to be used to estimate $di/d\Delta$.

The agreement between the observed and theoretical travel time curve for the main focal branch of PKS is

believed good enough to justify the use of the theoretical travel times to analyze, to a first approximation, the energy content of PKS_1 phases.

Energy

The equation used to determine the theoretical energy content of SKP, PKS, $_pSKP$, $_sSKP$, $_pPKS$, and $_sPKS$ was

$$A_t = C - \log \left| Q \sqrt{\frac{F_1 F_2 \cdots e^{-\int \kappa dD} \, d\cos i_h / d\Delta}{\sin \Delta \cos i_o}} \right| \qquad (16)$$

It is derived from equations presented by Gutenberg (1944), and is based on a theory originated by Zoeppritz (1912). The basic assumption in its use is that energy is governed by the geometry of the ray paths, an assumption which, as pointed out by Fu (1947), is not inherent in Fermat's principle of least time.

C is a constant related to the amount of energy imparted to a particular wave type at its source. Gutenberg (1945) has found that C is approximately the same for both longitudinal and transverse waves. His value of 6.3 was used for all calculations.

Q is the ratio of ground displacement to incident amplitude. It depends upon the angle of incidence of the

ray at the surface and upon Poisson's ratio, and was determined from equations given by Gutenberg (1944). Velocities of 5.5 km/sec for compressional waves and 3.2 km/sec for shear waves, and a radius for the earth of 6.37 km were used to compute the angles of incidence from the ray parameters given in table 4. The velocities used for the compressional and shear waves correspond to a Poisson's ratio of 0.239.

$F_1 F_2 \ldots$ are factors which indicate the energy ratios of refracted and reflected waves to incident waves. They are obtained from the Knott-Zoeppritz equations derived for plane waves traveling in homogeneous layers separated by sharp, planar discontinuities. They are not valid for an angle of grazing incidence to a discontinuity. The values for refraction at the core boundary were taken from Dana (1944) who used velocities of 13.7 km/sec for longitudinal and 7.25 km/sec for shear waves outside the core; and velocities of 8.0 km/sec for longitudinal and 0.0 for shear waves in the core. He also used 5.4 gms/cc for the density outside the core and 10.1 gms/cc for the density inside the core. For the calculation of the angles of incidence of the rays at the core from the ray parameters given in table 4, a radius for the core of 3.45 km was used. For the reflected phases ($_pSKP$, $_pPKS$, $_sSKP$ and $_sPKS$),

surface energy ratios were computed from equations given by Gutenberg (1944). The surface conditions were assumed to be the same as those used to determine the values of Q.

$e^{-\int \kappa dD}$ accounts for absorption along the ray path. Gutenberg's (1945a) value of .00012/km, based upon his analysis of the energy content of P, P'P', and P'P'P', is used for SKP. The path length for SKP was computed from straight line segments in the mantle and the core drawn so as to subtend the same amount of epicentral distance as do each of the curved ray segments of SKP computed by equa. 7. The attenuation factor obtained for SKP amplitudes averages about $\frac{1}{2}$. The values for this factor have a maximum change of only 4% for the entire SKP travel time curve.

Δ is the epicentral distance. Values for it were taken from table 4.

i_h is the angle of emission of a ray from the hypocenter. It was determined from the ray parameters given in table 4, by using initial velocities of 7.5 km/sec for PKS and 4.0 km/sec for SKP, and 6,370 km for the radius of the earth. The energy computed is quite sensitive to the factor $\cos i_h/d\Delta$. Fig. 60 shows a plot of $di_h/d\Delta$ for PKS versus the slope of the travel time curve, $dt/d\Delta$.

i_s is the angle of surface incidence at the recording station. It was computed from the ray parameters given in

table 4. The surface conditions were assumed to be the same as those used to determine the values of Q.

In figs. 61 to 63, the theoretical energy parameters for various SKP phases are plotted against epicentral distances. In order that the theoretical focal point coincide with the observed focal point at $131\frac{1}{2}^{\circ}$, 2° were added to the epicentral distances. Dashed lines denote the upper focal branch, and solid lines denote the main focal branch. The data for the figures were obtained from tables 5a and 5b.

The graphs indicate that the most significant amplitudes are those of the main focal branch of horizontal PKS and ${}_{p}$PKS, and vertical SKP and ${}_{s}$SKP. Although the energies of the two focal branches are the same at the focal point, amplitudes for the upper focal branch fall off rapidly with increasing distance. This may well explain why no clear indication of the upper focal branch was noted for epicentral distances greater than 138°. However, because Knott's equations are not valid for grazing incidences to the core, and because $di/d\Delta$ changes rapidly, the theoretical data given for the upper focal branch lose physical significance for distances greater than 135°.

Although the energy parameters were computed for shocks of normal depth, the parameters are believed valid for the analysis of shocks of intermediate depths. For

shocks of intermediate depth, there should be a slight decrease in epicentral distance to the SKP focal point. This decrease amounts to only a fraction of a degree and is smaller for SKP than PKS. For shocks of intermediate depth, the additional increase in the size of the cone of emitted energy subtended by the core would be negligible if it were not for the fact that there is a marked increase of velocity from shallow to intermediate depths. The initial velocities of 7.5 km/sec used for PKS and 4.0 km/sec used for SKP are probably too high for shocks originating in the upper granitic layers and too low for shocks originating below the Mohorovičić discontinuity. Higher velocities at the point at which a shock originates mean higher values for $di/d\Delta$, and hence more energy for the core phases.

Table 6 gives the residuals for the observed minus the theoretical "A" values for some of the more prominent SKP phases. The residuals are given for shocks of normal, 60 km, and 100 km depths. Data are presented for the long and short period instruments in separate rows. Question marks signify doubtful data; and blanks, no available data. The energies of $_pPKS$ and $_pSKP$, and those of $_sSKP$ and $_sPKS$ are inseparable by virtue of identical travel times. Since the horizontal amplitudes of $_pPKS$ should be twenty times larger than those of $_pSKP$, little error should result in

Theoretical Energy Parameters

A_t

Δ	SKP		PKS		pSKP	
	Vert.	Horiz.	Vert.	Horiz.	Vert.	Horiz.
144.78°	7.64	8.51	8.50	7.38	8.10	7.38
144.66	7.64	8.51	8.49	7.37	8.10	7.38
143.84	7.62	8.48	8.46	7.35	8.07	7.36
143.03	7.61	8.45	8.43	7.33	8.04	7.34
142.24	7.58	8.41	8.39	7.31	8.00	7.32
141.47	7.56	8.38	8.36	7.29	7.97	7.30
140.72	7.54	8.35	8.33	7.26	7.94	7.28
139.99	7.51	8.32	8.29	7.24	7.91	7.25
139.28	7.50	8.29	8.25	7.22	7.88	7.24
138.59	7.48	8.26	8.23	7.20	7.85	7.22
137.92	7.46	8.23	8.20	7.19	7.82	7.20
137.27	7.44	8.20	8.18	7.16	7.80	7.18
136.65	7.42	8.17	8.14	7.13	7.76	7.15
136.06	7.40	8.14	8.11	7.12	7.75	7.13
135.49	7.37	8.11	8.08	7.10	7.70	7.11
134.95	7.35	8.08	8.05	7.07	7.67	7.09
134.44	7.32	8.04	8.02	7.05	7.63	7.07
133.97	7.30	8.01	7.98	7.03	7.60	7.05
133.52	7.28	7.98	7.95	7.00	7.57	7.02
133.11	7.25	7.94	7.91	6.97	7.53	6.99
132.75	7.21	7.90	7.87	6.94	7.49	6.96
132.42	7.18	7.86	7.82	6.90	7.45	6.92
132.15	7.13	7.80	7.76	6.85	7.39	6.87
131.92	7.07	7.74	7.70	6.79	7.33	6.81
131.76	6.98	7.62	7.59	6.69	7.23	6.71
131.67	6.78	7.43	7.39	6.50	7.02	6.53
131.66	[illegible]	[illegible]	[illegible]	[illegible]	[illegible]	[illegible]
131.74	6.97	7.60	7.56	6.69	7.20	6.71
131.95	7.12	7.75	7.70	6.84	7.35	6.86
132.30	7.23	7.84	7.79	6.93	7.45	6.96
132.87	7.33	7.94	7.88	7.03	7.54	7.05
133.73	7.43	8.03	7.97	7.12	7.63	7.15
135.12	7.56	8.16	8.09	7.25	7.76	7.28
137.77	7.91	8.50	8.39	7.56	8.00	7.59
142.44	[illegible]	[illegible]	[illegible]	[illegible]	[illegible]	[illegible]

Table 5a.

Theoretical Energy Paremeters

A_t

Δ	$_pPKS$		$_sSKP$		$_sPKS$	
	Vert.	Horiz.	Vert.	Horiz.	Vert.	Horiz.
144.78°	8.50	7.38	7.65	8.52	9.42	8.30
144.66	8.50	7.38	7.65	8.51	9.42	8.30
143.84	8.47	7.36	7.63	8.50	9.38	8.27
143.03	8.44	7.34	7.62	8.46	9.33	8.24
142.24	8.40	7.32	7.59	8.42	9.28	8.20
141.47	8.37	7.30	7.57	8.39	9.24	8.17
140.72	8.34	7.28	7.55	8.36	9.20	8.13
139.99	8.31	7.25	7.53	8.33	9.15	8.10
139.28	8.26	7.24	7.51	8.30	9.10	8.08
138.59	8.25	7.22	7.49	8.27	9.07	8.04
137.92	8.22	7.20	7.48	8.25	9.04	8.02
137.27	8.19	7.18	7.46	8.22	9.00	7.99
136.65	8.16	7.15	7.43	8.19	8.96	7.95
136.06	8.13	7.13	7.41	8.16	8.92	7.92
135.49	8.10	7.11	7.39	8.13	8.89	7.89
134.95	8.06	7.08	7.37	8.09	8.83	7.86
134.44	8.03	7.07	7.34	8.06	8.79	7.83
133.97	8.00	7.03	7.32	8.03	8.75	7.80
133.52	7.97	7.02	7.30	8.00	8.71	7.76
133.11	7.93	6.99	7.27	7.96	8.66	7.73
132.75	7.89	6.96	7.23	7.92	8.62	7.69
132.42	7.84	6.92	7.20	7.88	8.56	7.64
132.15	7.79	6.87	7.15	7.82	8.50	7.58
131.92	7.72	6.81	7.09	7.76	8.42	7.52
131.76	7.60	6.71	7.00	7.65	8.31	7.41
131.67	7.42	6.53	6.81	7.45	8.10	7.21
131.66	$-\infty$	$-\infty$	$-\infty$	$-\infty$	$-\infty$	$-\infty$
131.74	7.59	6.71	6.99	7.63	8.26	7.38
131.95	7.73	6.86	7.13	7.78	8.40	7.53
132.30	7.82	6.96	7.26	7.87	8.48	7.62
132.87	7.91	7.05	7.35	7.97	8.56	7.71
133.73	8.00	7.15	7.46	8.06	8.64	7.80
135.12	8.12	7.28	7.59	8.19	8.76	7.92
137.77	8.43	7.59	7.74	8.54	9.06	8.22
142.44	∞	∞	∞	∞	∞	∞

Table 5b.

attributing all the energy recorded on the horizontal instruments as resulting from $_{p}$PKS. Since the vertical amplitudes of $_{s}$SKP should be twenty-five times larger than those of $_{s}$PKS, little error should result in attributing all the energy recorded on the vertical instruments as resulting from $_{s}$SKP. For shallow shocks, the values of A_o for $_{s}$SKP and $_{p}$PKS were assumed to be those computed for $_{3}$SKP in figs. 44 and 46. The energy comparisons for $\Delta = 132^{\circ}$ give a crude measure of the "focal energy", and may have significance because the actual focus is rather broad. The comparisons for $\Delta = 135$ to 140° have, of course, more physical meaning.

The residuals indicate that the energy shifts from long to short period waves as the focal depth increases. This probably results from the fact that the elastic moduli rise more rapidly with depth than the density, a factor which would raise the frequency of the vibrational modes carrying the dominant energy released in an elastic rebound.

The vertical residuals are relatively small; hence, the observed and theoretical energies of SKP and $_{s}$SKP are in good agreement. The large positive values for the horizontal residuals indicate that the observed energies of PKS and $_{p}$PKS are several times smaller than the theoretical energies. The problem of too little energy being recorded by horizontal instruments is not satisfactorily

$A_o - A_t$

		SKP Vertical		PKS Horizontal		pPKS Horizontal		sSKP Vertical	
		132°	135-140°	132°	135-140°	132°	135-140°	132°	135-140°
h = N	S.P.	+.10	+.35	+.80		+.35		+.10	+.30
	L.P.	-.35	-.15	+.30	+.15	+.25	+.30	-.30	-.15
h = 60 km.	S.P.	+.30	+.30?	+.30		+.50?		+.25	+.20
	L.P.	-.10?	.00?	+.30	+.40	+.25	+.45	-.10?	.00
h = 100 km.	S.P.	.00		+.50		+.35??		+.10?	
	L.P.	-.30?		+.40	+.00	+.55??	+.35	.00??	

Table 6.

explained.

Because of the reciprocity of the transmission coefficients associated with the core, they should affect the energy content of PKS and SKP phases equally. A large error in the boundary conditions assumed for the core boundary would produce a consistent error in the computed energies for both PKS and SKP phases.

The hypothesis that the energy imparted to the PKS phase at the hypocenter is smaller than that predicted would contradict the observation of too much energy on both horizontal and vertical instruments for PcP by Martner (1950) and for PKP by Denson (1950).

The assumption that the horizontal components of PKS surface amplitudes are too low because the angles of incidence of the shear rays at the surface are smaller than those calculated seems untenable for:

1. The velocity of 3.2 km/sec used to calculate the angles of incidence of the shear waves at the surface should be relatively close to the actual velocities at the recording stations. To obtain lower angles of incidence at the surface, the velocity used must be smaller. The reduction in velocity necessary to make the horizontal residuals small would be unreasonable.

2. As a consequence of their thicknesses being comparable to a wavelength, the low velocity crustal layers may be too thin to affect the paths of the incident rays. If this be true, the incident angles of the rays at the surface would be expected to be larger rather than smaller than the values computed.

3. Too much energy for the horizontal component

relative to that for the vertical component was found by Martner for PcP and by Denson for PKP. This points to larger, rather than smaller angles of incidence at the surface.

The value computed for $di/d\Delta$ depends heavily on the second derivative of the travel time curve. Because the curvature of the theoretical travel time curve is less than that of the new curve (see fig. 2), theoretical energies calculated by use of the new curve would be smaller, and, accordingly, the computed values for A_t would be larger by 0.1. This would reduce the horizontal residuals by a small amount. The short period vertical residuals would also be reduced, but the long period vertical residuals would be increased. The curvature of the theoretical travel time curve is less than that of Jeffrey's travel time curve. Values computed for A_t by using Jeffrey's curve would be smaller by 0.1. This would reduce the long period vertical residuals, but would increase all other residuals.

SKP, PKP, AND THE INNER CORE

SKP_2 may have been observed between distances of 135 and 138°. Such a narrow range of observations probably results from the fact that at distances less than 135°, SKP_2 cannot be distinguished from SKP_1, and at distances greater than 138°, SKP_2 records with very small amplitudes. Few of the points used to determine the observed SKP travel times (see figs. 16 to 18 in pocket on back cover) will line up with a slope steep enough to suggest the upper focal branch. PKP_2 has been well observed by Gutenberg (1934) from the focal point near 143° to a maximum distance of 180°.

Amplitude data for SKP indicate that for waves of periods of 1 to 5 seconds, the focal point occurs at 131½° and that for waves of periods of 5 to 10 seconds, the focal point is broadly defined between 130 and 131°. For PKP, Denson (1950) notes that the focal point for short period waves occurs at 147°, and that the focal point for long period waves occurs at 143°. Thus, the dependence of the position of the focal point upon the wave periods is less marked for SKP than for PKP.

Denson suspects that the PKP caustic may be affected by diffraction in accordance with Airy's theory. For SKP, the backward extension from the focus of short period waves

to only 129° and that of long period waves to 125° strongly suggests a diffraction phenomenon.

Denson observes that long period PKP_1 waves persist with large amplitudes to distances as far as 157°. The new curve for SKP in fig. 2, which is based indirectly upon Denson's results for PKP, indicates that SKP_1 should extend to 149°. Actually, long period SKP phases could not be observed with certainty beyond 145°. This may be due partly to the interference of SKP phases by late PP phases.

Denson notes that the amplitudes of short period PKP_1 waves fall off rapidly between 147 and 157°. Amplitudes of SKP_1 fall off rapidly between 131½ and 140°. A paucity of data renders difficult the determination of the maximum epicentral distance to which short period waves extend, but it is not believed to exceed 143°. Gutenberg (1938) suggests that PKP_1 may extend to epicentral distances greater than that which is subtended by the ray which grazes the inner core. The observed data for both PKP and SKP indicate that as a result of diffraction, the longer period waves may extend into the shadow zone produced by the inner core.

Denson noted that P'' recorded with high amplitudes between 120 and 125°. Correspondingly, SKP'' would be expected to record with high amplitudes between 114 and

122° on both short and long period instruments. SKP" data from long period instruments at distances between 122 and 125° was not available. The period data for SKP" thus appear to harmonize with that for P". The inability to identify SKP" between 125° and the SKP focal point may result from the fact that SKP" motion is too small to be distinguished from microseisms.

The separation of long and short period energy noted by Denson for PKP is not so apparent for SKP. The focal point of SKP depends to a less extent upon frequency. The caustics of the later SKP phases occur at the same distance as does that of the initial, main SKP phase. Some of the multiple phases have travel times nearly independent of the wave periods. The en echelon nature of the travel time curves for the multiple phases are not so apparent for SKP as for PKP; although, a shift of SKP energy to the later phases for increasing distance from the focal point is observed.

For PKP, Denson suspects that short period waves arriving at epicentral distances between 120 and 147° and long period waves arriving between 145 and 157° have separated from each other during their passage through the earth. For SKP, a smaller magnitude of separation is indicated. Possibly, short period SKP" waves arriving between approx-

imately 114 and 125° are separated from long period waves arriving between 140 and 145°.

The twin pulses observed for SKP" may signify the two branches of a focal point. However, the two branches would not be expected to be distinguished from each other unless the focal point occurs at a distance several degrees shorter than the 115½° indicated by the new curve in fig. 2.

The observations of SKP" are essentially in harmony with those for P" and they corroborate to a limited degree Gutenberg's hypothesis of a large, but continuous increase in velocity in the transition zone at the boundary of the inner core.

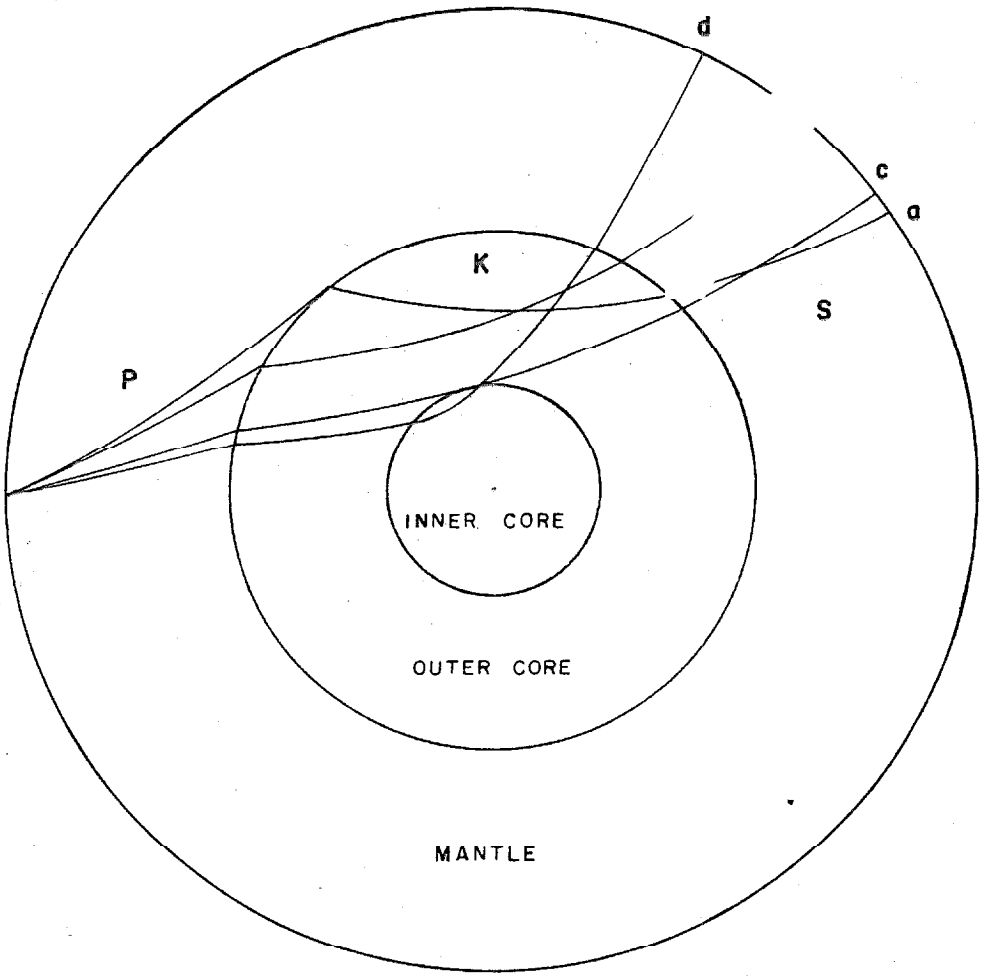

Ray paths of PKS

Figure 1.

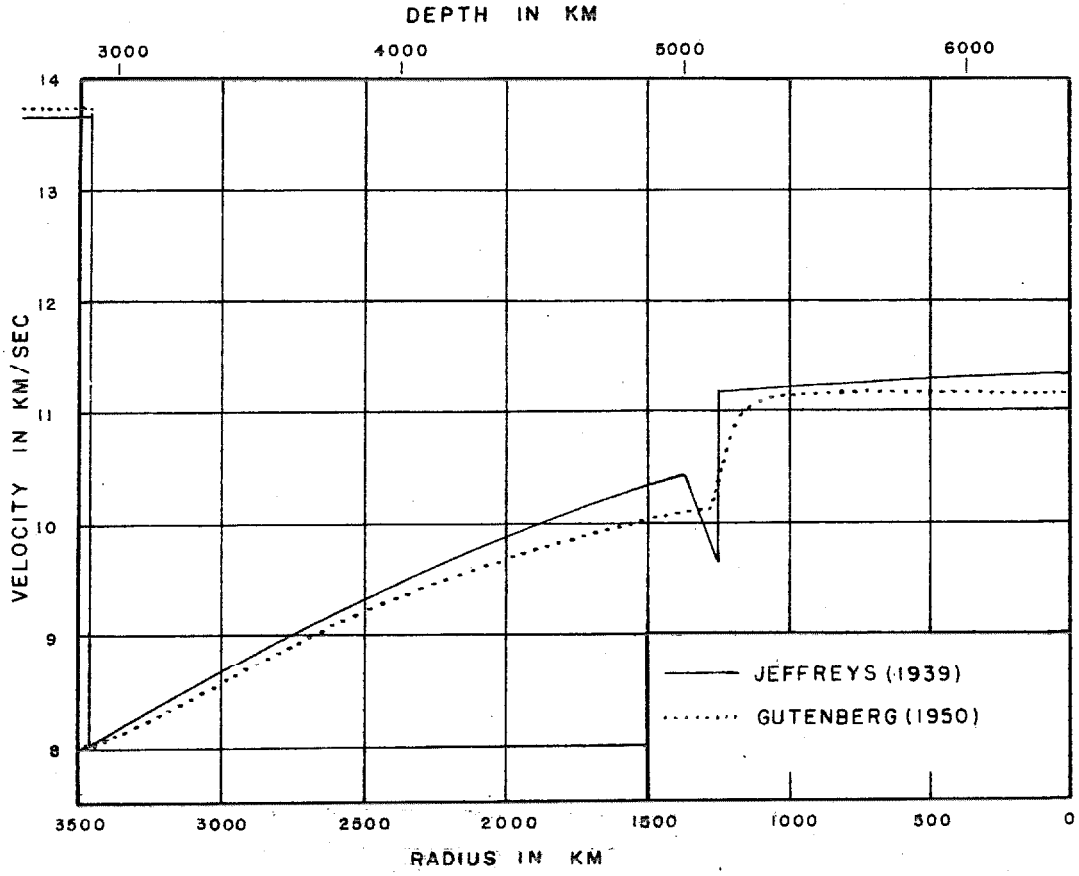

Calculated velocity of longitudinal waves in the core

Figure 3.

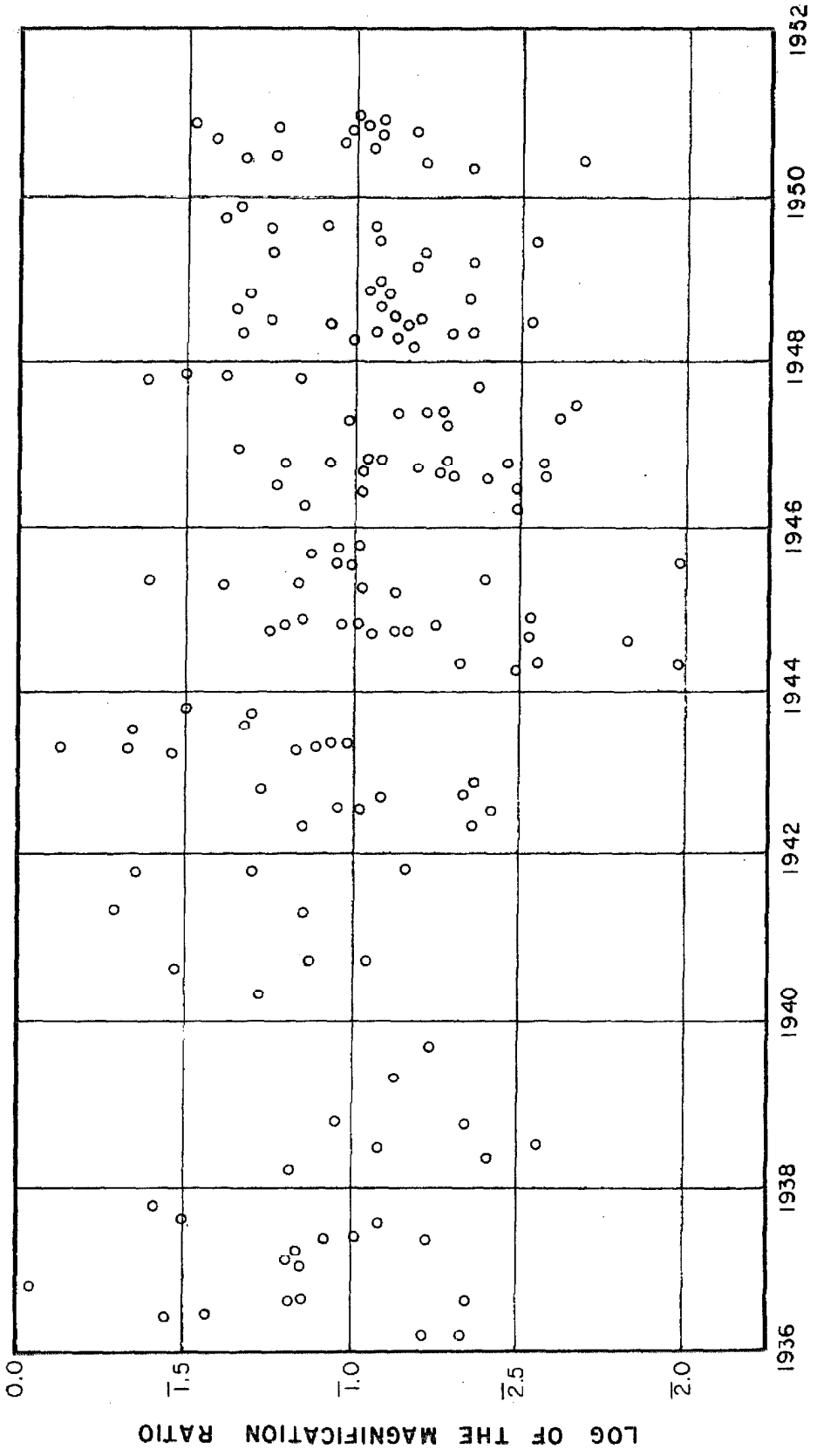

Sensitivity of the short period, vertical Benioff seismometer at Pasadena

Figure 4.

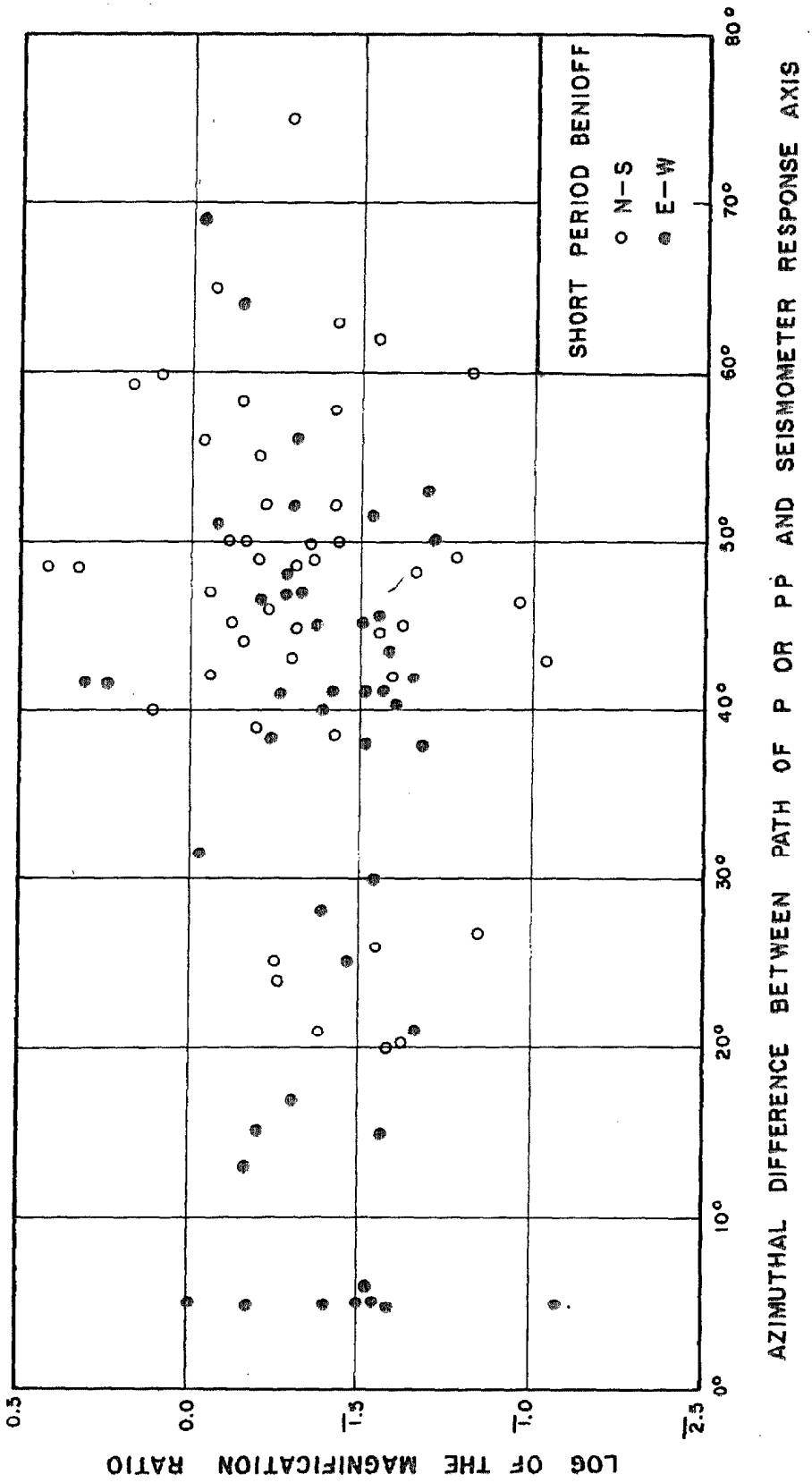
SHORT PERIOD BENIOFF
○ N-S
● E-W
0°
10°
20°
30°
40°
30°
60°
70°
80°
AZIMUTHAL DIFFERENCE BETWEEN PATH OF P OR PP AND SEISMOMETER RESPONSE AXIS
0.5
0.0
1.5
1.0
2.5
LOG OF THE MAGNIFICATION RATIO

Figure 5.

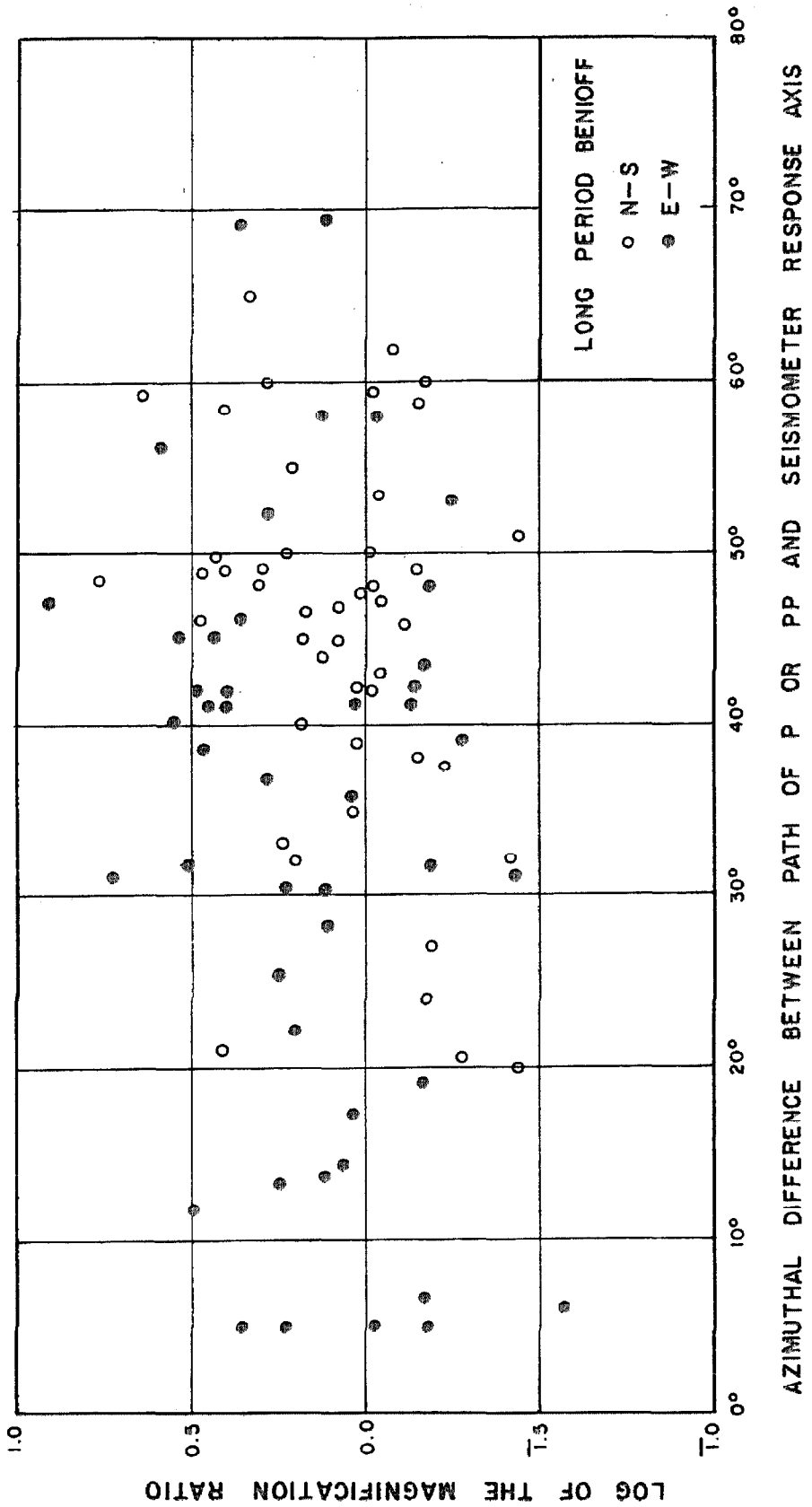
LONG PERIOD BENIOFF
o N-S
● E-W
LOG OF THE MAGNIFICATION RATIO
1.0
0.3
0.0
-1.3
-1.0
0°
10°
20°
30°
40°
50°
60°
70°
80°
AZIMUTHAL DIFFERENCE BETWEEN PATH OF P OR PP AND SEISMOMETER RESPONSE AXIS

Figure 6.

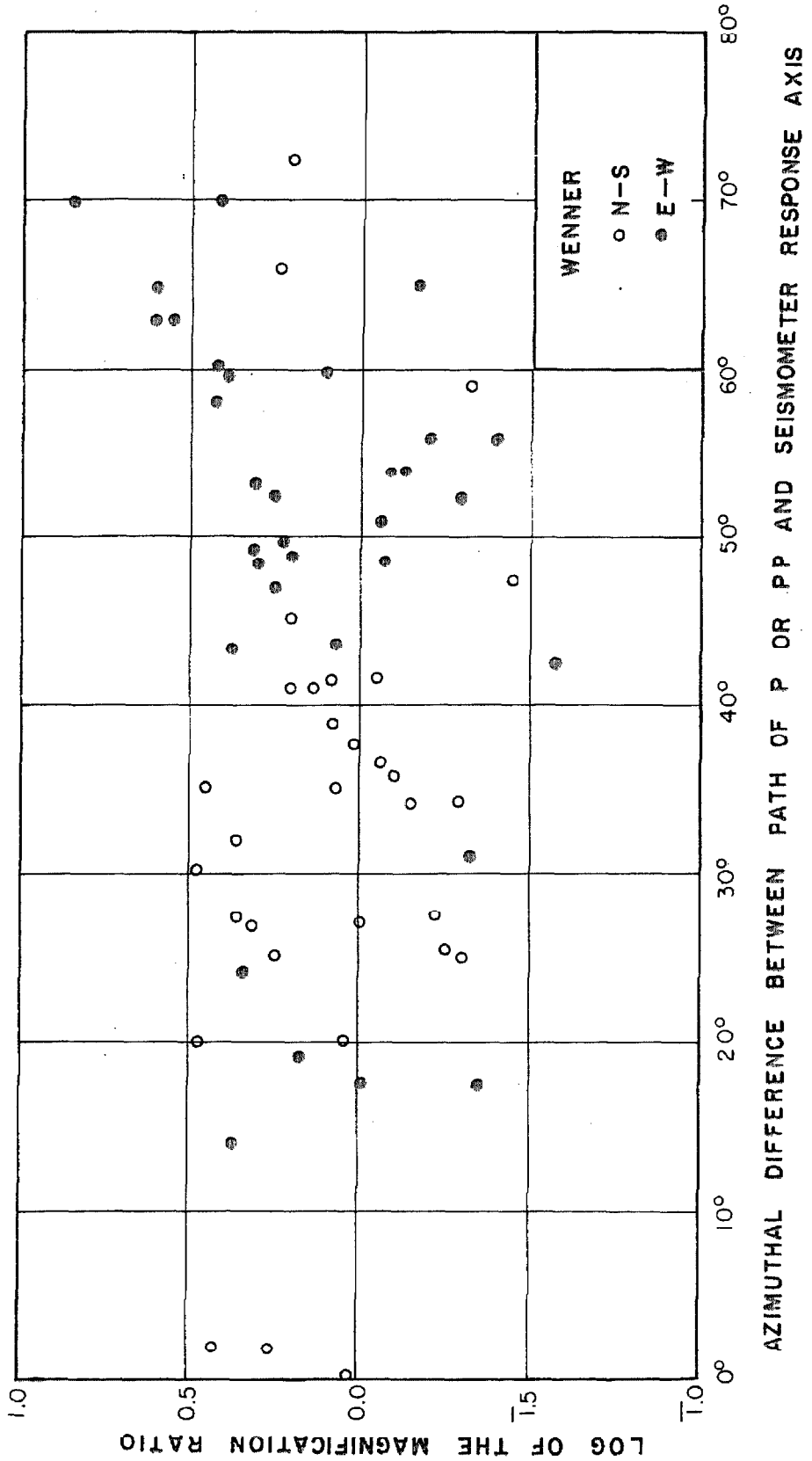
WENNER
o N-S
• E-W
0°
10°
20°
30°
40°
50°
60°
70°
80°
AZIMUTHAL DIFFERENCE BETWEEN PATH OF P OR PP AND SEISMOMETER RESPONSE AXIS
1.0
0.5
0.0
1.5
1.0
LOG OF THE MAGNIFICATION RATIO

Figure 7.

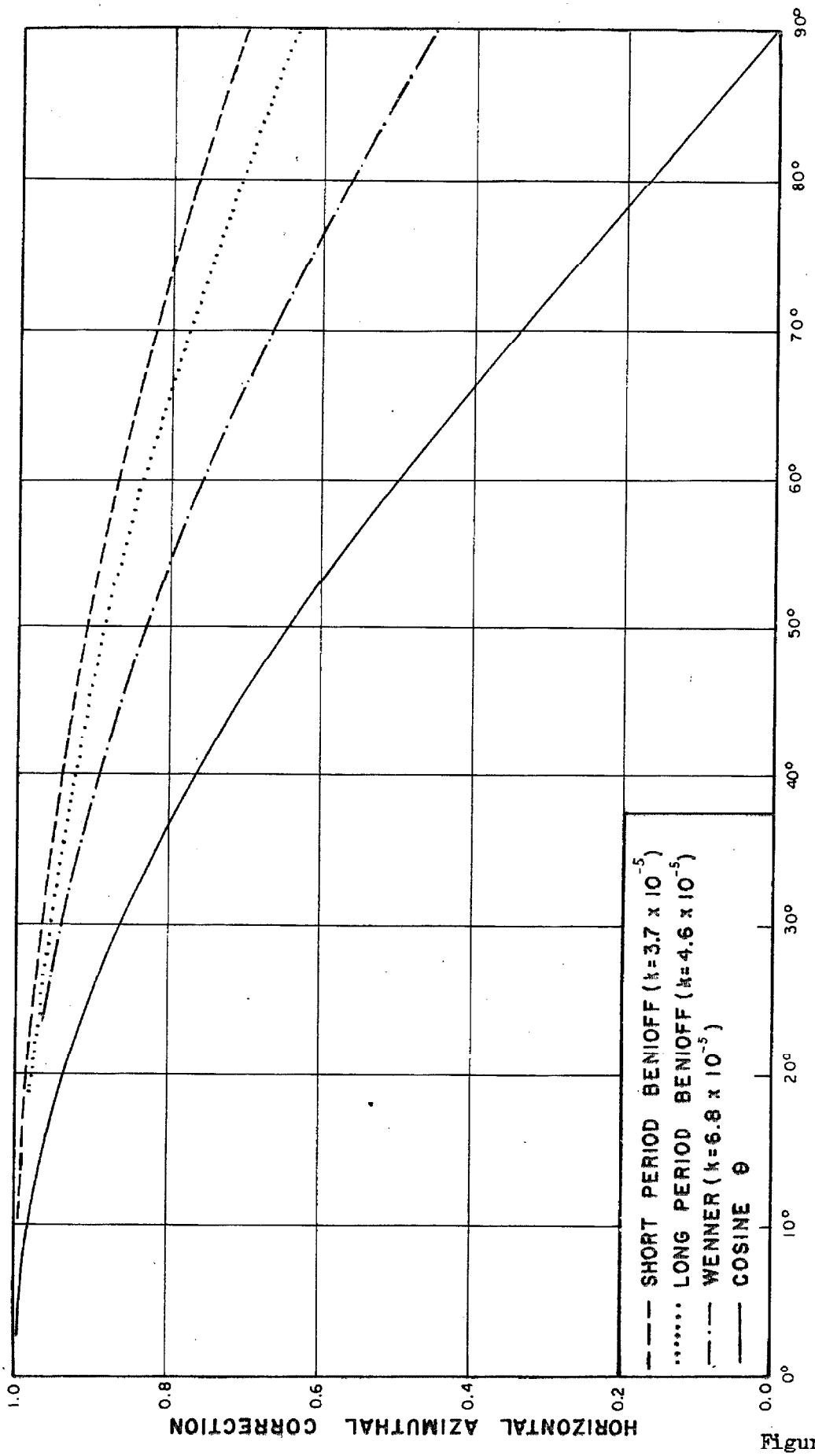
HORIZONTAL AZIMUTHAL CORRECTION
1.0
0.8
0.6
0.4
0.2
0.0
0°
10°
20°
30°
40°
50°
60°
70°
80°
90°
AZIMUTHAL DIFFERENCE BETWEEN PATH OF P OR PP AND SEISMOGRAPH RESPONSE AXIS
SHORT PERIOD BENIOFF (k=3.7 x 10⁻⁵)
LONG PERIOD BENIOFF (k=4.6 x 10⁻⁵)
WENNER (k=6.8 x 10⁻⁵)
COSINE θ

Figure 8.

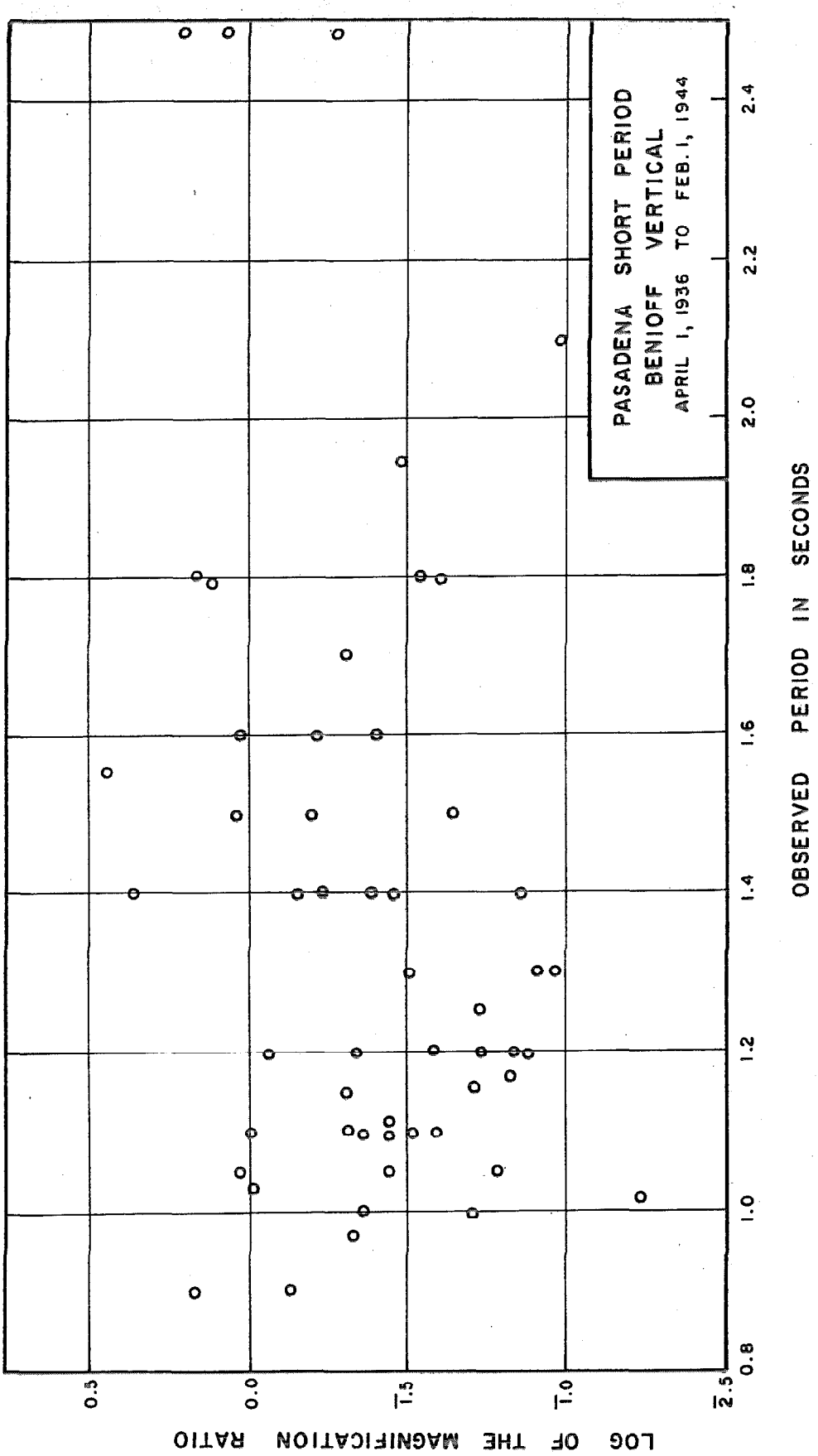
PASADENA SHORT PERIOD
BENIOFF VERTICAL
APRIL 1, 1936 TO FEB. 1, 1944
0.8
1.0
1.2
1.4
1.6
1.8
2.0
2.2
2.4
OBSERVED PERIOD IN SECONDS
0.5
0.0
1.5
1.0
2.5
LOG OF THE MAGNIFICATION RATIO

Figure 9.

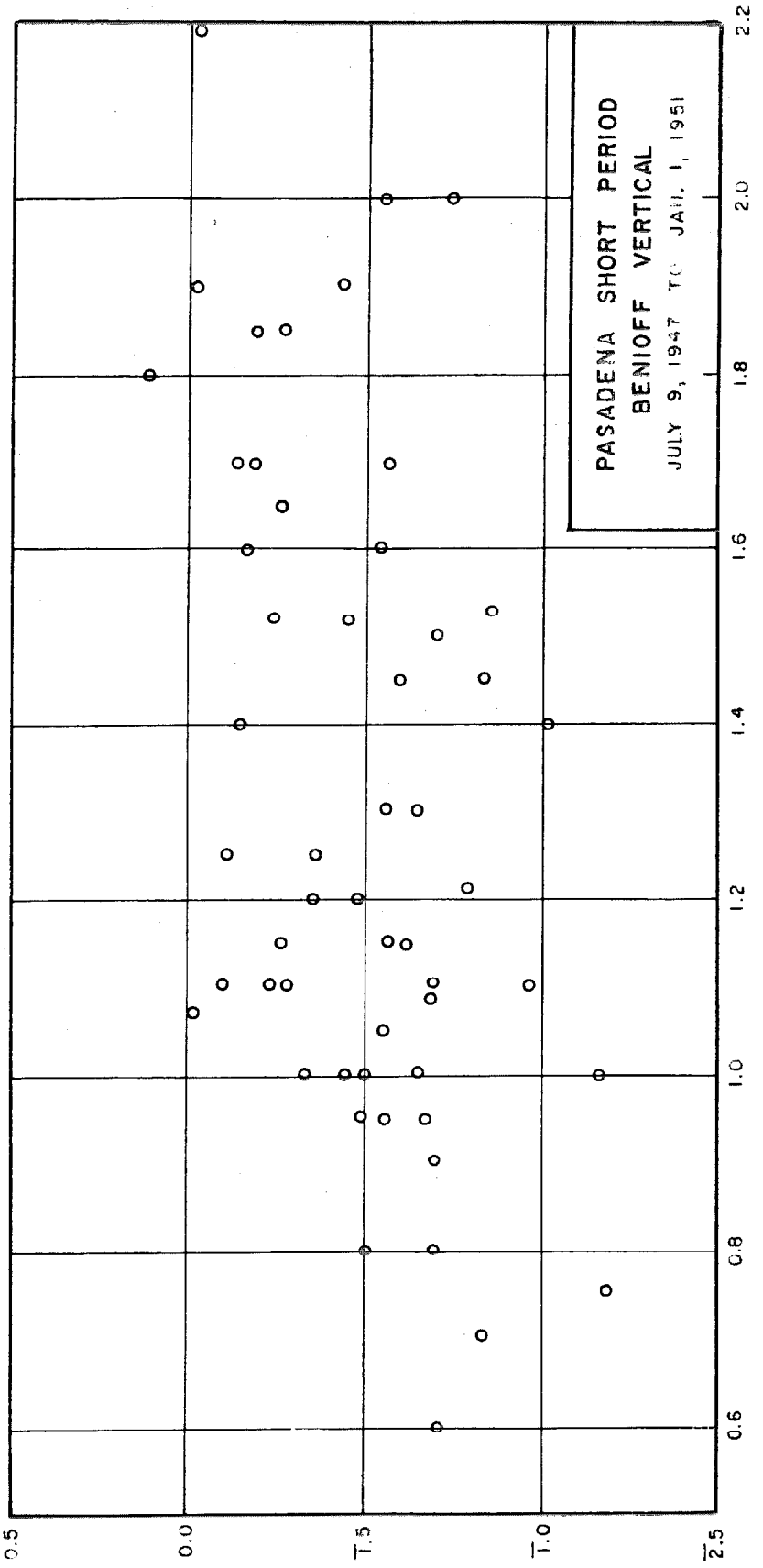
PASADENA SHORT PERIOD
BENIOFF VERTICAL
JULY 9, 1947 TO JAN. 1, 1951
0.5
0.0
$\bar{1}.5$
$\bar{1}.0$
$\bar{2}.5$
LOG OF THE MAGNIFICATION RATIO
0.6
0.8
1.0
1.2
1.4
1.6
1.8
2.0
2.2
OBSERVED PERIOD IN SECONDS

Figure 10.

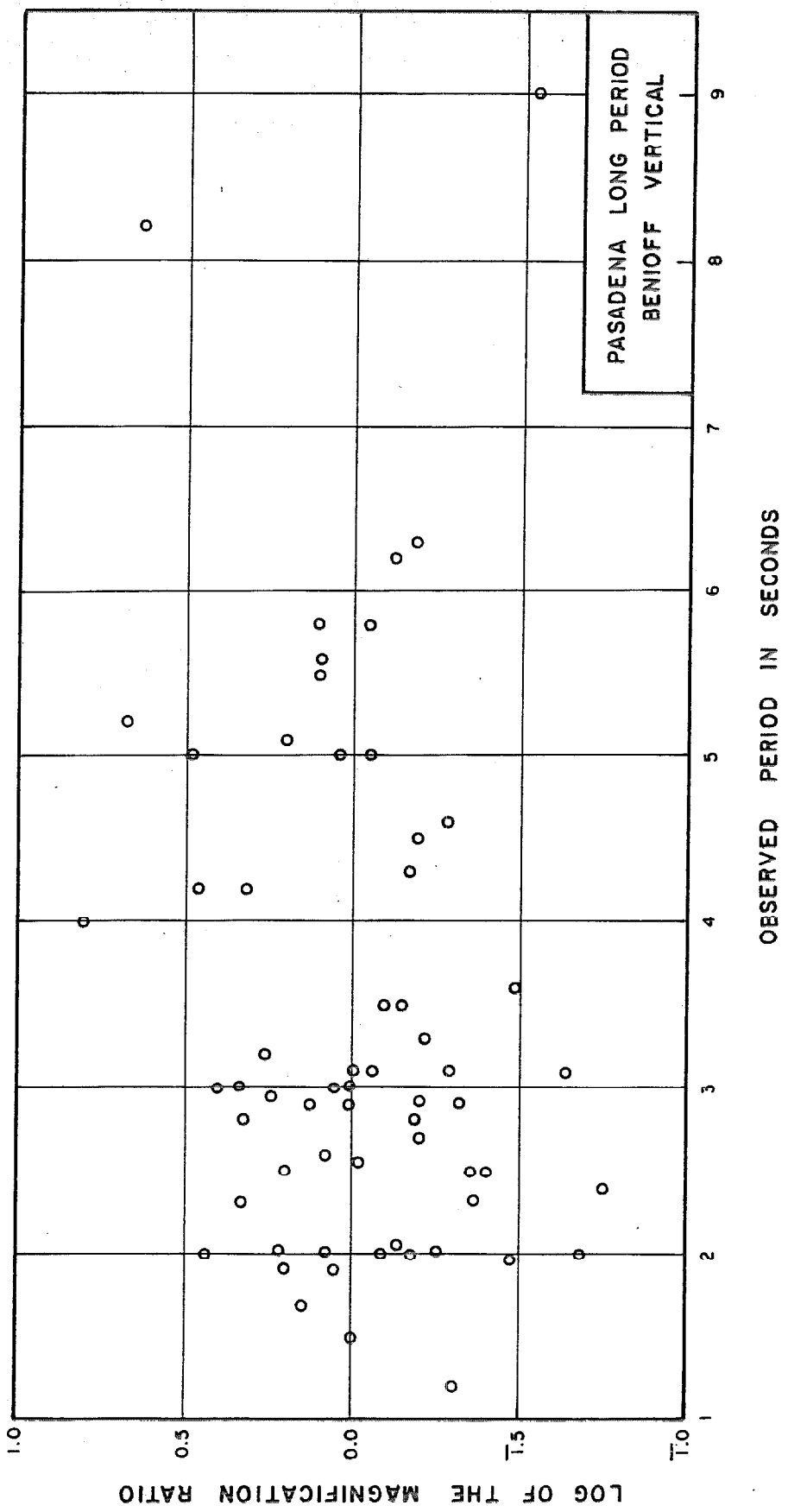
PASADENA LONG PERIOD
BENIOFF VERTICAL
OBSERVED PERIOD IN SECONDS
1
2
3
4
5
6
7
8
9
LOG OF THE MAGNIFICATION RATIO
1.0
0.5
0.0
1.5
2.0

Figure 11.

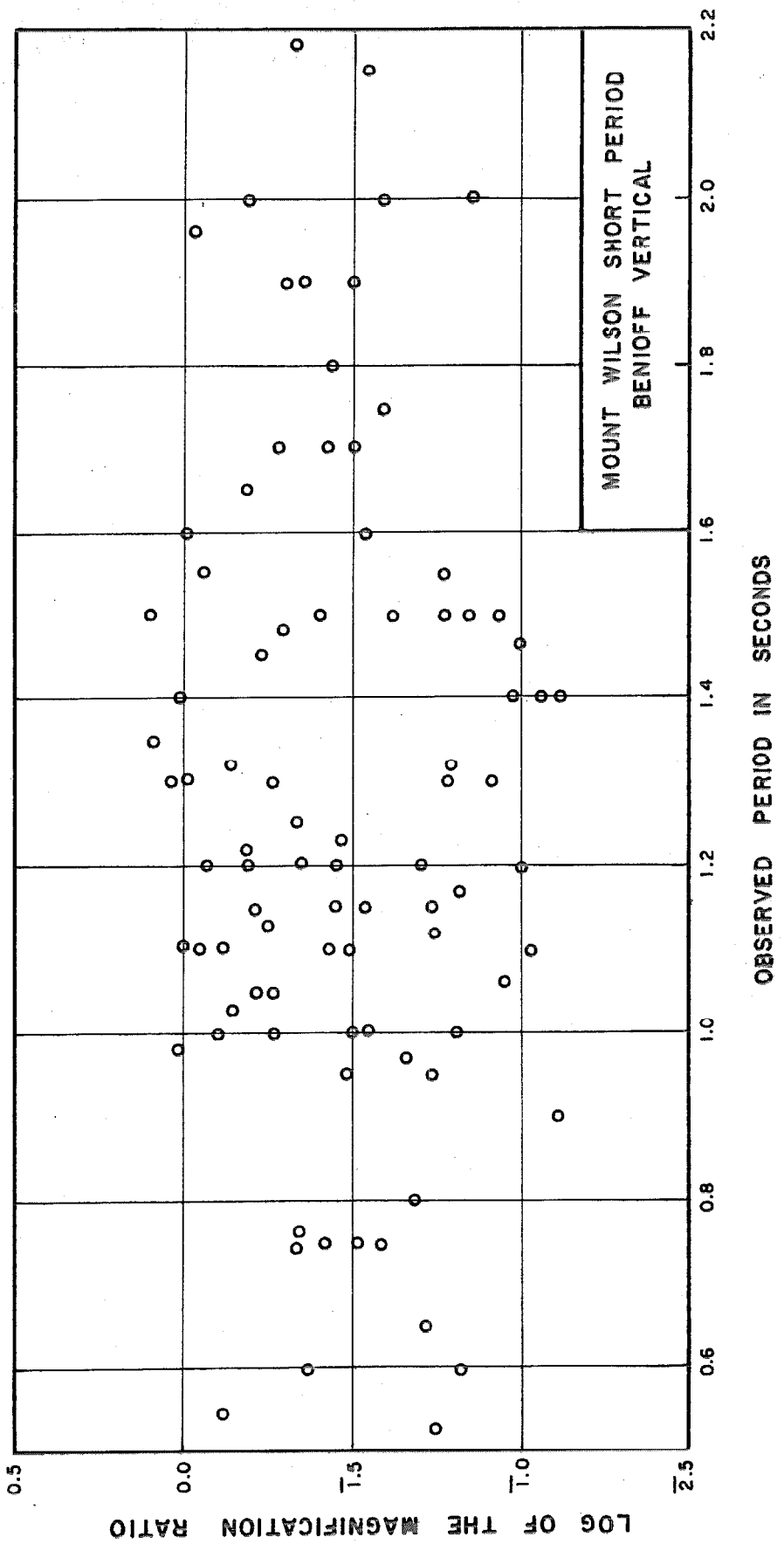
MOUNT WILSON SHORT PERIOD
BENIOFF VERTICAL
OBSERVED PERIOD IN SECONDS
0.6
0.8
1.0
1.2
1.4
1.6
1.8
2.0
2.2
LOG OF THE MAGNIFICATION RATIO
0.5
0.0
1.5
1.0
2.5

Figure 12.

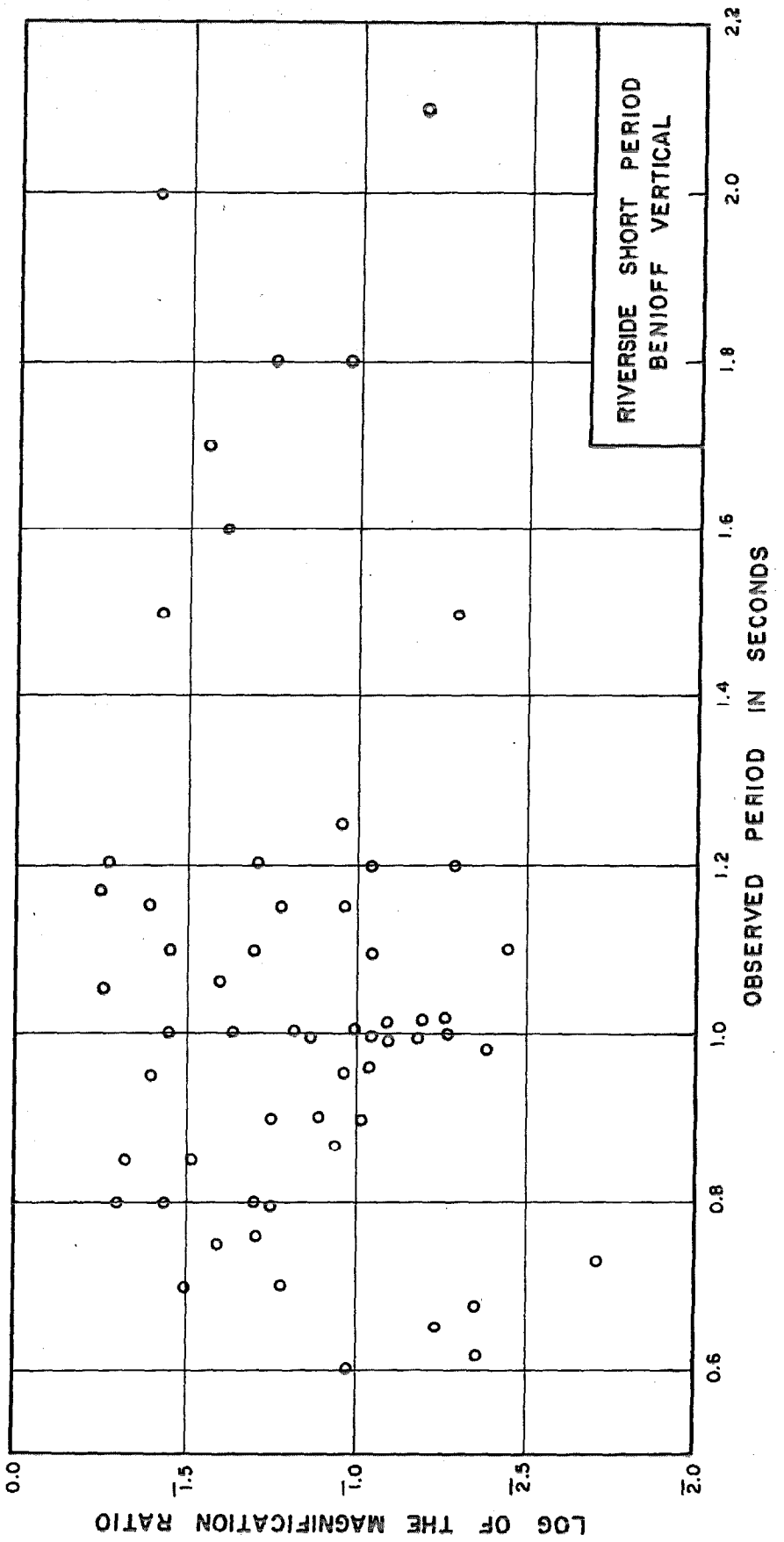
RIVERSIDE SHORT PERIOD
BENIOFF VERTICAL
OBSERVED PERIOD IN SECONDS
0.6
0.8
1.0
1.2
1.4
1.6
1.8
2.0
2.2
LOG OF THE MAGNIFICATION RATIO
0.0
1.5
1.0
2.5
2.0

Figure 13.

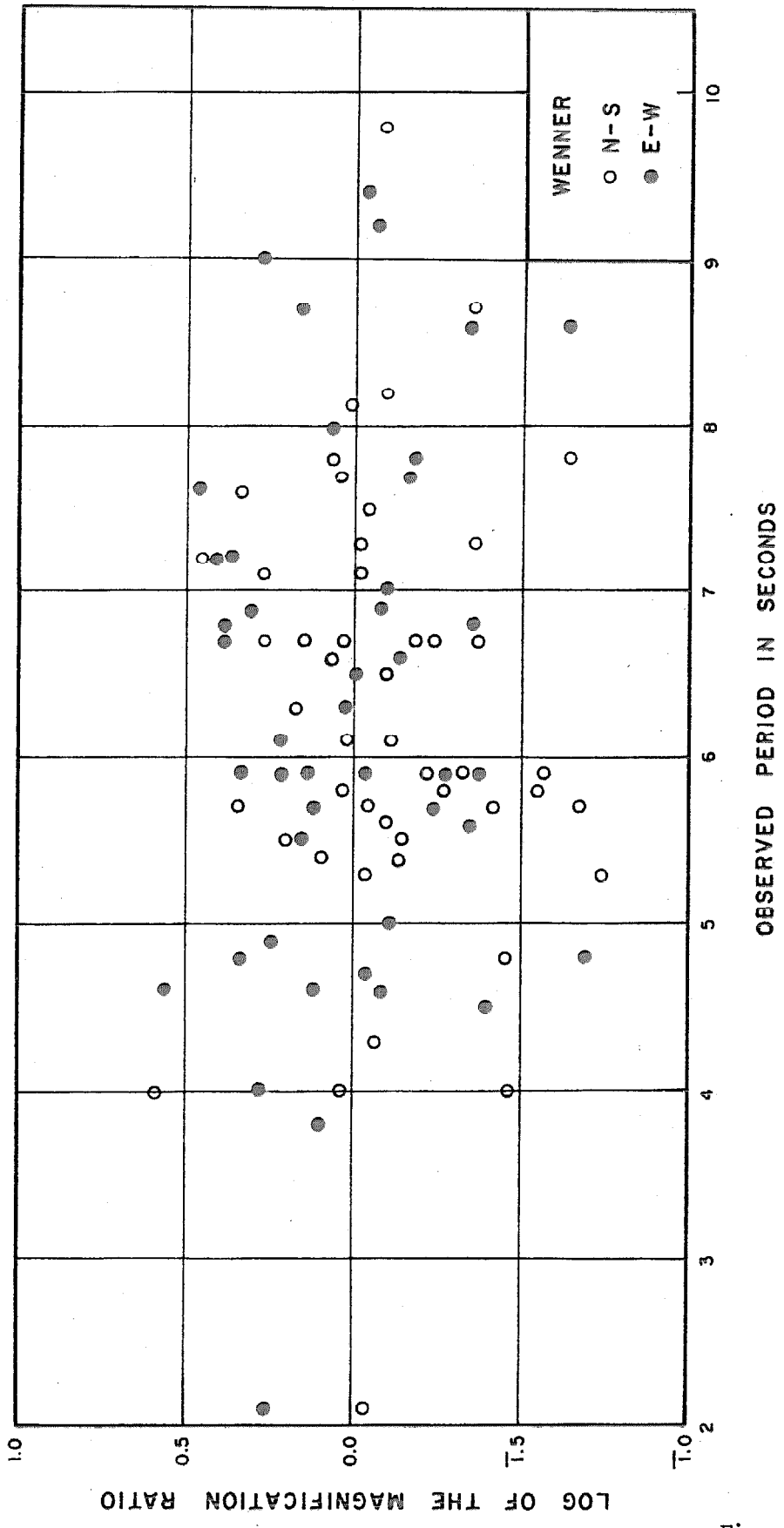
WENNER
N-S
E-W
1.0
0.5
0.0
-1.5
-1.0
2
3
4
5
6
7
8
9
10
LOG OF THE MAGNIFICATION RATIO
OBSERVED PERIOD IN SECONDS

Figure 14.

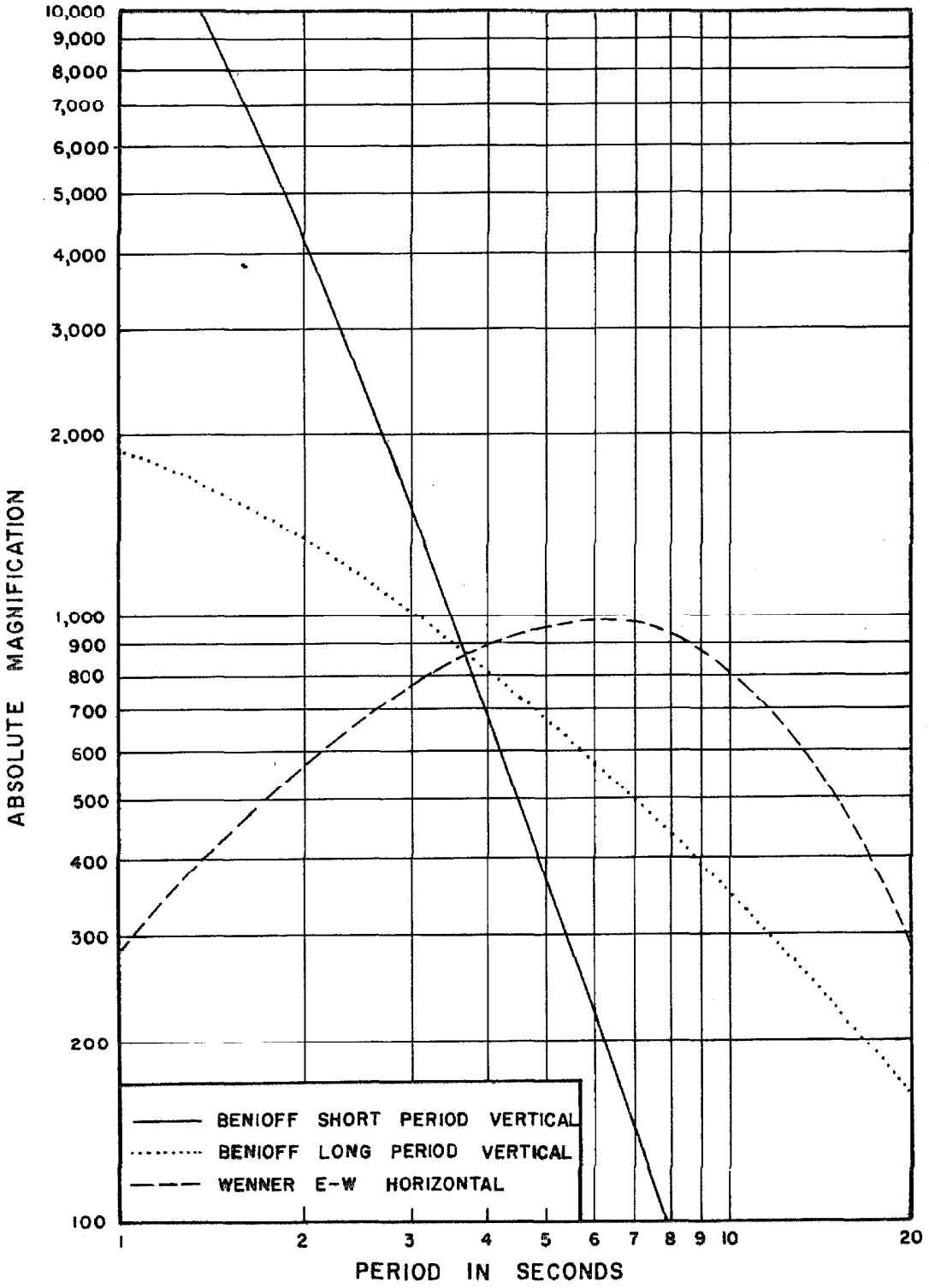
ABSOLUTE MAGNIFICATION
10,000
9,000
8,000
7,000
6,000
5,000
4,000
3,000
2,000
1,000
900
800
700
600
500
400
300
200
100
1
2
3
4
5
6
7
8
9
10
20
PERIOD IN SECONDS
BENIOFF SHORT PERIOD VERTICAL
BENIOFF LONG PERIOD VERTICAL
WENNER E-W HORIZONTAL

Figure 15.

SHOCKS SHOWN IN FIGURES 19 TO 30 .

(Minute marks are indicated in all photographs.)

Fig.	Date	Origin Time G.C.T.	Epicenter	Focal Depth	Magnitude	Recording Instrument	Station	Δ
	June 24, 1933	21:54:46	5½S, 104 3/4E	Normal	7.5	short period experimental vertical	Pasadena	131.2°
						long period experimental vertical		
	March 21, 1940	13:52:52	10S, 108E	Normal	6 3/4	short period Benioff vertical	Pasadena	131.5
	Feb. 28, 1934	14:21:42	5S, 150E	Normal	7.2	long period Wenner E-W horizontal	Huancayo	131.8
	March 21, 1943	20:35:43	5 3/4S, 152½E	Normal	7.3	long period Wenner E-W horizontal	Huancayo	129.5
	Sept. 27, 1937	08:55:10	9½S, 111E	Normal	7.2	short period Benioff vertical	Tucson	135.2
	May 8, 1946	05:20:22	0, 99½E	Normal	7.1	long period Benioff vertical	Pasadena	131.0
							Tucson	137.0

Continued next page

Continued

Fig.	Date	Origin Time G.C.T.	Epicenter	Focal Depth	Magnitude	Recording Instrument	Station	Δ
	Sept. 21, 1934	12:38:54	2N, 99E	100 km	6¼	short period Benioff vertical	Pasadena	129.9°
	Jan. 2, 1936	22:34:30	0, 99½E	60 km	7.0	short period Benioff vertical	Pasadena	131.0
						long period Benioff vertical		
	Aug. 18, 1938	09:30:04	4S, 103E	100 km	6.9	short period Benioff vertical	Pasadena	131.4
	March 9, 1943	09:48:55	60S, 27W	Normal	7.3	short period Benioff vertical	Pasadena	119.4
	Feb. 9, 1948	14:54:22	0, 122½E	160 km	7.2	short period Benioff vertical	Pasadena	114.0
	March 22, 1944	00:43:18	8½S, 123½E	220 km	7.5	short period Benioff vertical	Pasadena	118.1
							Tucson	124.5

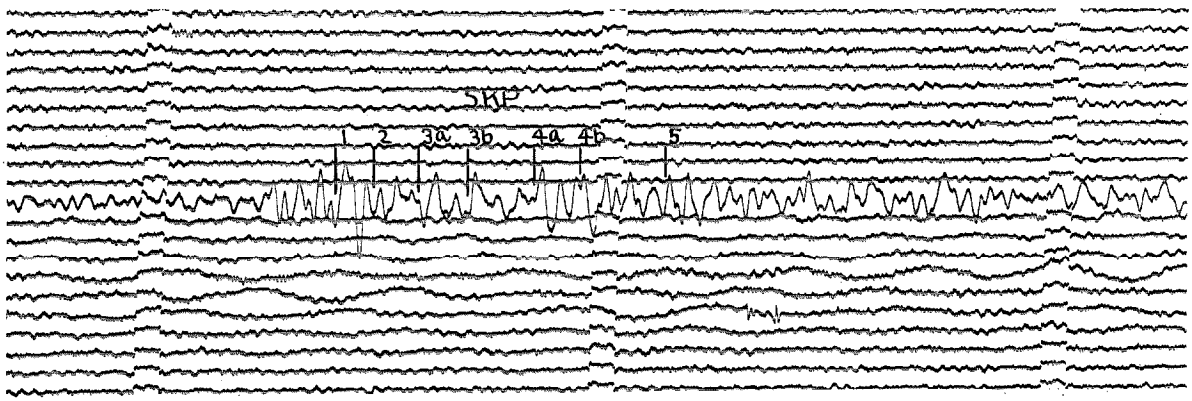

Figure 19a.

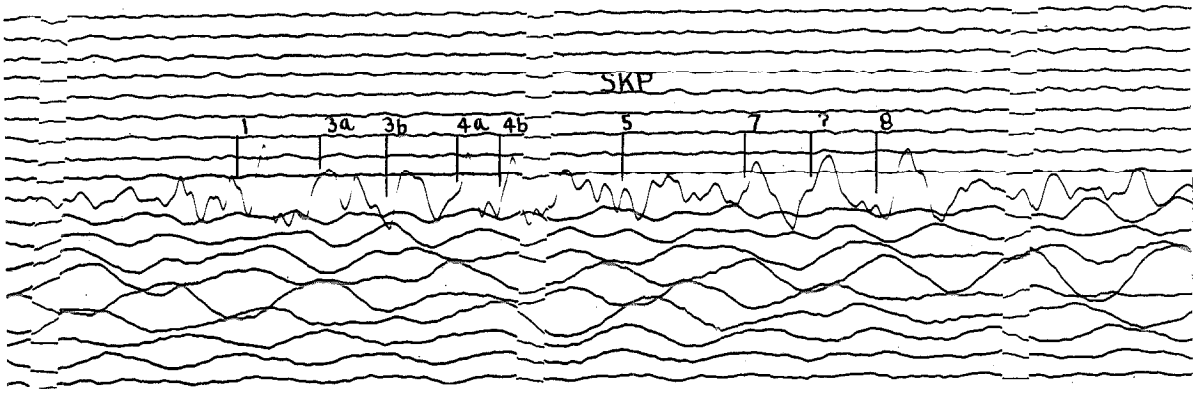

Figure 19b.

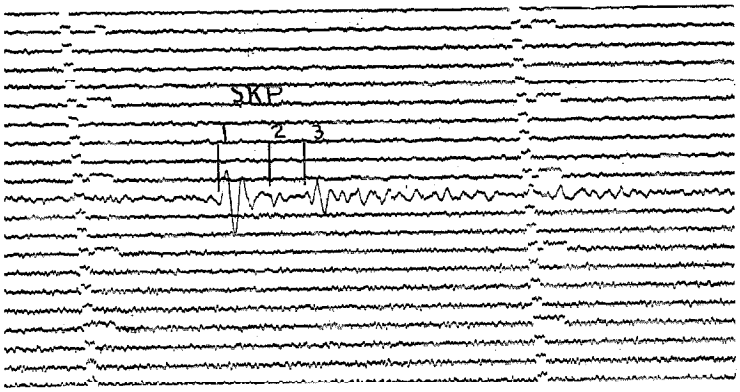

Figure 20.

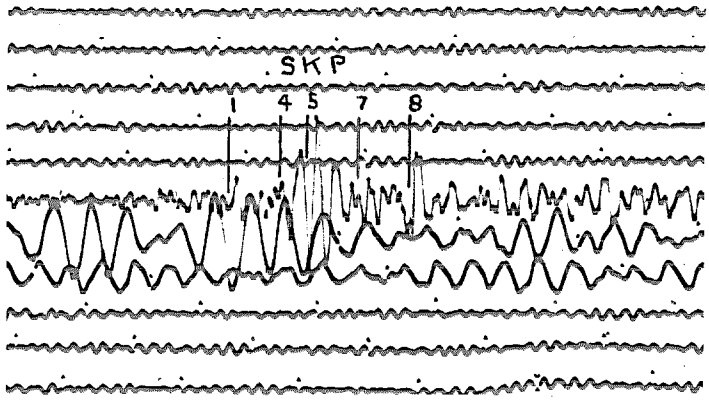

Figure 21.

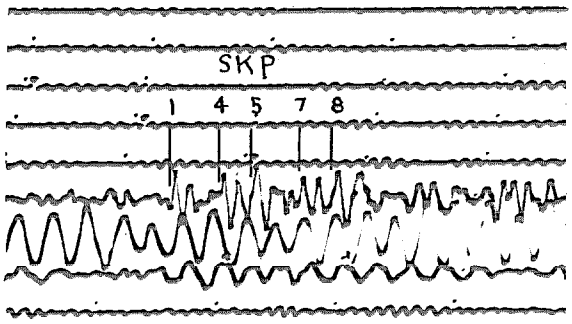

Figure 22.

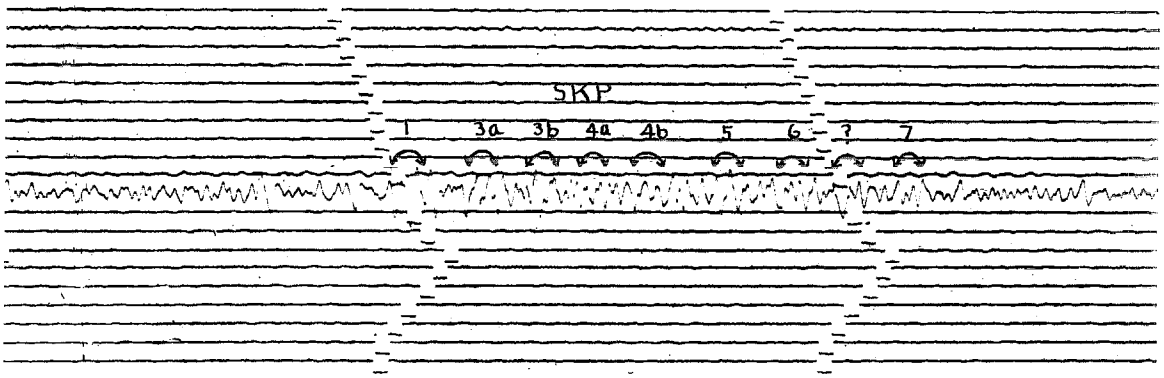

Figure 23.

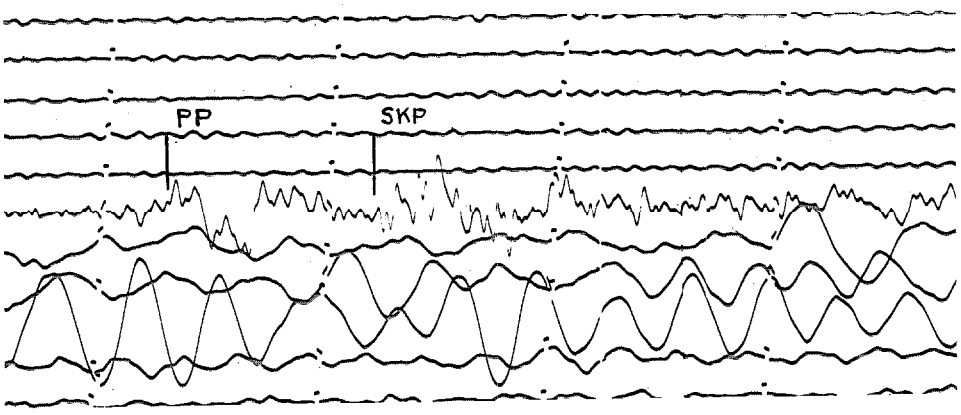

Figure 24a.

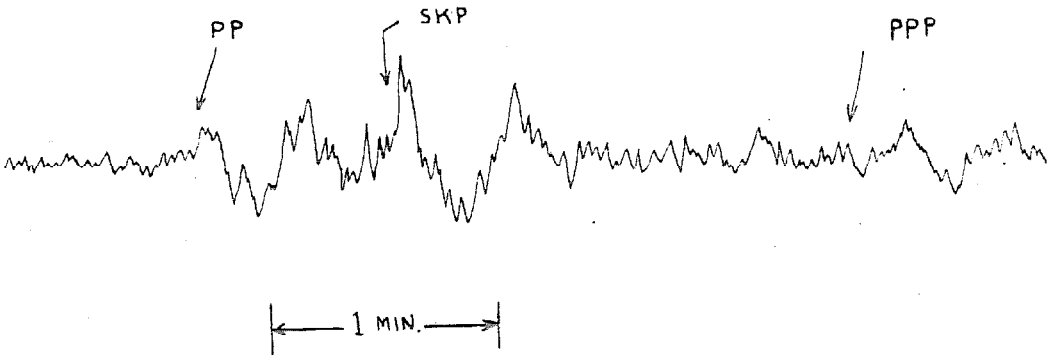

Figure 24b.

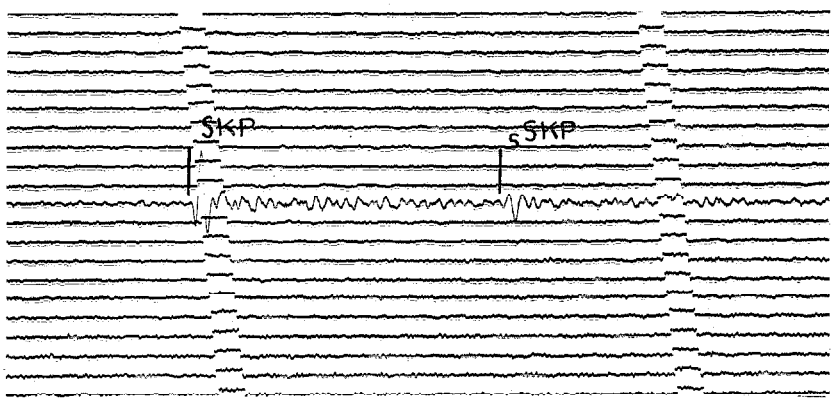

Figure 25.

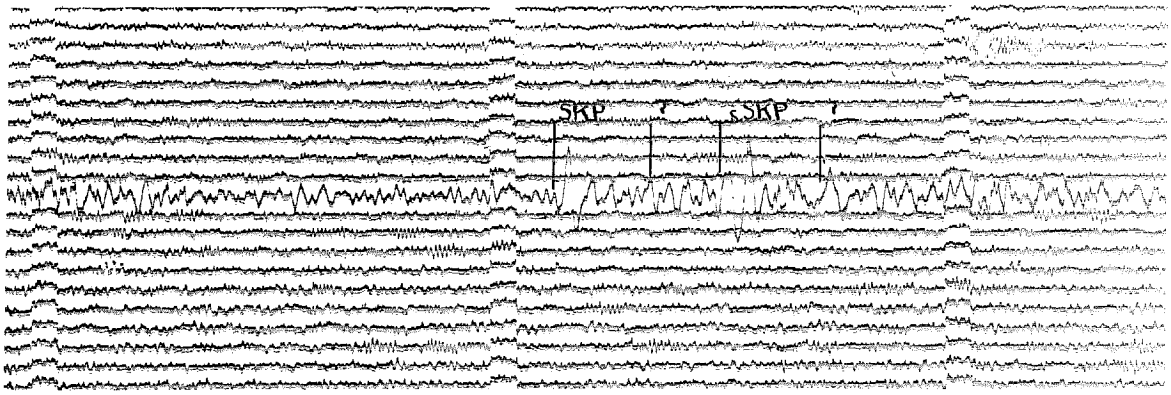

Figure 26a.

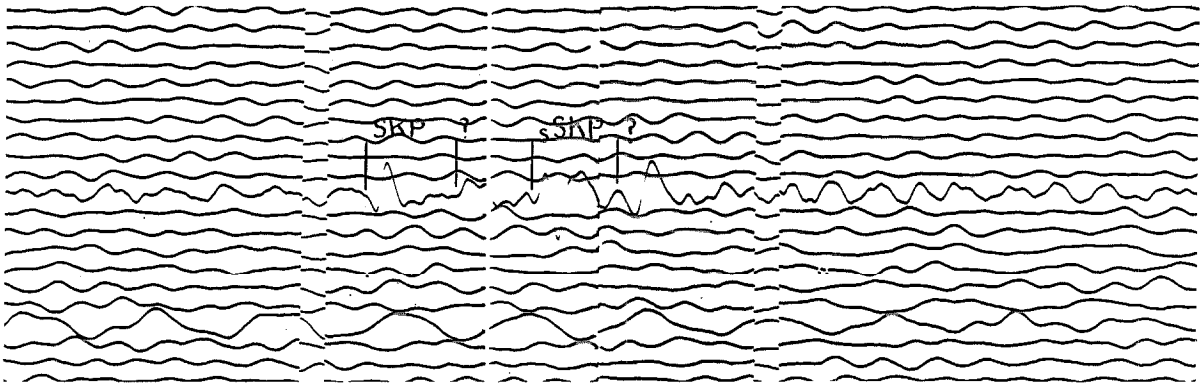

Figure 26b.

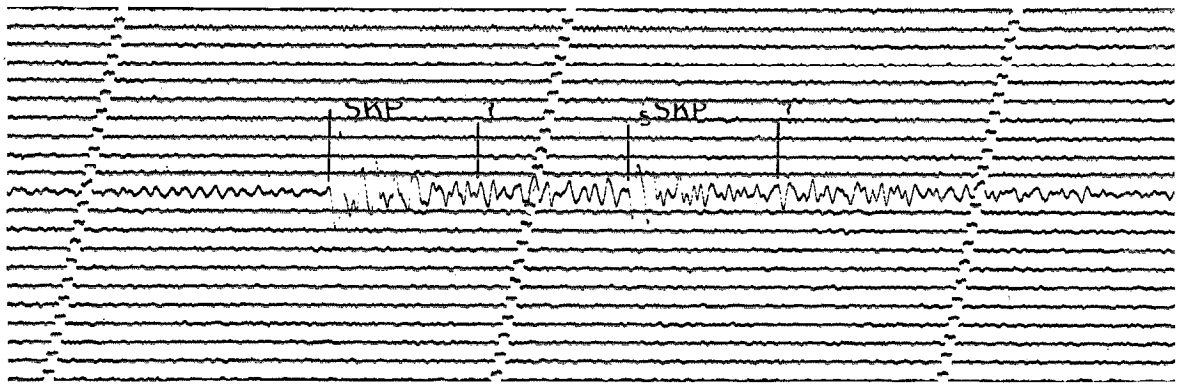

Figure 27.

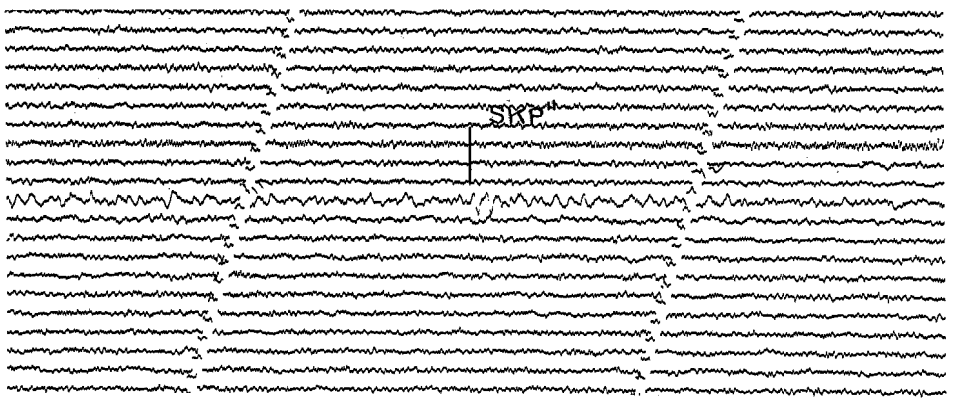

Figure 28.

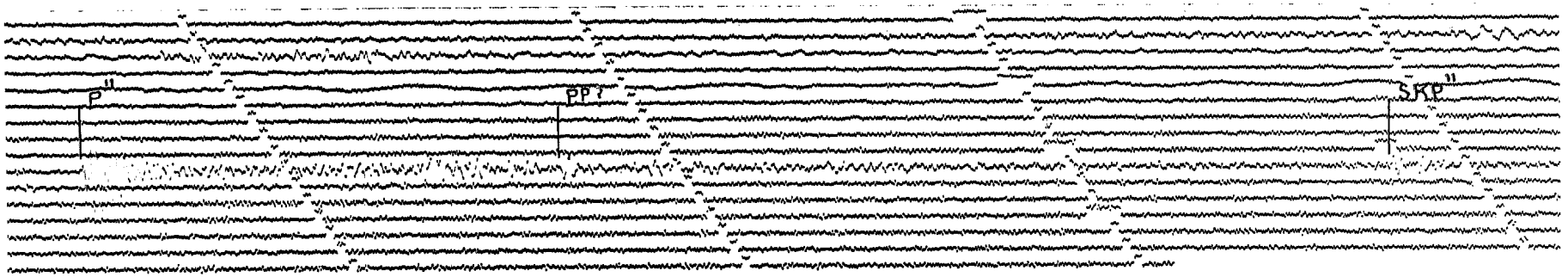

Figure 29.

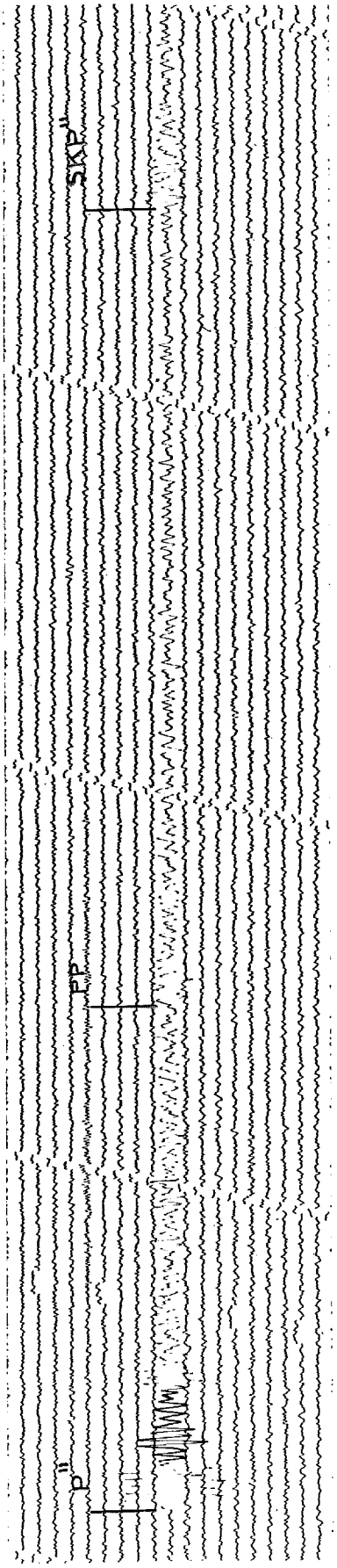

Figure 30a.

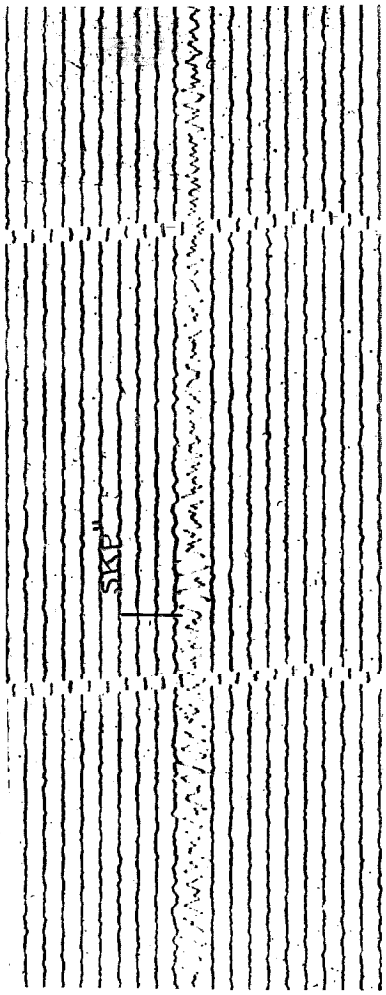

Figure 30b.

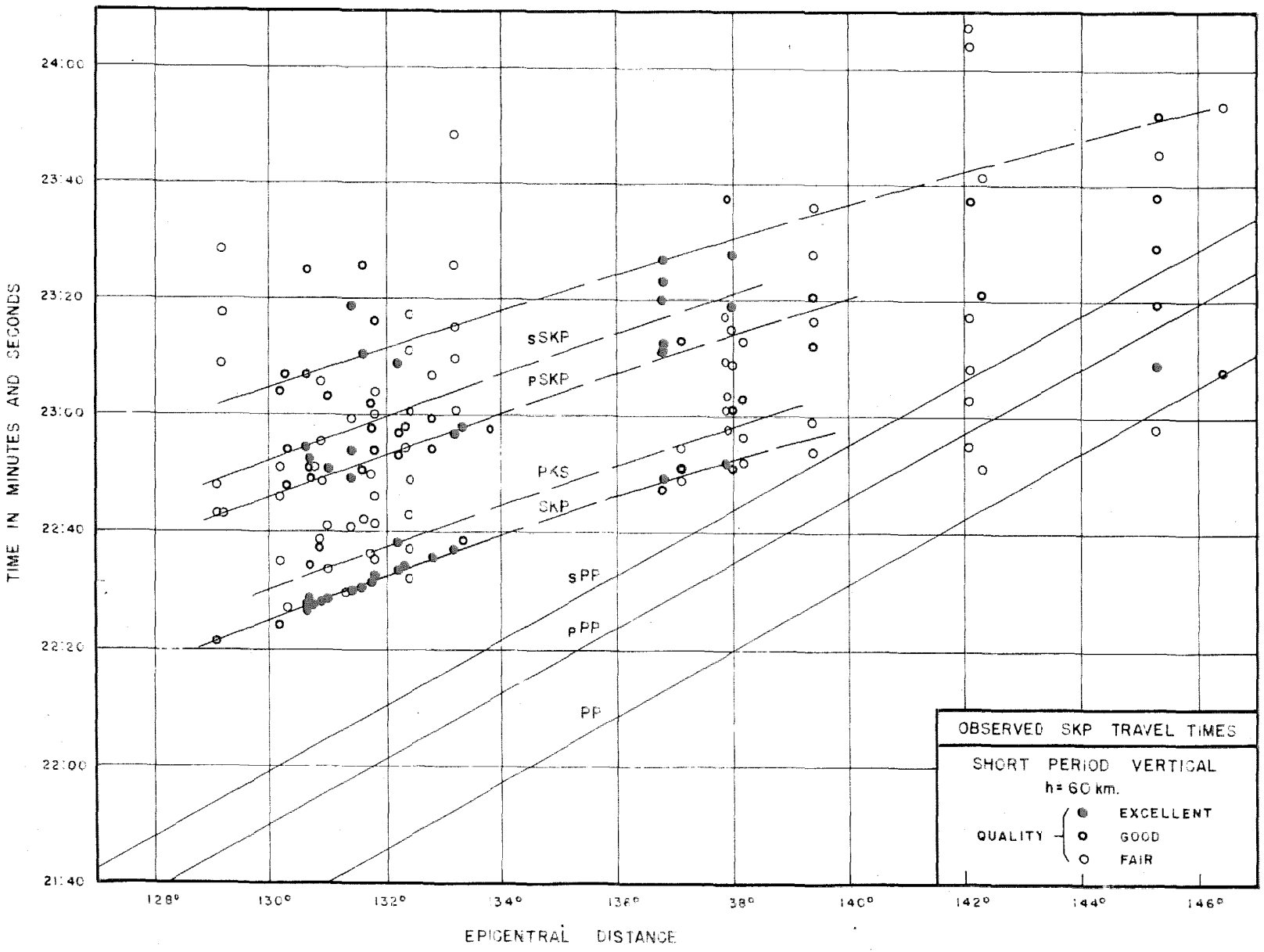
TIME IN MINUTES AND SECONDS
24:00
23:40
23:20
23:00
22:40
22:20
22:00
21:40
128°
130°
132°
134°
136°
138°
140°
142°
144°
146°
EPICENTRAL DISTANCE
sSKP
pSKP
PKS
SKP
sPP
pPP
PP
OBSERVED SKP TRAVEL TIMES
SHORT PERIOD VERTICAL
h = 60 km.
QUALITY
EXCELLENT
GOOD
FAIR

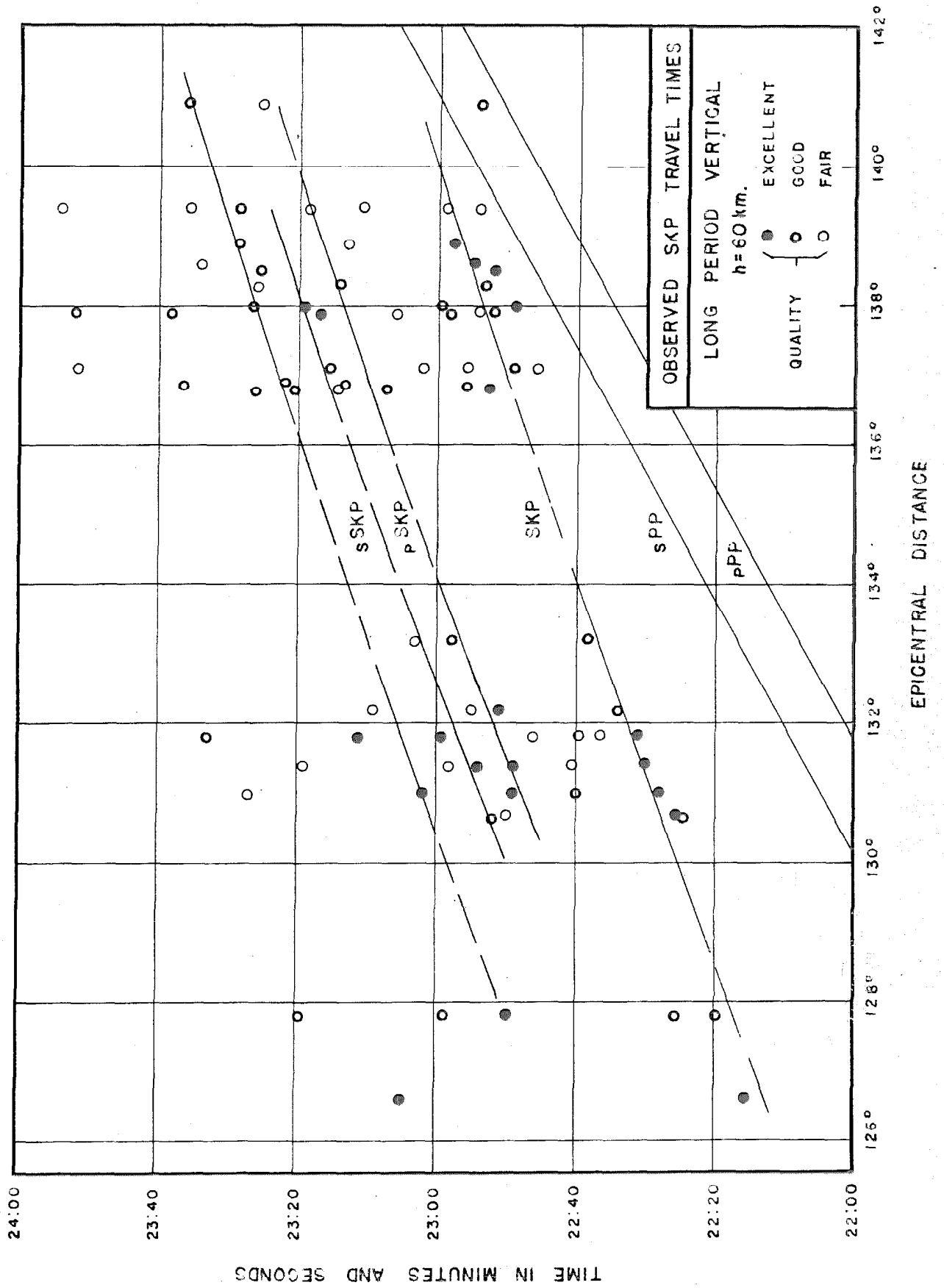
OBSERVED SKP TRAVEL TIMES
LONG PERIOD VERTICAL
h=60 km.
QUALITY
EXCELLENT
GOOD
FAIR
sSKP
pSKP
SKP
sPP
pPP
126°
128°
130°
132°
134°
136°
138°
140°
142°
EPICENTRAL DISTANCE
24:00
23:40
23:20
23:00
22:40
22:20
22:00
TIME IN MINUTES AND SECONDS

Figure 32.

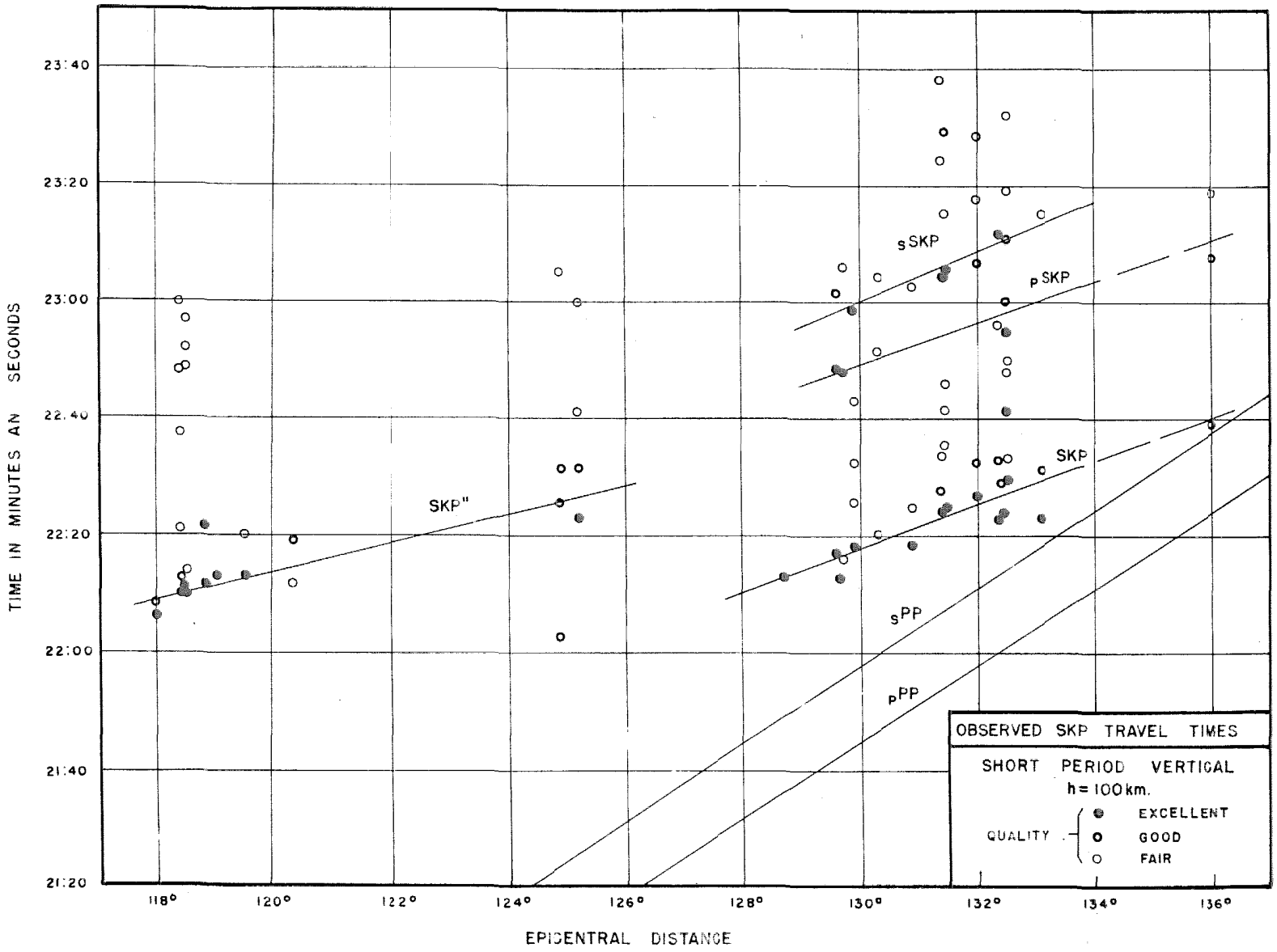
TIME IN MINUTES AN SECONDS
23:40
23:20
23:00
22:40
22:20
22:00
21:40
21:20
118°
120°
122°
124°
126°
128°
130°
132°
134°
136°
EPICENTRAL DISTANCE
SKP"
sSKP
pSKP
SKP
sPP
pPP
OBSERVED SKP TRAVEL TIMES
SHORT PERIOD VERTICAL
h = 100 km.
QUALITY
EXCELLENT
GOOD
FAIR

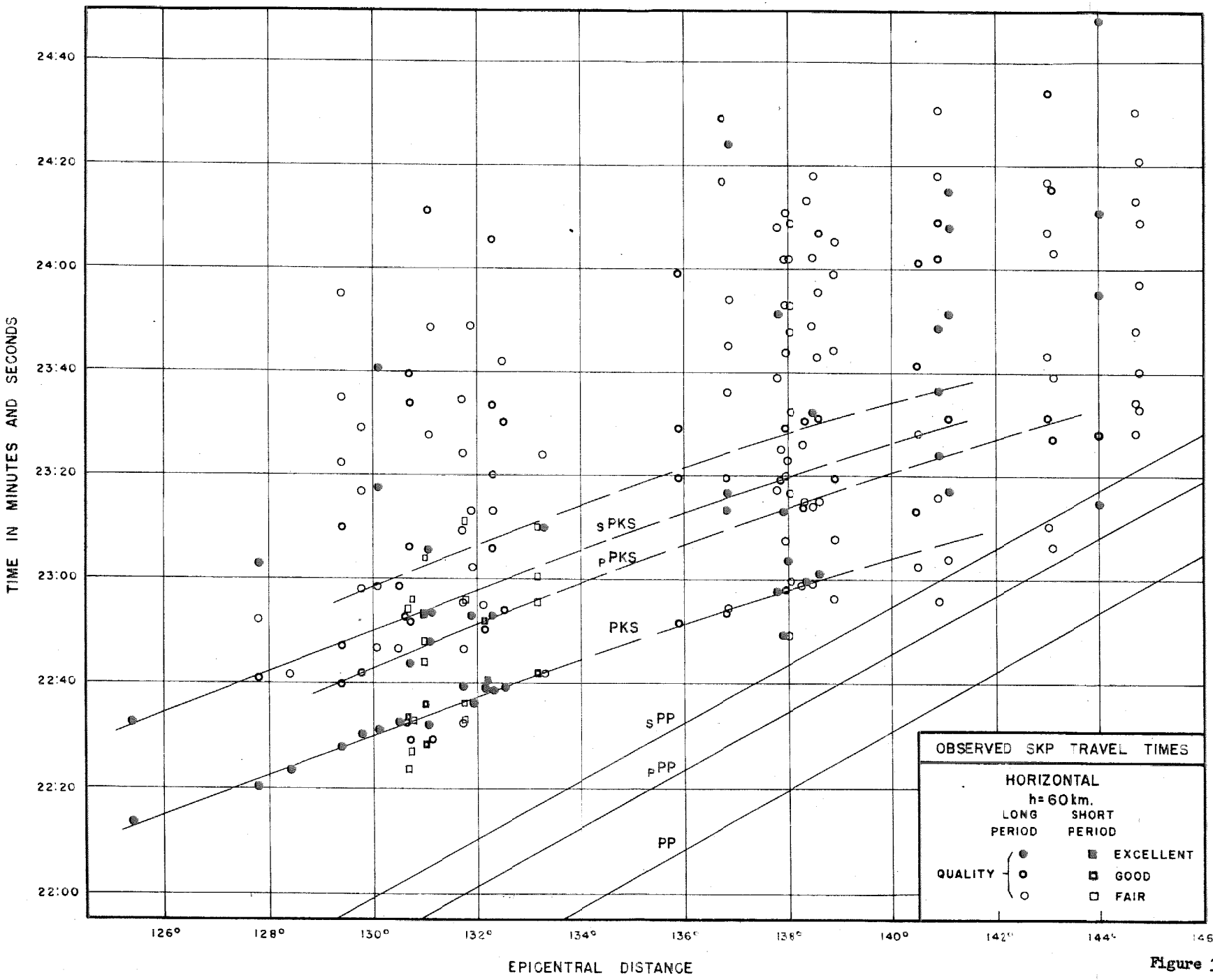
TIME IN MINUTES AND SECONDS
24:40
24:20
24:00
23:40
23:20
23:00
22:40
22:20
22:00
126°
128°
130°
132°
134°
136°
138°
140°
142°
144°
146°
EPICENTRAL DISTANCE
sPKS
pPKS
PKS
sPP
pPP
PP
OBSERVED SKP TRAVEL TIMES
HORIZONTAL
h=60km.
LONG PERIOD
SHORT PERIOD
QUALITY
EXCELLENT
GOOD
FAIR

Figure 33.

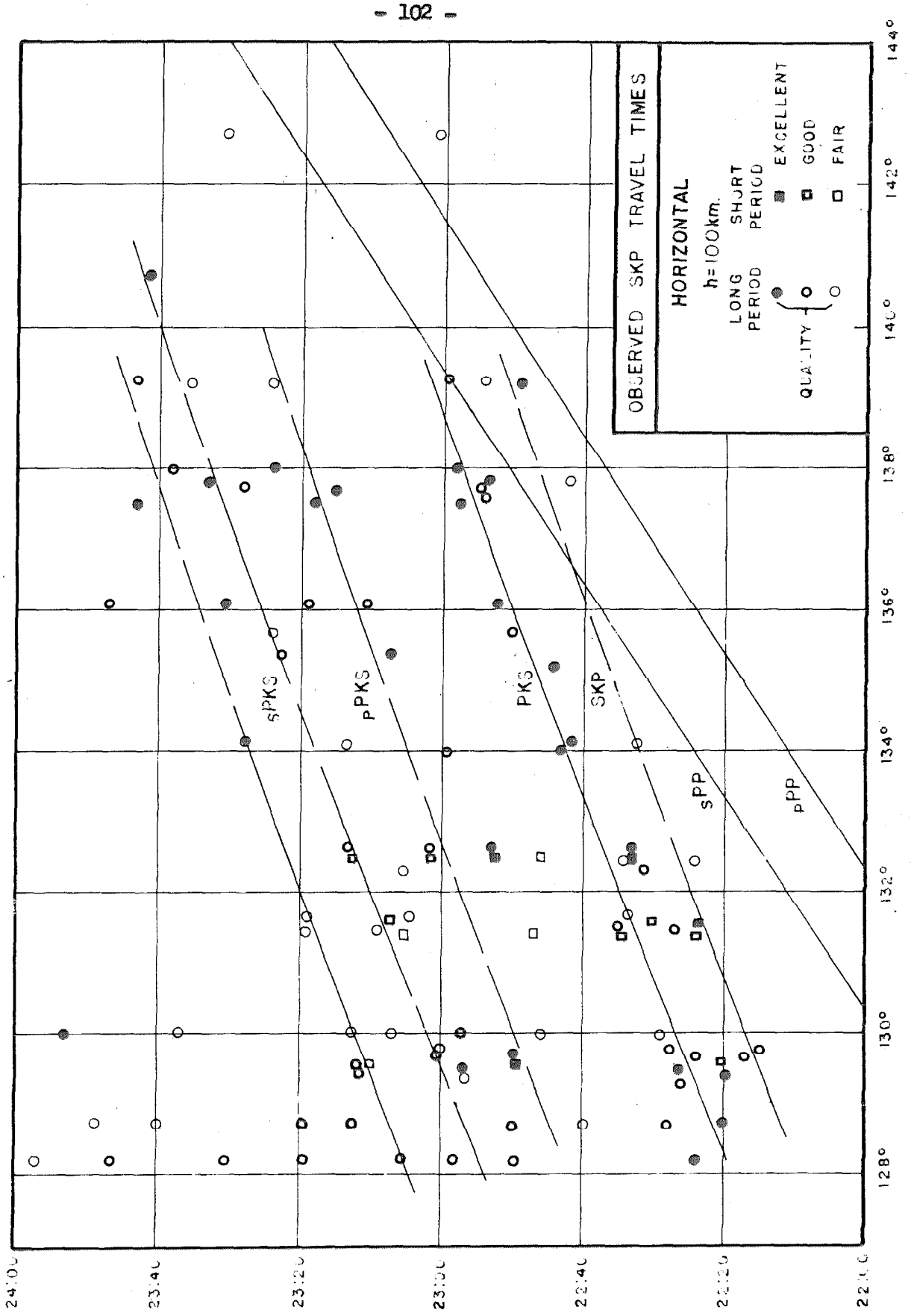
OBSERVED SKP TRAVEL TIMES
HORIZONTAL
h=100km.
LONG PERIOD
SHORT PERIOD
QUALITY
EXCELLENT
GOOD
FAIR
sPKS
pPKS
PKS
SKP
sPP
pPP
128°
130°
132°
134°
136°
138°
140°
142°
144°
EPICENTRAL DISTANCE
TIME IN MINUTES AND SECONDS

Figure 35.

EXPLANATION OF SYMBOLS USED IN FIGURES 36 TO 53 .

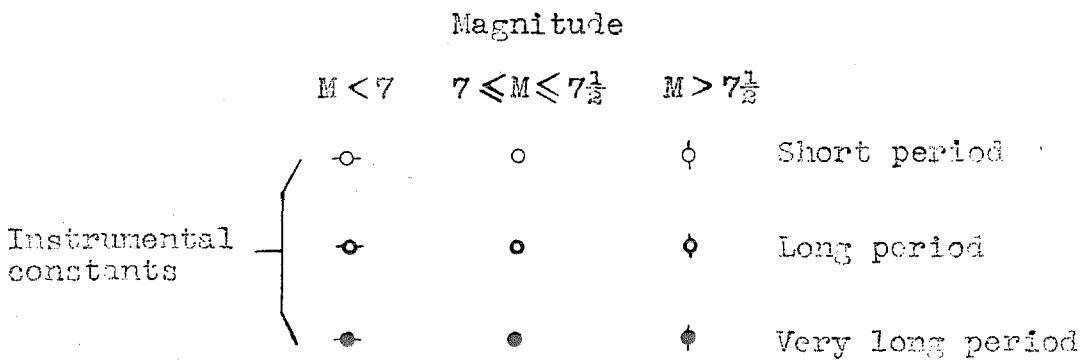

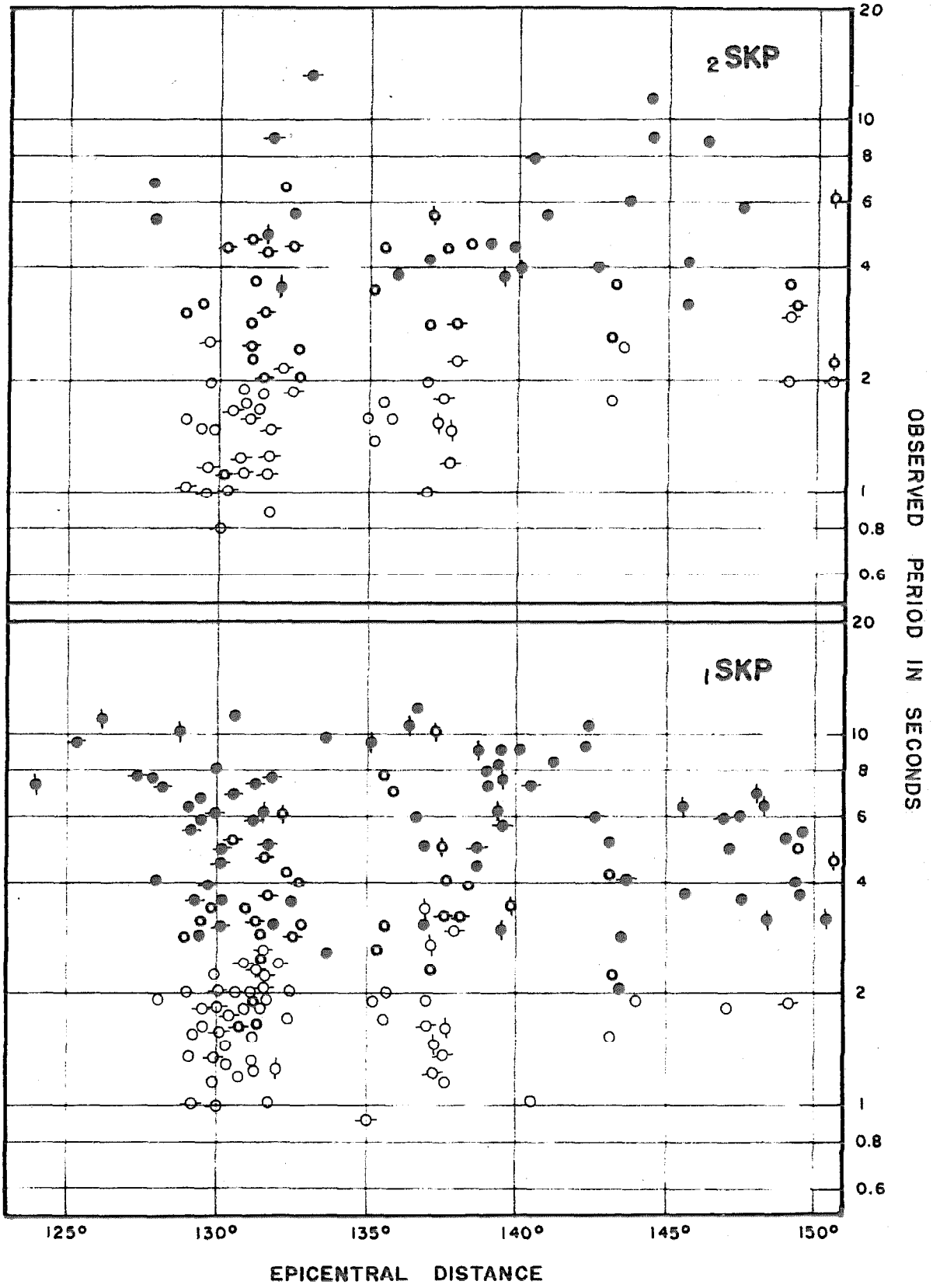
2 SKP
1 SKP
20
10
8
6
4
2
1
0.8
0.6
125°
130°
135°
140°
145°
150°
EPICENTRAL DISTANCE
OBSERVED PERIOD IN SECONDS

Figure 36.

h = N

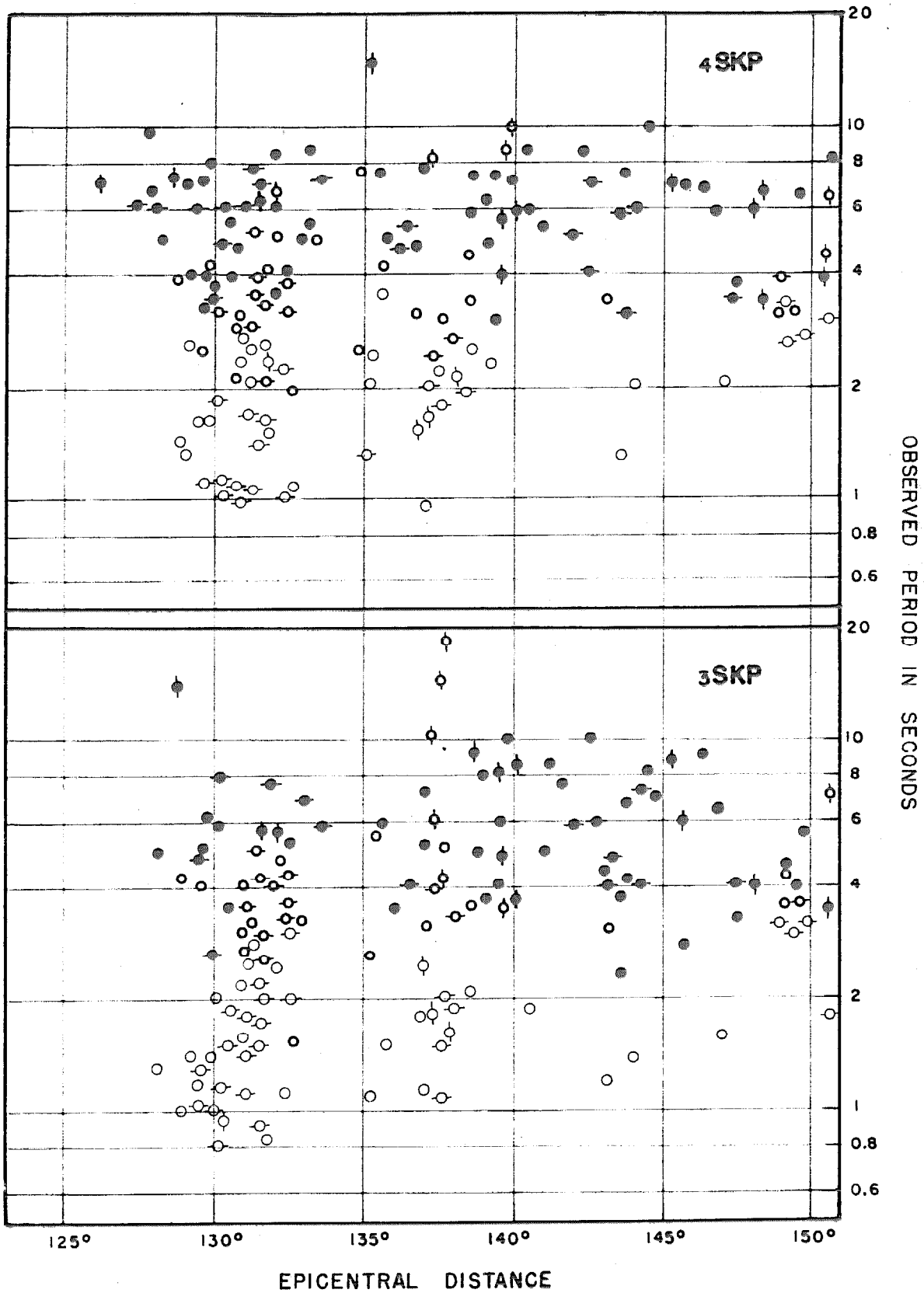
4SKP
3SKP
20
10
8
6
4
2
1
0.8
0.6
125°
130°
135°
140°
145°
150°
EPICENTRAL DISTANCE
OBSERVED PERIOD IN SECONDS

Figure 37.

h=N

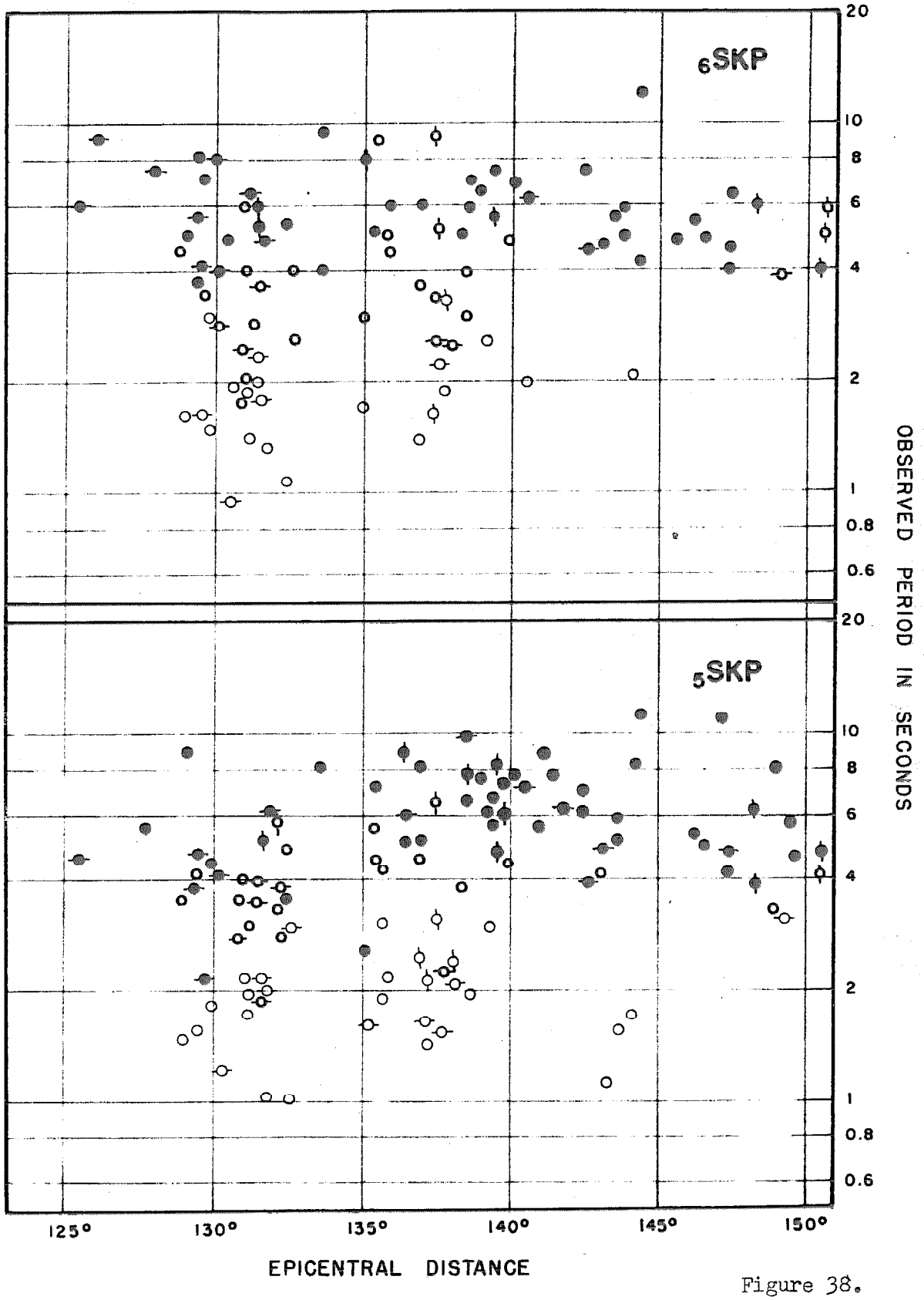
6SKP
5SKP
20
10
8
6
4
2
1
0.8
0.6
125°
130°
135°
140°
145°
150°
EPICENTRAL DISTANCE
OBSERVED PERIOD IN SECONDS
h=N

Figure 38.

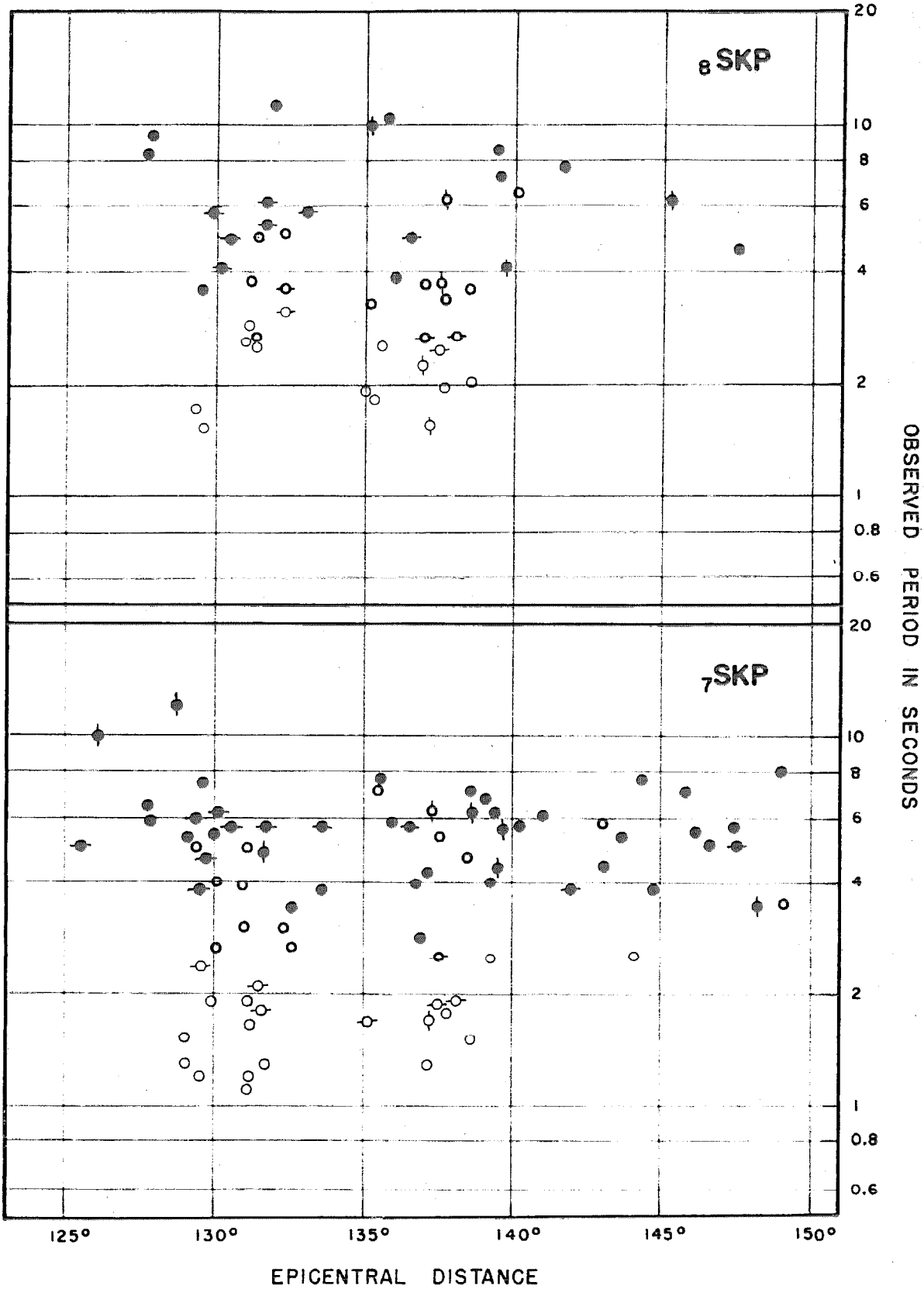
8SKP
7SKP
20
10
8
6
4
2
1
0.8
0.6
125°
130°
135°
140°
145°
150°
EPICENTRAL DISTANCE
OBSERVED PERIOD IN SECONDS
h=N

Figure 39.

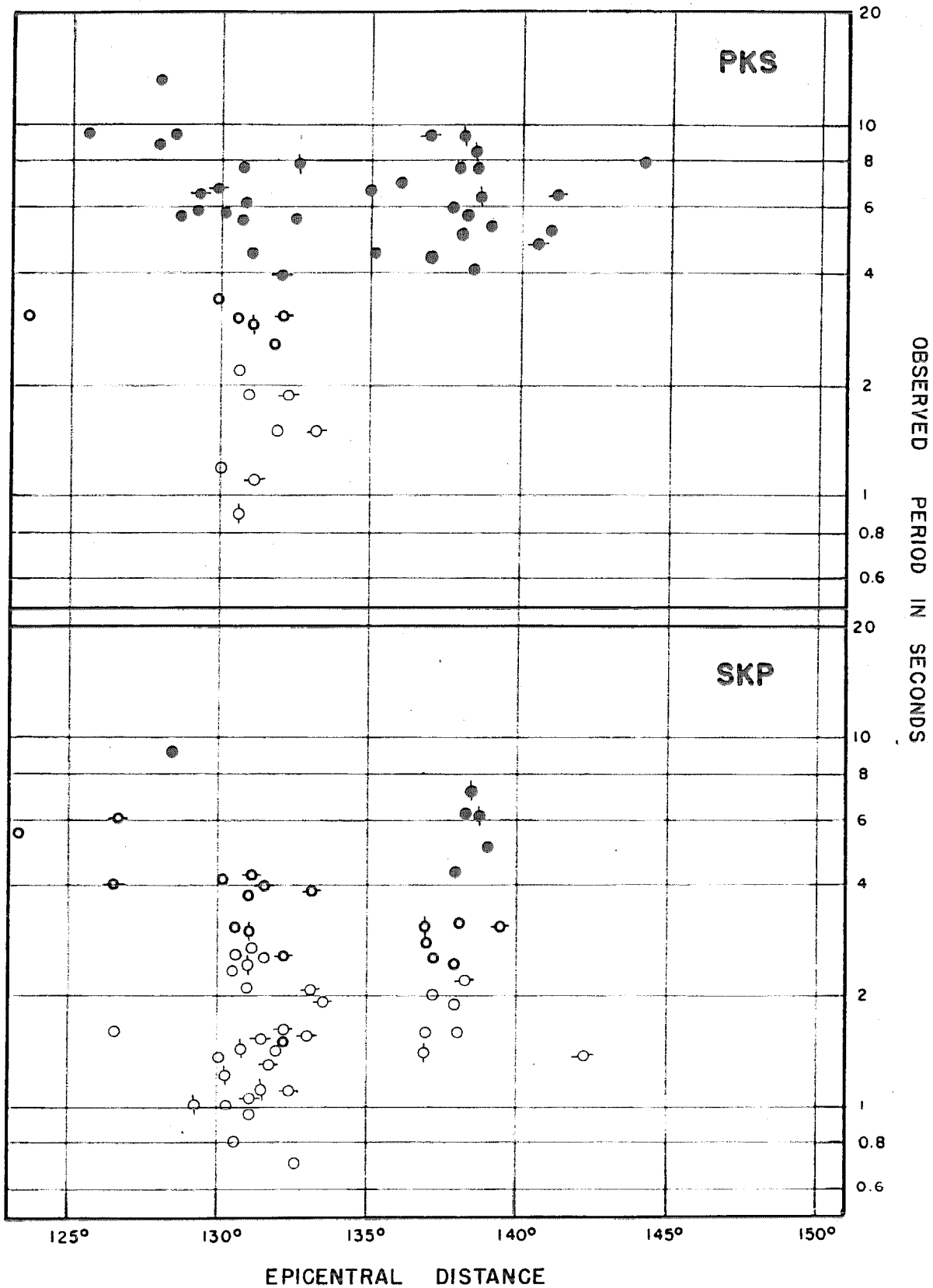
PKS
SKP
20
10
8
6
4
2
1
0.8
0.6
OBSERVED PERIOD IN SECONDS
125°
130°
135°
140°
145°
150°
EPICENTRAL DISTANCE
h = 60 km.

Figure 40.

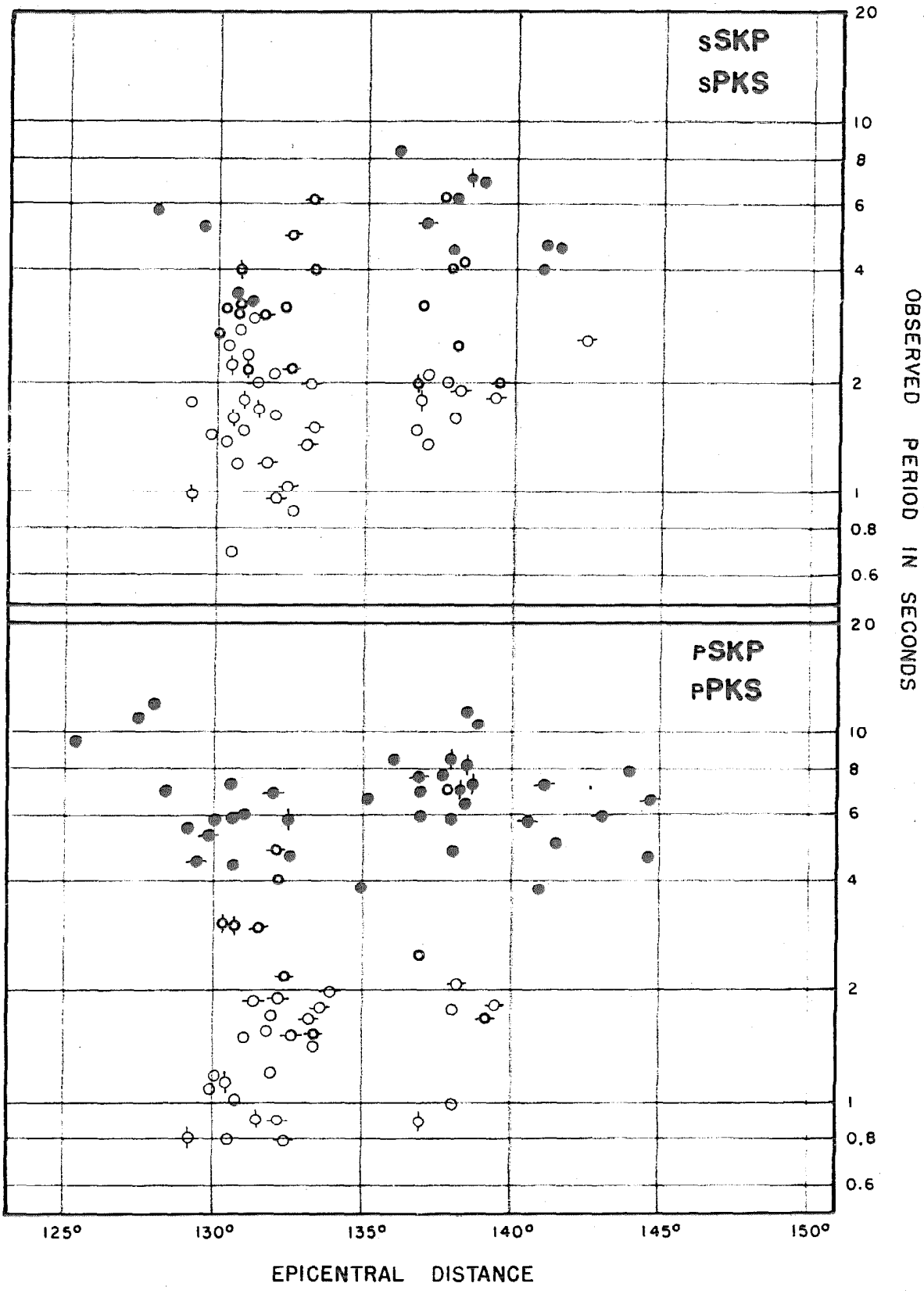
sSKP
sPKS
pSKP
pPKS
20
10
8
6
4
2
1
0.8
0.6
125°
130°
135°
140°
145°
150°
EPICENTRAL DISTANCE
OBSERVED PERIOD IN SECONDS
h = 60 km.

Figure 41.

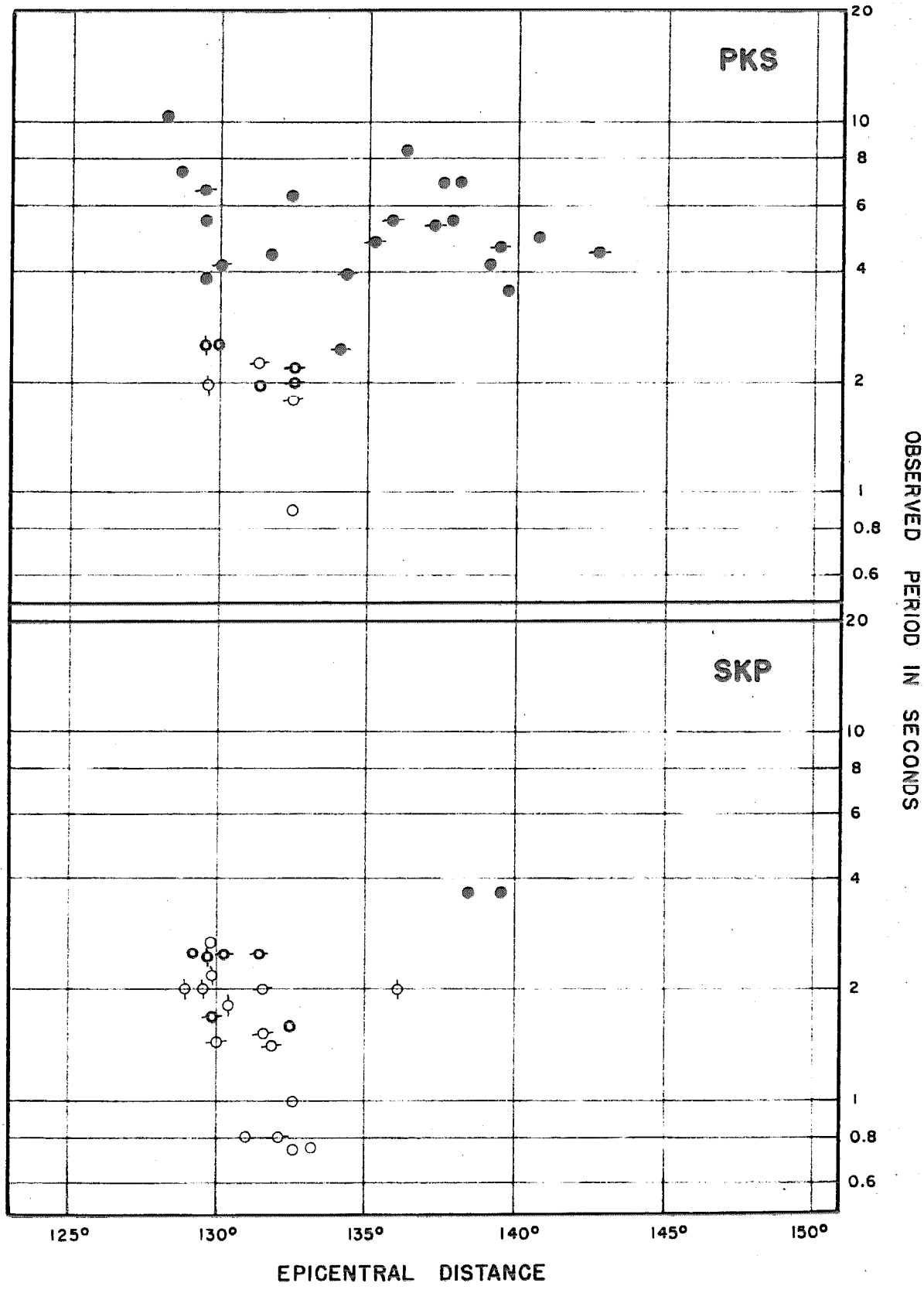
PKS
SKP
20
10
8
6
4
2
1
0.8
0.6
125°
130°
135°
140°
145°
150°
EPICENTRAL DISTANCE
OBSERVED PERIOD IN SECONDS
h = 100 Km.

Figure 42.

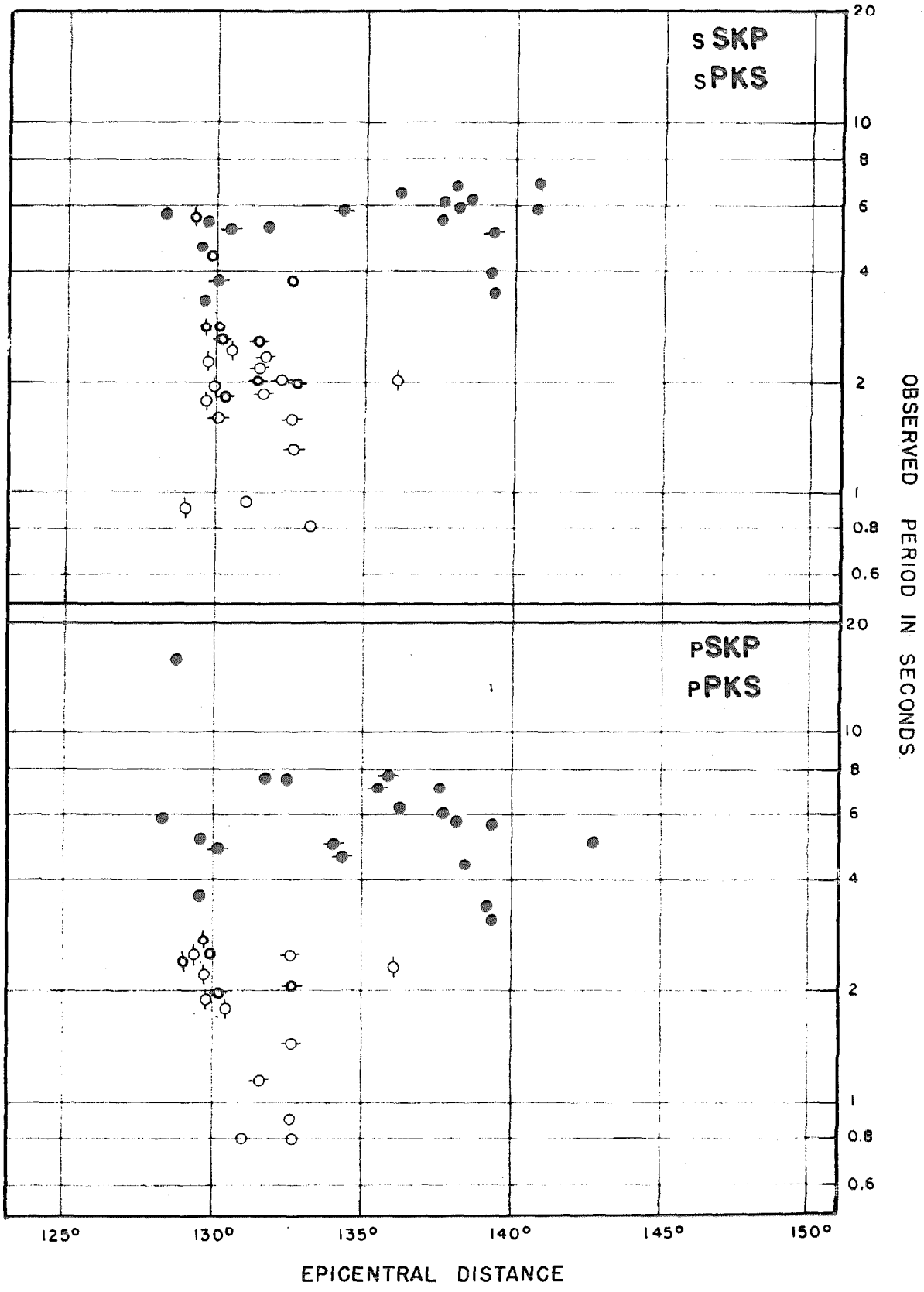
sSKP
sPKS
pSKP
pPKS
20
10
8
6
4
2
1
0.8
0.6
125°
130°
135°
140°
145°
150°
EPICENTRAL DISTANCE
OBSERVED PERIOD IN SECONDS
h=100 km.

Figure 43.

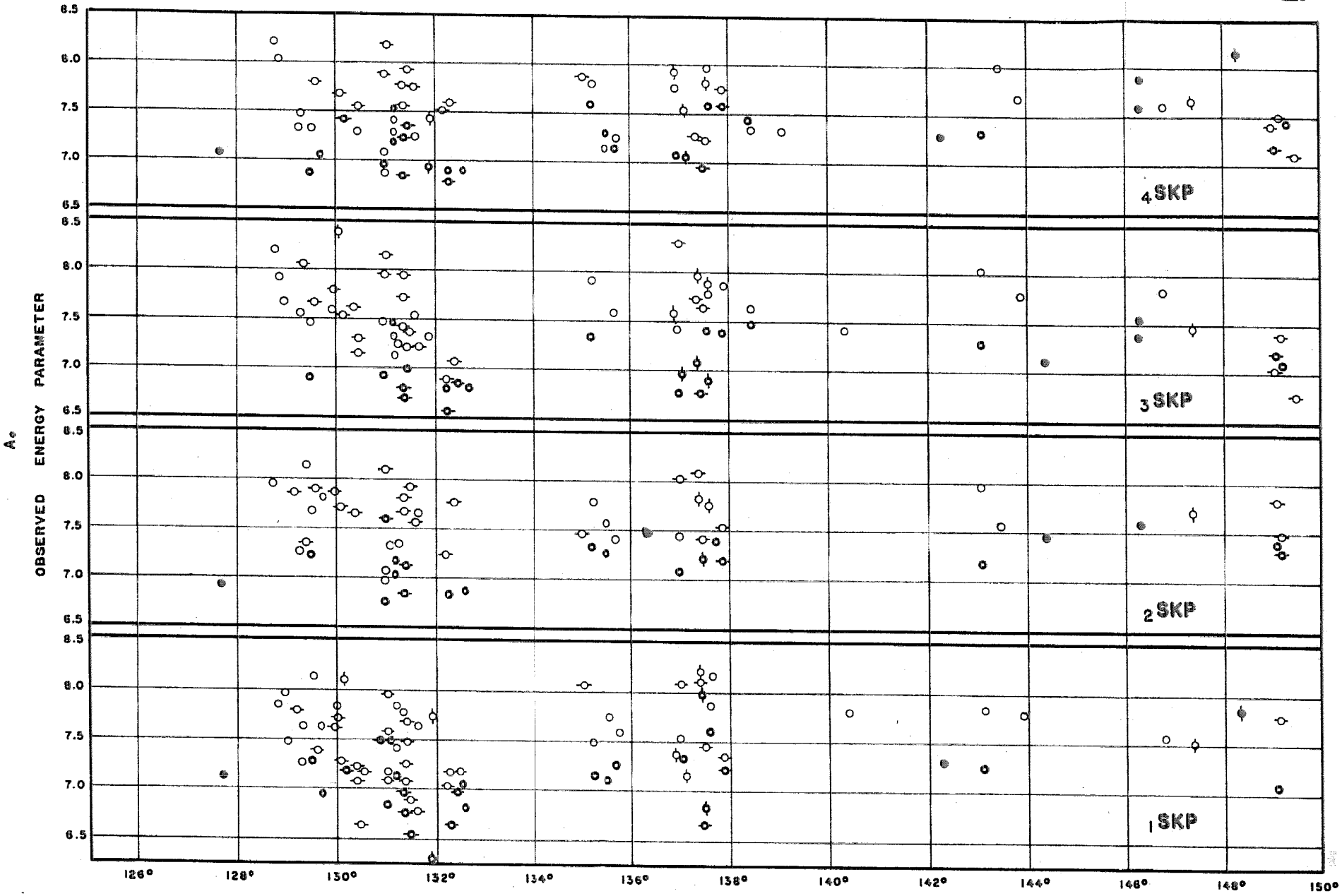
OBSERVED ENERGY PARAMETER
A_e
6.5
7.0
7.5
8.0
8.5
4 SKP
3 SKP
2 SKP
1 SKP
126°
128°
130°
132°
134°
136°
138°
140°
142°
144°
146°
148°
150°
EPICENTRAL DISTANCE
h = N
VERTICAL

Figure 44.

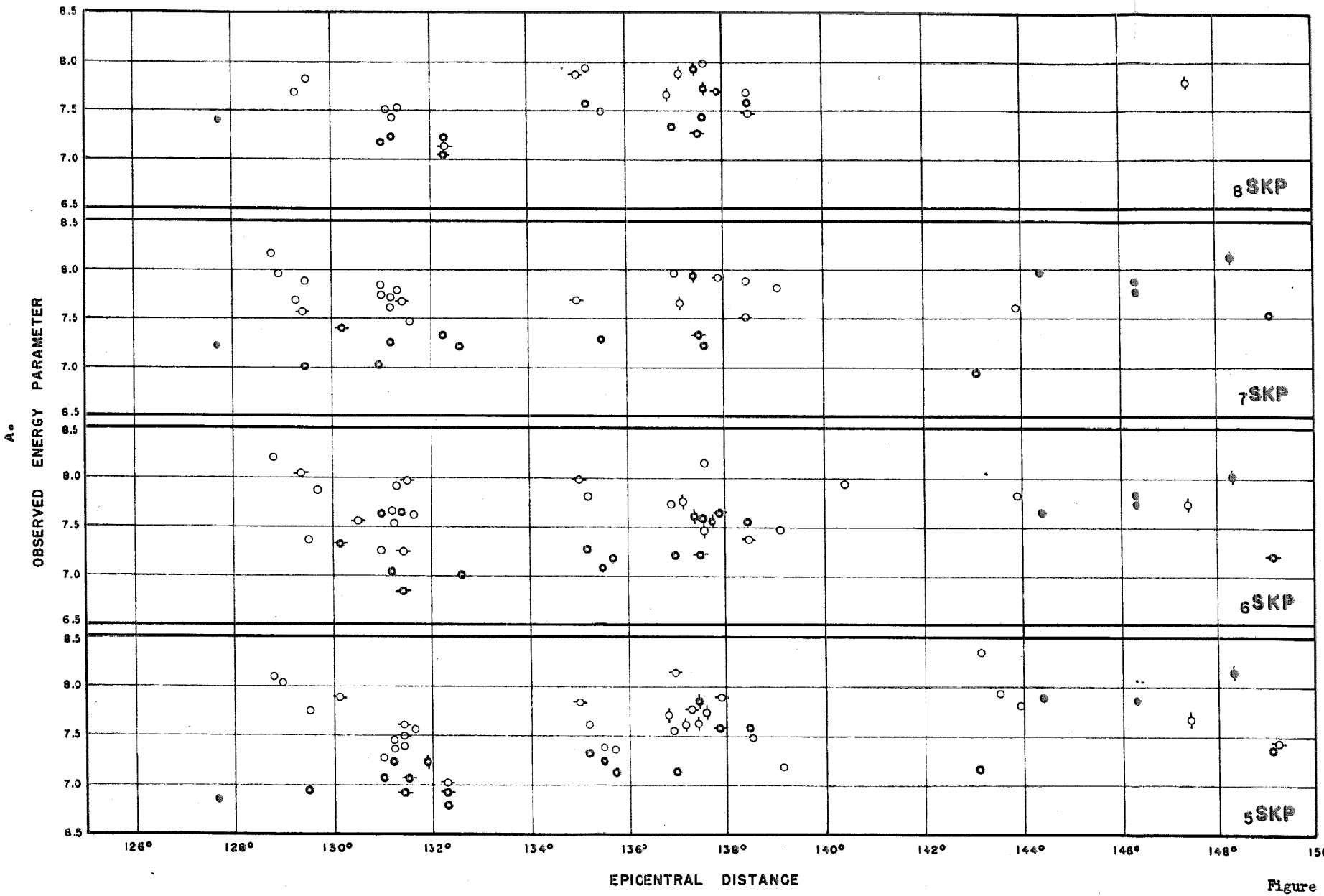

Figure 45.

h=N VERTICAL

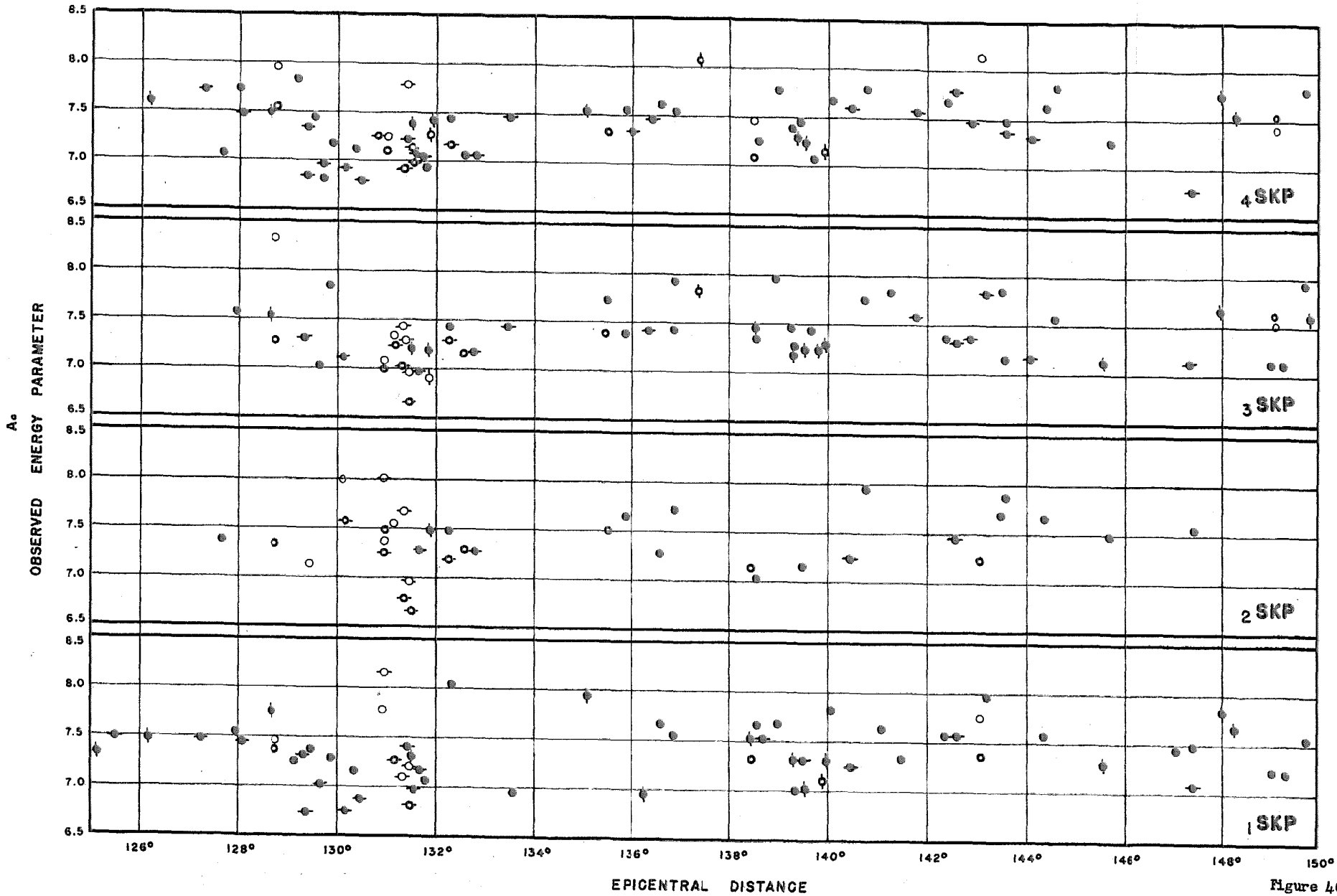

Figure 46.

h = N

HORIZONTAL

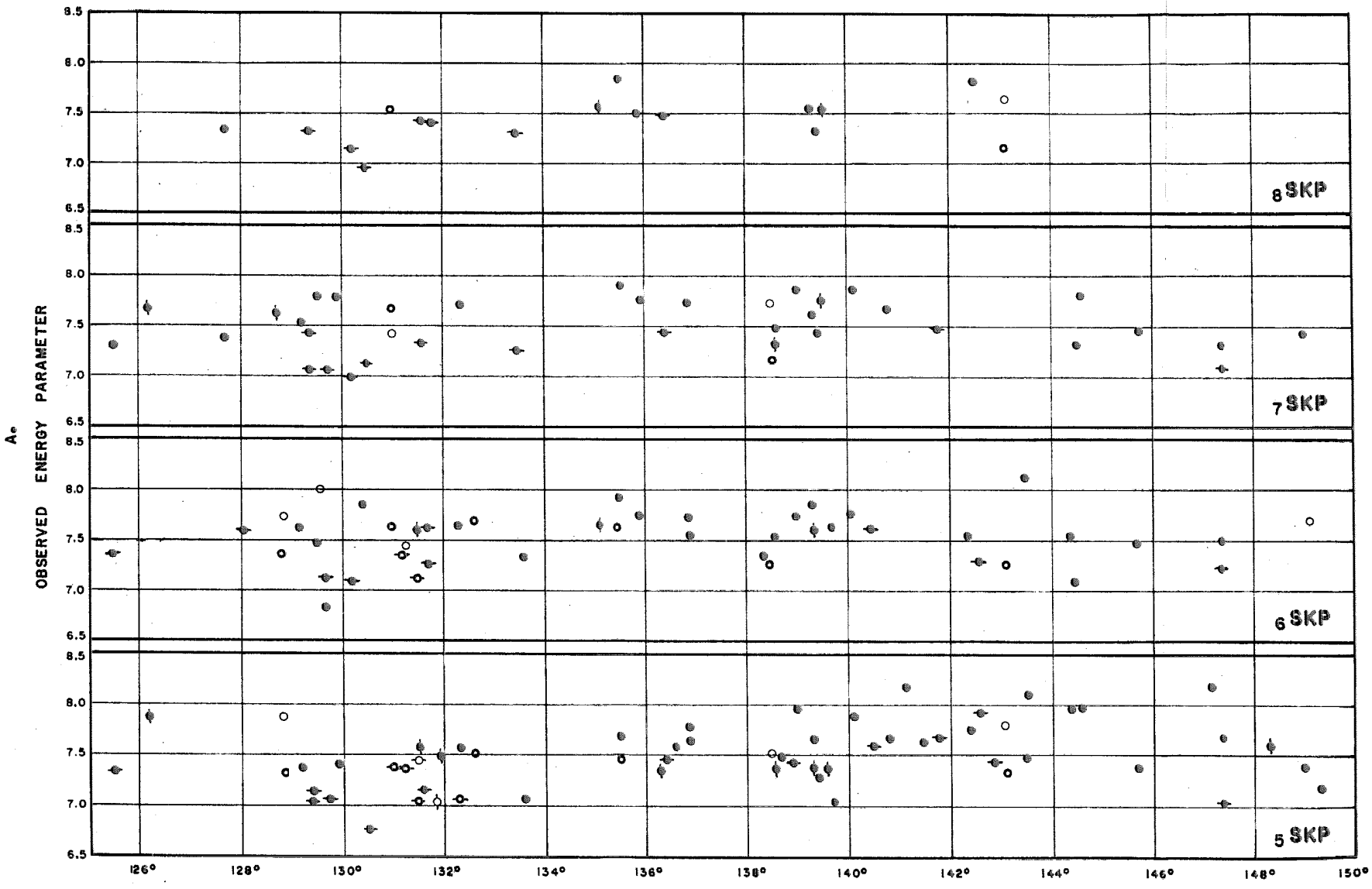

Figure 47.

h = N

HORIZONTAL

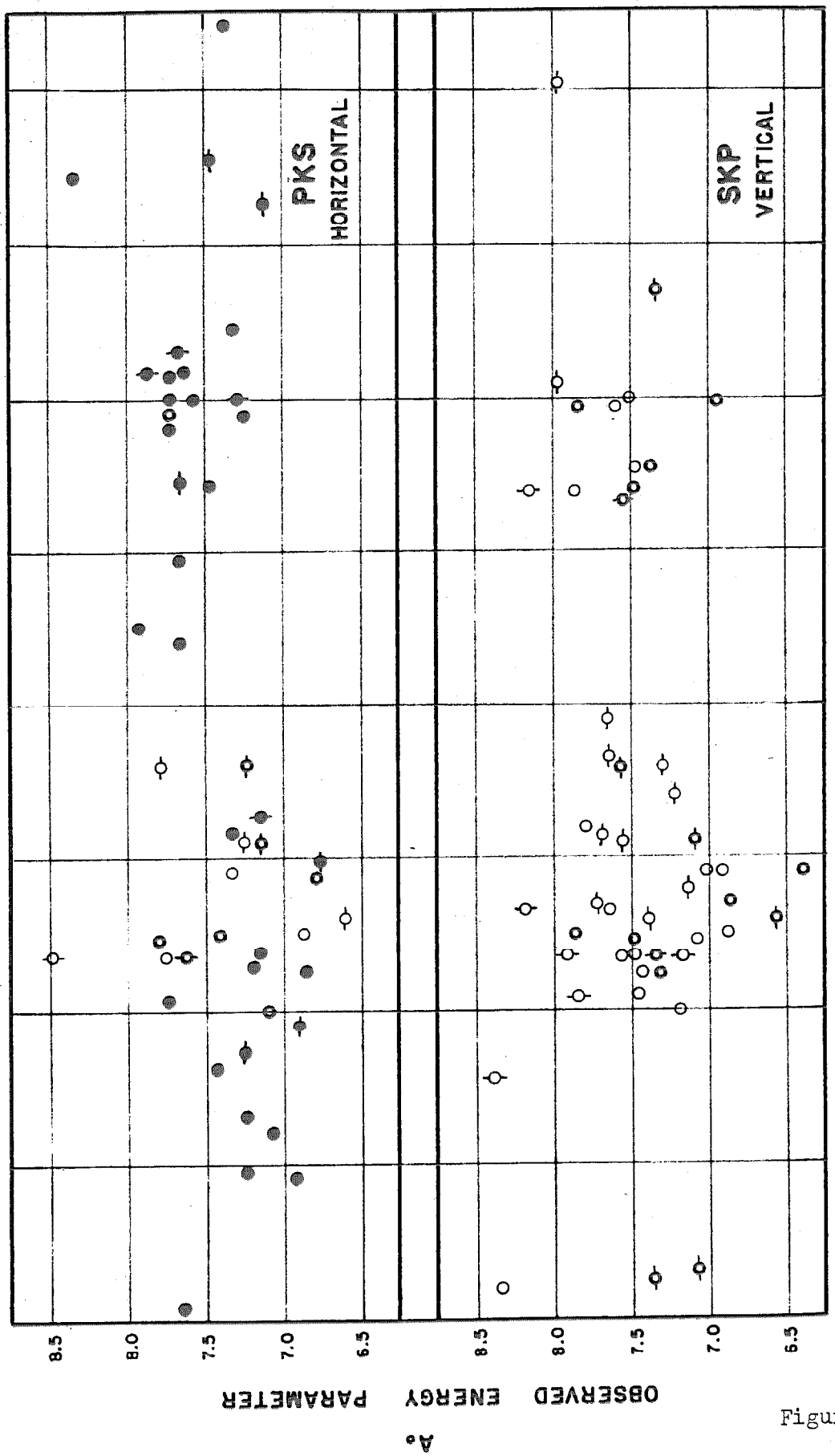
PKS
HORIZONTAL
SKP
VERTICAL
8.5
8.0
7.5
7.0
6.5
126°
128°
130°
132°
134°
136°
138°
140°
142°
EPICENTRAL DISTANCE
h = 60 km
OBSERVED ENERGY PARAMETER
A°

Figure 48.

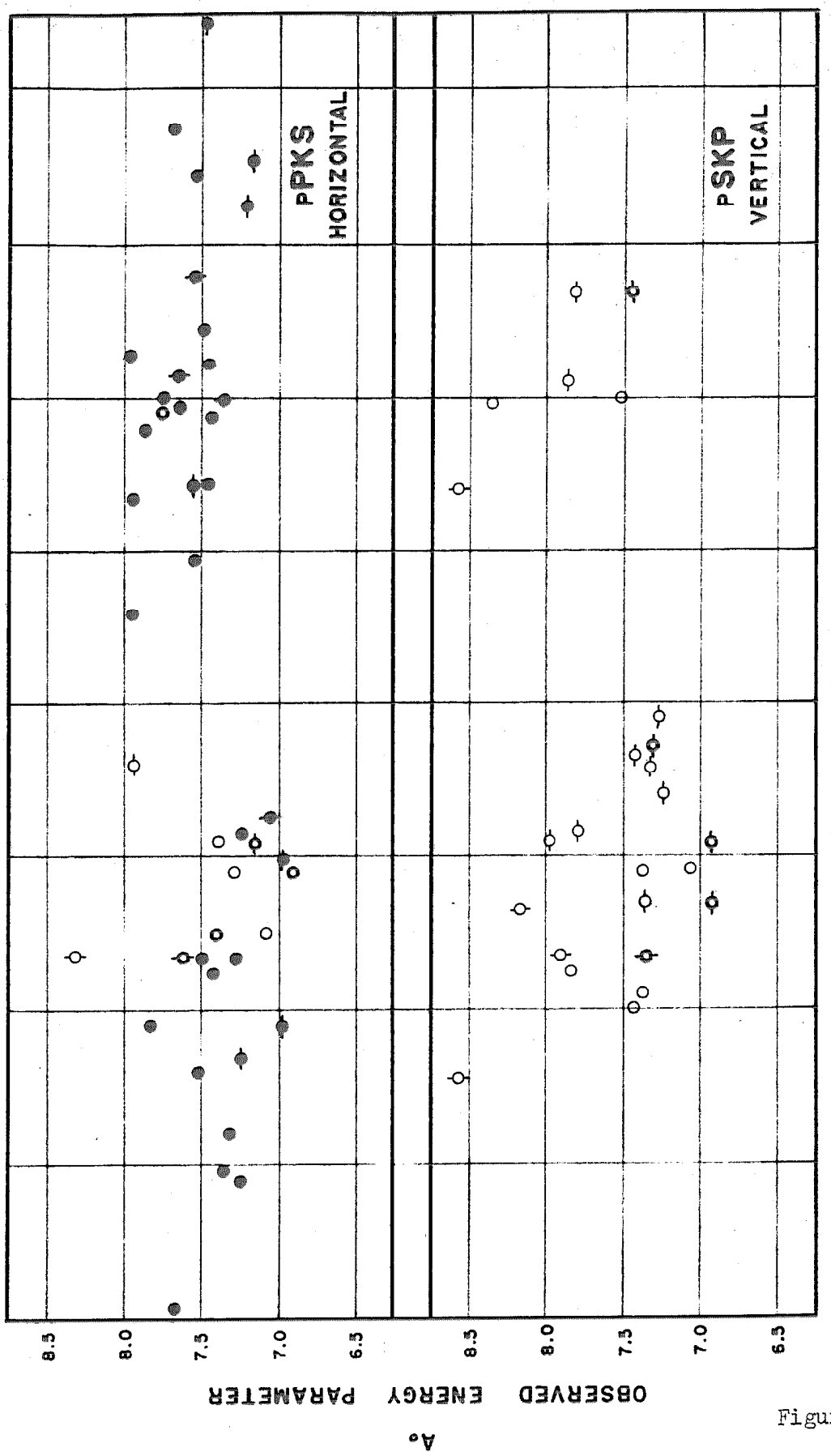
pPKS
HORIZONTAL
pSKP
VERTICAL
8.5
8.0
7.5
7.0
6.5
126°
128°
130°
132°
134°
136°
138°
140°
142°
EPICENTRAL DISTANCE
h = 60 km
OBSERVED ENERGY PARAMETER
A°

Figure 49.

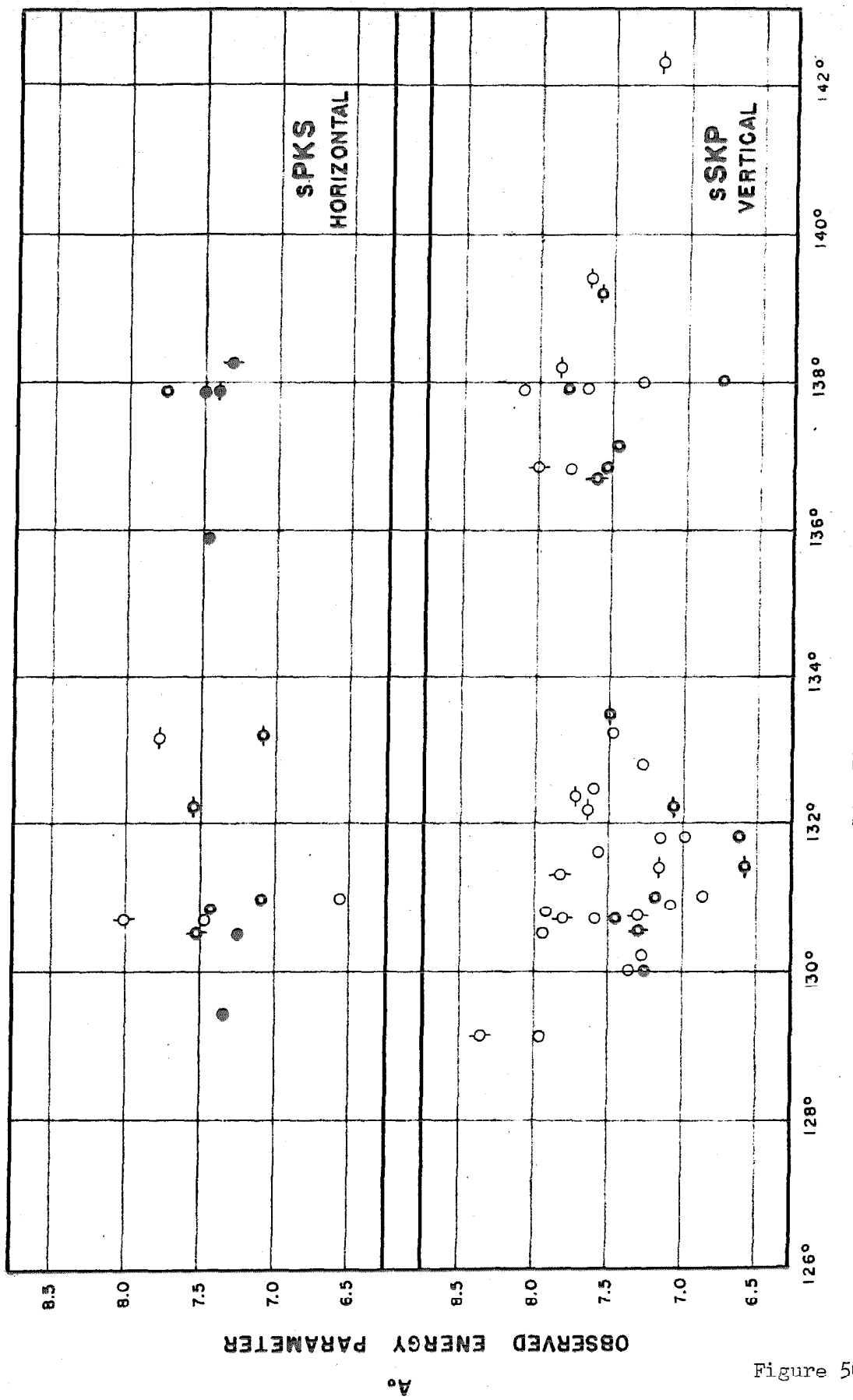
sPKS
HORIZONTAL
sSKP
VERTICAL
8.5
8.0
7.5
7.0
6.5
126°
128°
130°
132°
134°
136°
138°
140°
142°
EPICENTRAL DISTANCE
h = 60 km
OBSERVED ENERGY PARAMETER
A°

Figure 50.

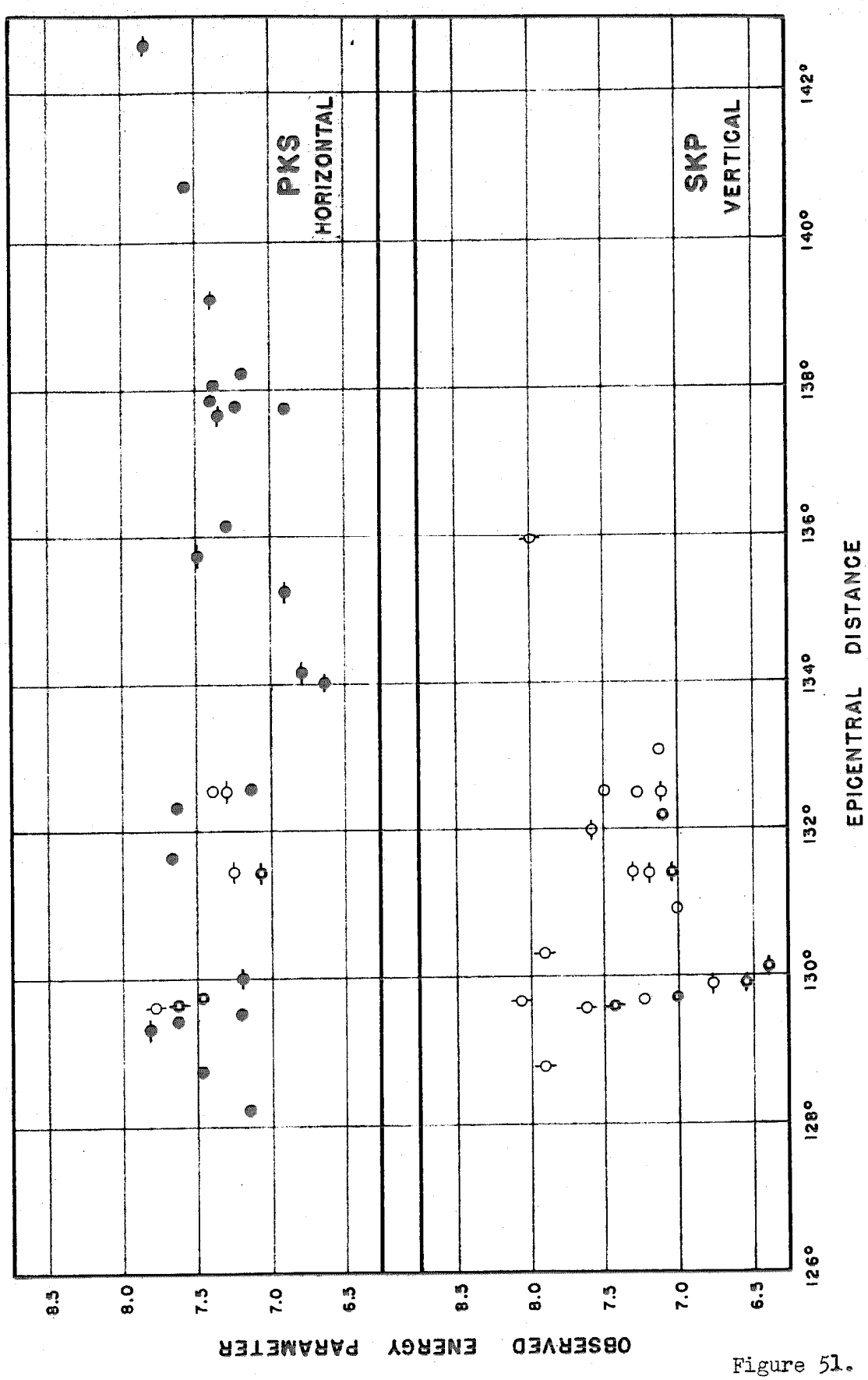
PKS
HORIZONTAL
SKP
VERTICAL
8.5
8.0
7.5
7.0
6.5
126°
128°
130°
132°
134°
136°
138°
140°
142°
EPICENTRAL DISTANCE
h = 100 km
OBSERVED ENERGY PARAMETER
A°

Figure 51.

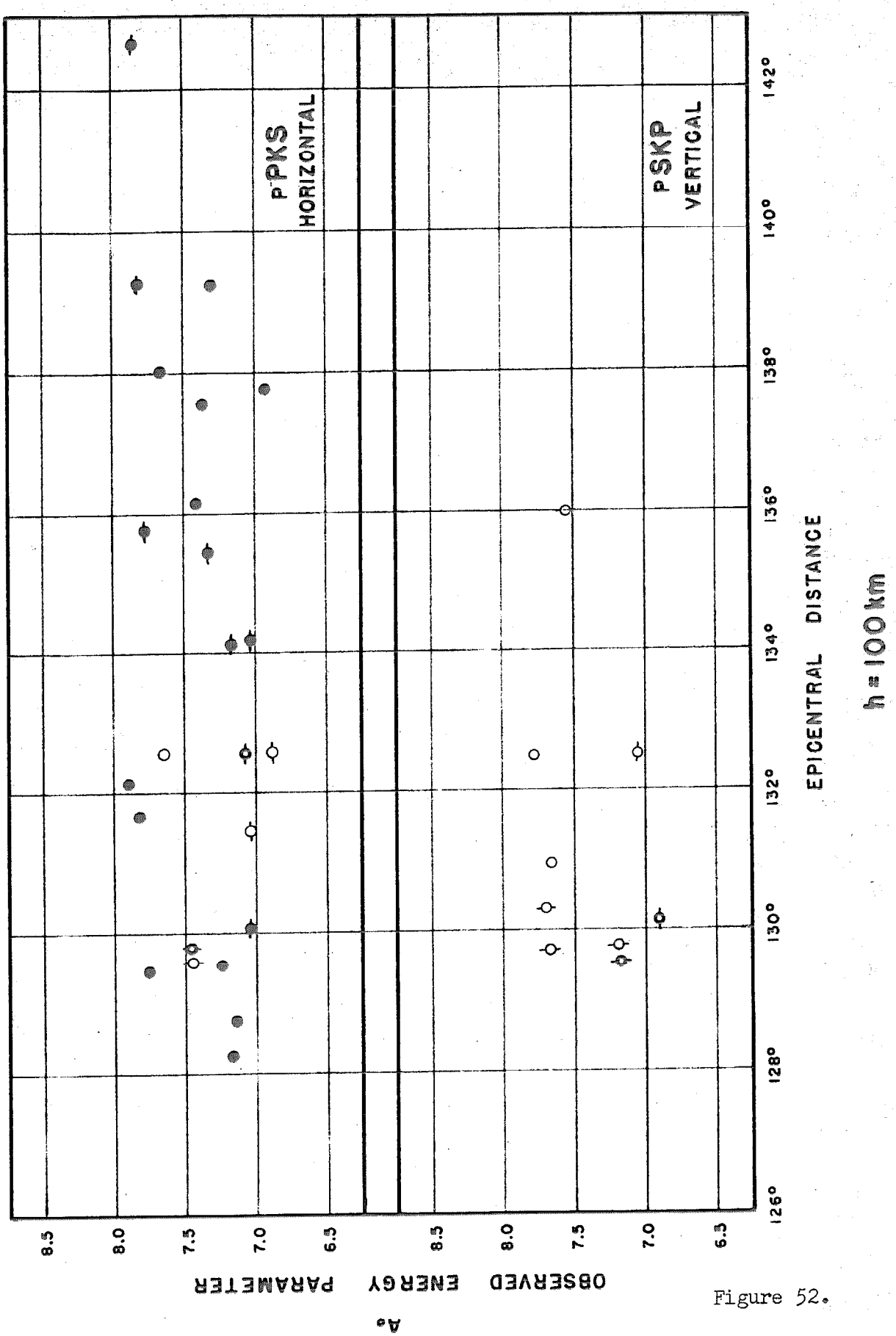
P'PKS
HORIZONTAL
PSKP
VERTICAL
OBSERVED ENERGY PARAMETER
A°
8.5
8.0
7.5
7.0
6.5
126°
128°
130°
132°
134°
136°
138°
140°
142°
EPICENTRAL DISTANCE
h = 100 km

Figure 52.

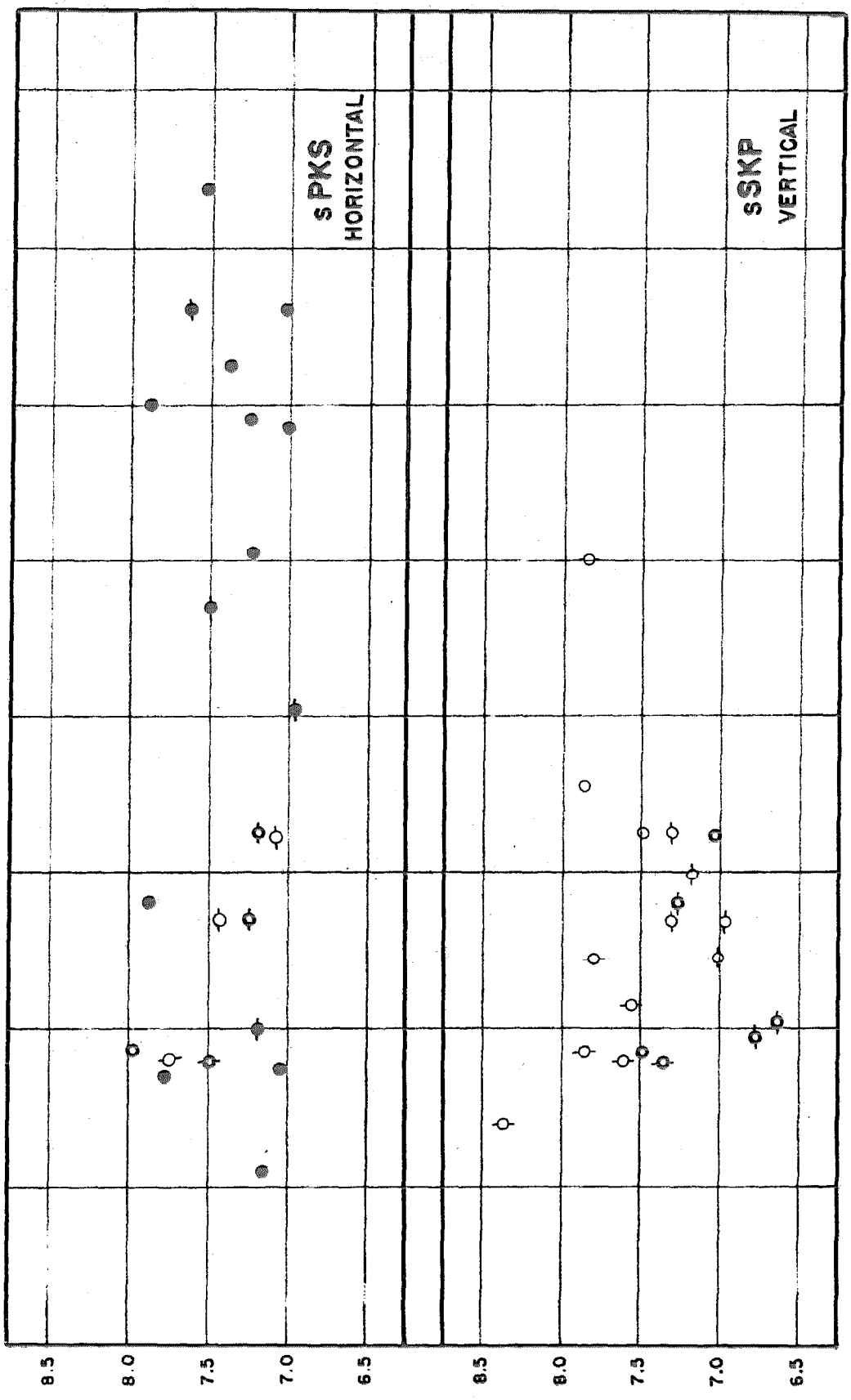
sPKS
HORIZONTAL
sSKP
VERTICAL
8.5
8.0
7.5
7.0
6.5
126°
128°
130°
132°
134°
136°
138°
140°
142°
EPICENTRAL DISTANCE
h = 100 km
OBSERVED ENERGY PARAMETER
A°

Figure 53.

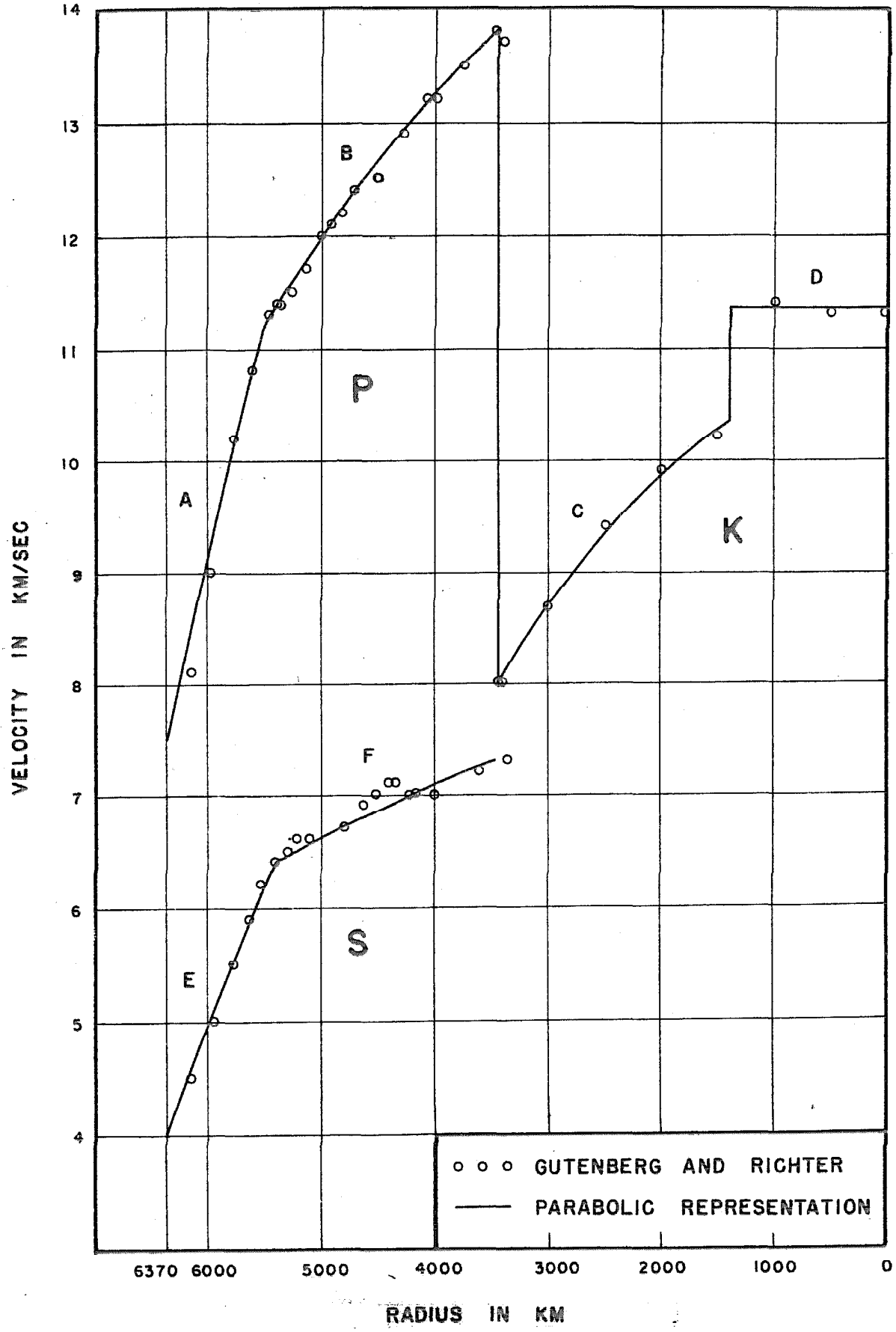
VELOCITY IN KM/SEC
14
13
12
11
10
9
8
7
6
5
4
A
B
C
D
E
F
P
S
K
o o o GUTENBERG AND RICHTER
PARABOLIC REPRESENTATION
6370 6000 5000 4000 3000 2000 1000 0
RADIUS IN KM

Figure 54.

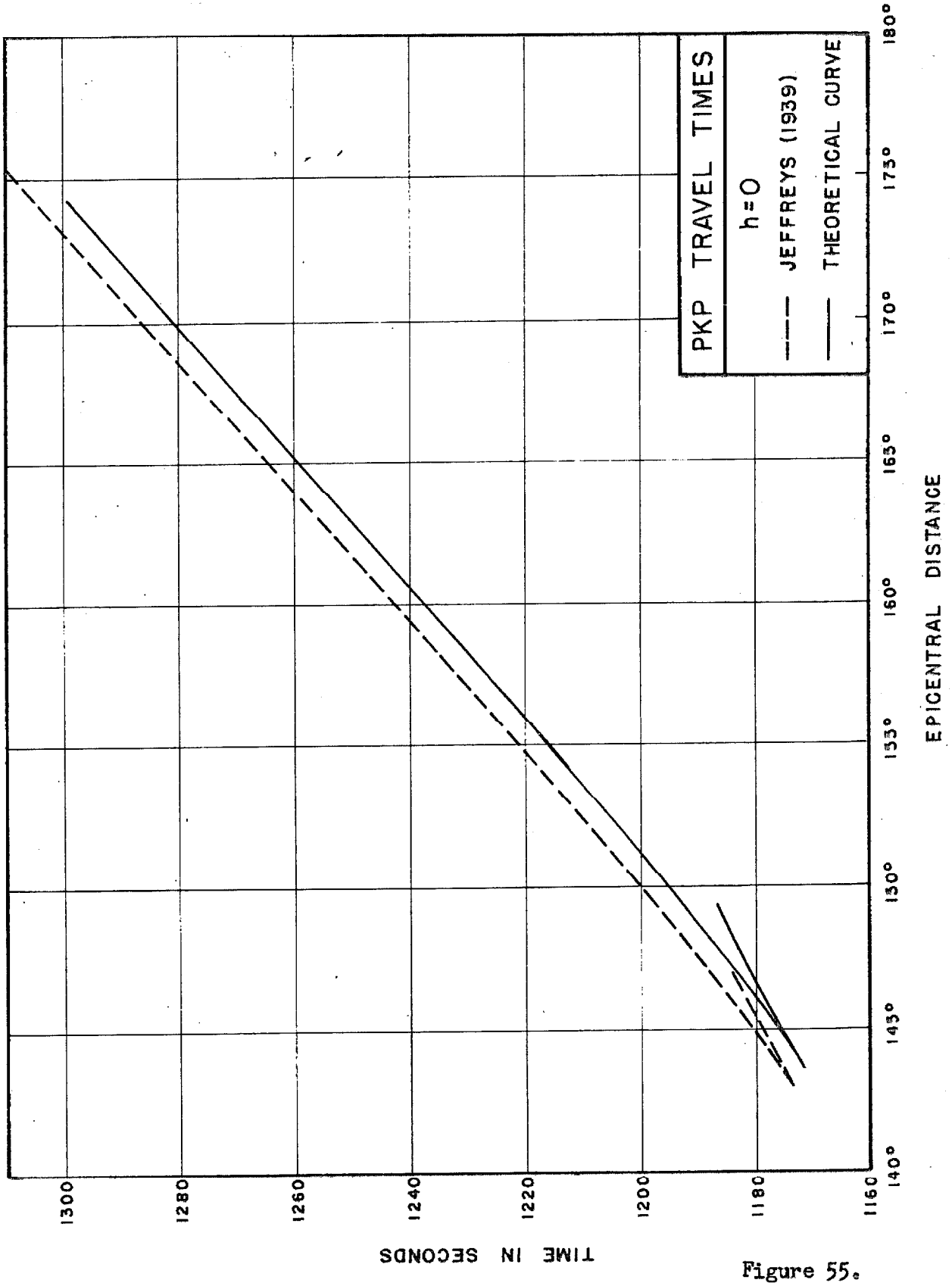
PKP TRAVEL TIMES
h=O
JEFFREYS (1939)
THEORETICAL CURVE
TIME IN SECONDS
1300
1280
1260
1240
1220
1200
1180
1160
140°
145°
150°
155°
160°
165°
170°
175°
180°
EPICENTRAL DISTANCE

Figure 55.

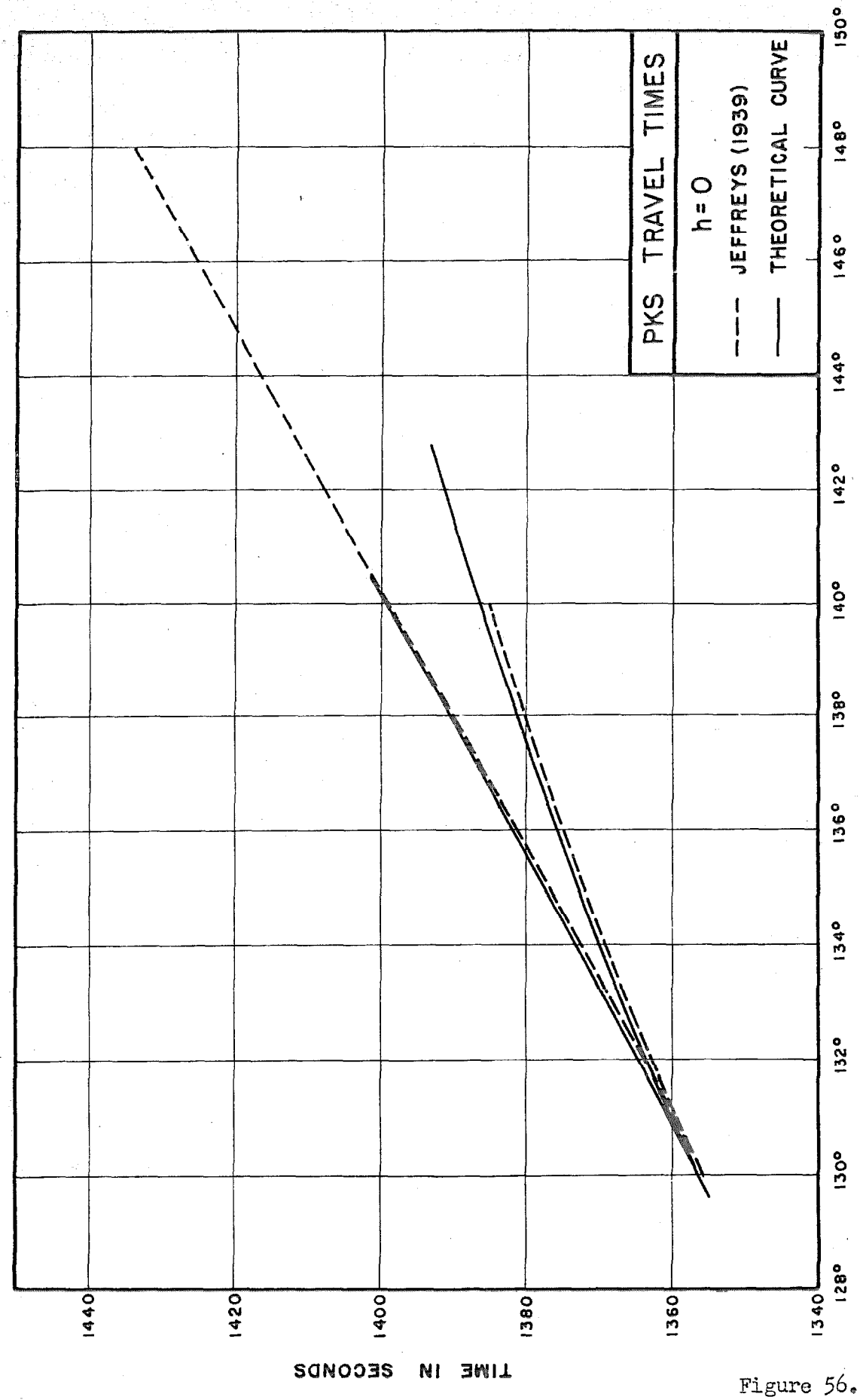
PKS TRAVEL TIMES
h = 0
JEFFREYS (1939)
THEORETICAL CURVE
TIME IN SECONDS
1440
1420
1400
1380
1360
1340
EPICENTRAL DISTANCE
128°
130°
132°
134°
136°
138°
140°
142°
144°
146°
148°
150°

Figure 56.

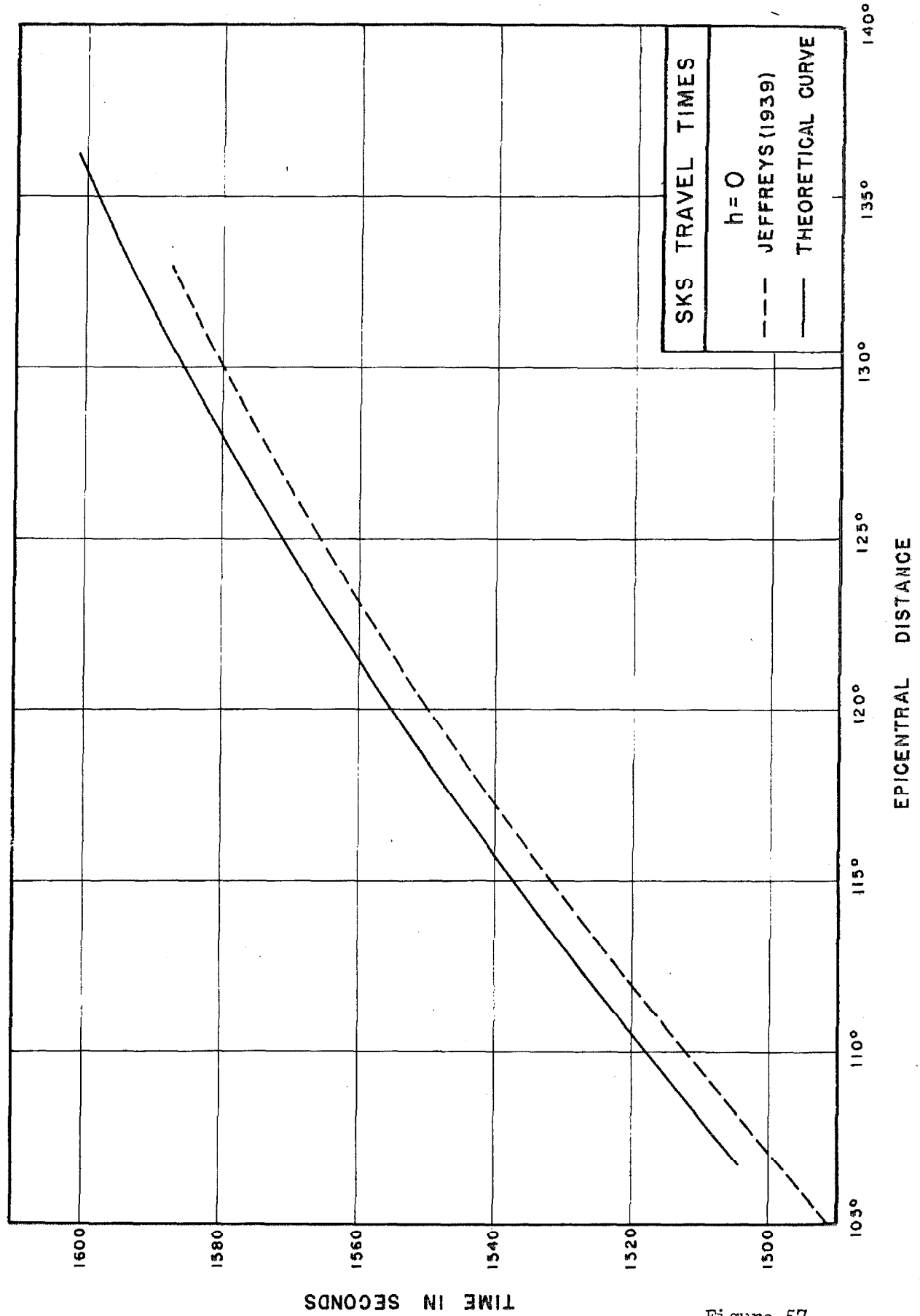
SKS TRAVEL TIMES
h = 0
JEFFREYS (1939)
THEORETICAL CURVE
TIME IN SECONDS
1600
1580
1560
1540
1320
1500
EPICENTRAL DISTANCE
103°
110°
115°
120°
125°
130°
135°
140°

Figure 57.

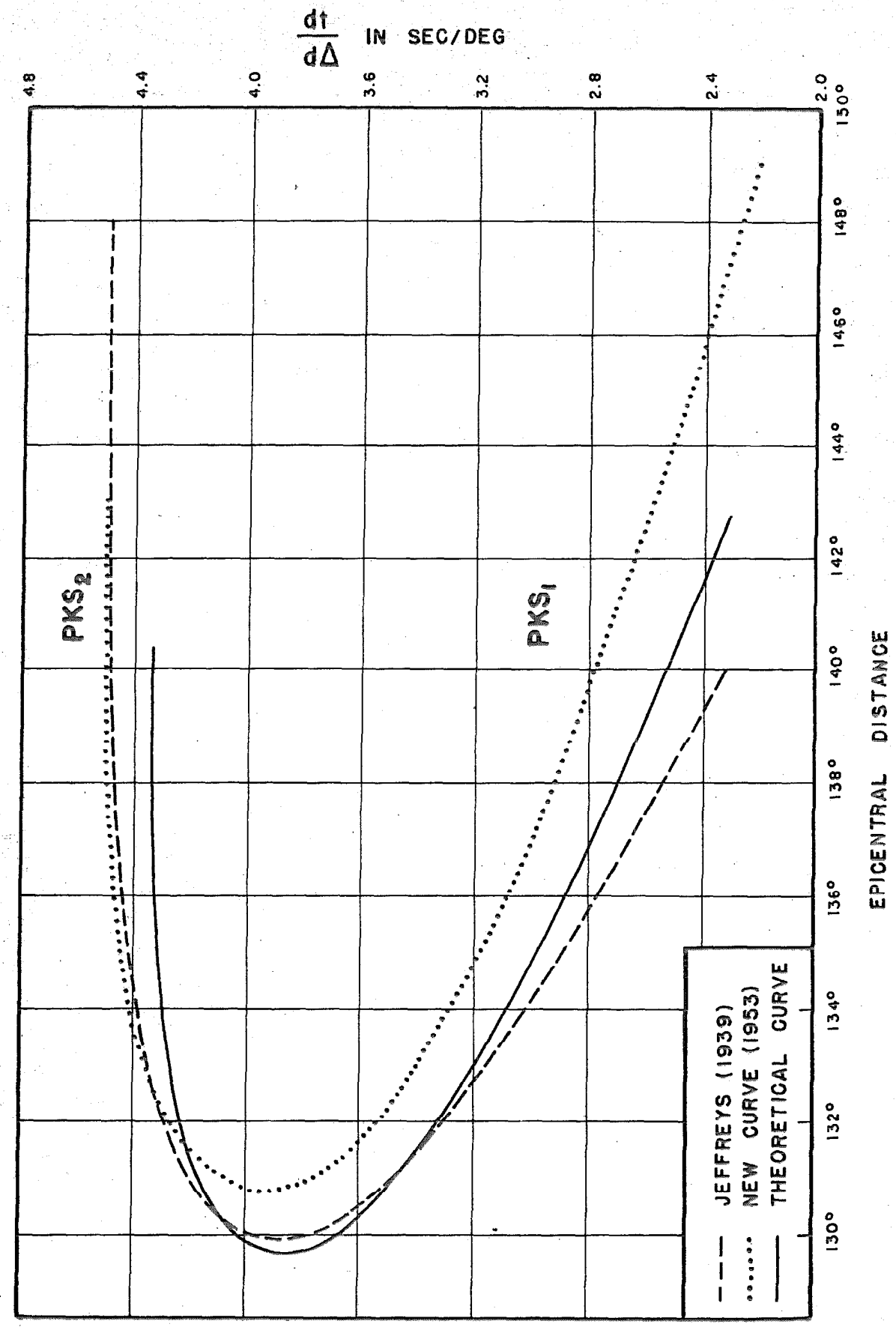
dt/dΔ IN SEC/DEG
4.8
4.4
4.0
3.6
3.2
2.8
2.4
2.0
150°
148°
146°
144°
142°
140°
138°
136°
134°
132°
130°
EPICENTRAL DISTANCE
PKS2
PKS1
JEFFREYS (1939)
NEW CURVE (1953)
THEORETICAL CURVE

Figure 58.

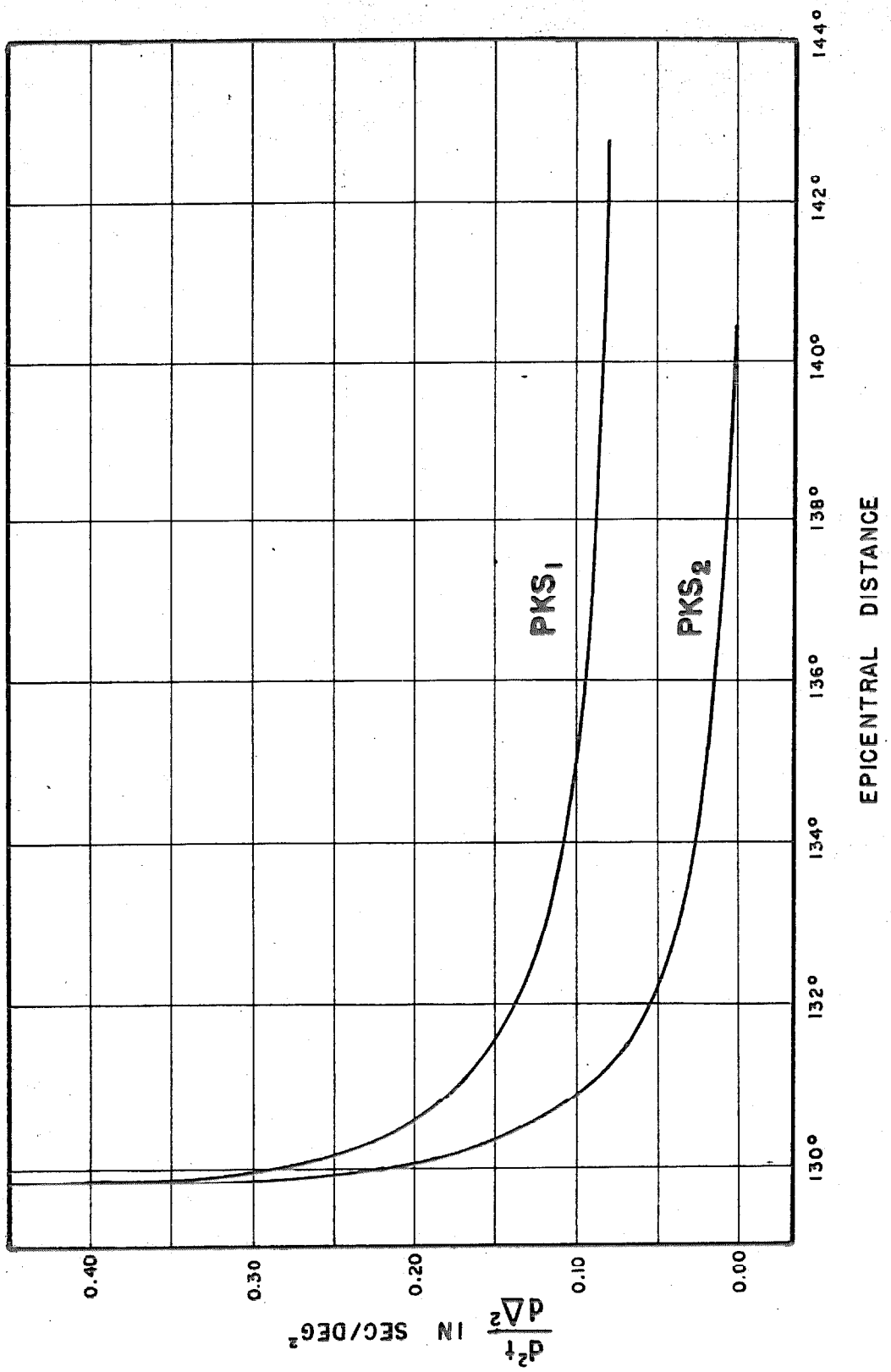
PKS1
PKS2
130°
132°
134°
136°
138°
140°
142°
144°
EPICENTRAL DISTANCE
0.40
0.30
0.20
0.10
0.00
d²t/dΔ² IN SEC/DEG²

Figure 59.

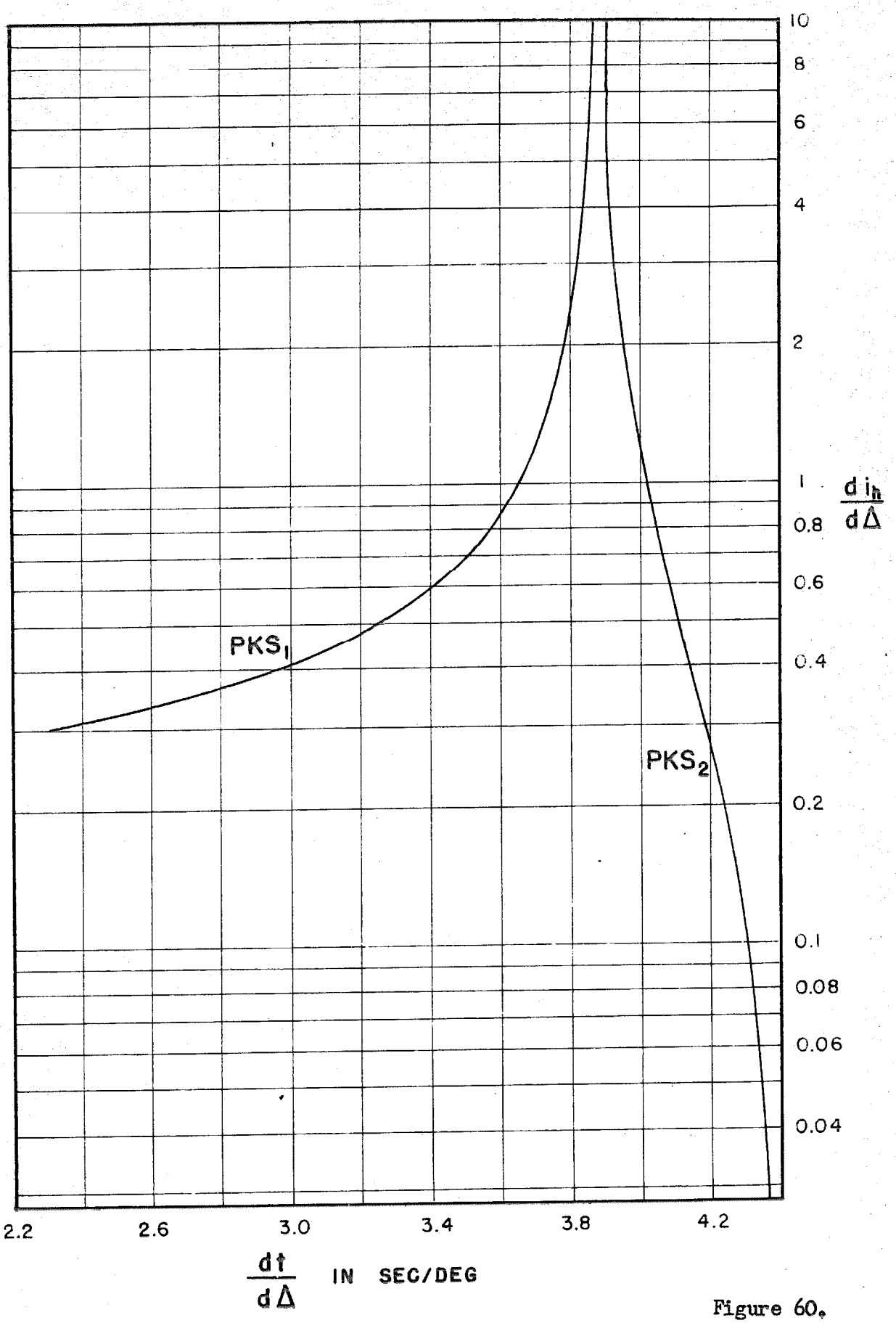
10
8
6
4
2
1
0.8
0.6
0.4
0.2
0.1
0.08
0.06
0.04
$\frac{d i_h}{d\Delta}$
PKS$_1$
PKS$_2$
2.2
2.6
3.0
3.4
3.8
4.2
$\frac{dt}{d\Delta}$ IN SEC/DEG

Figure 60.

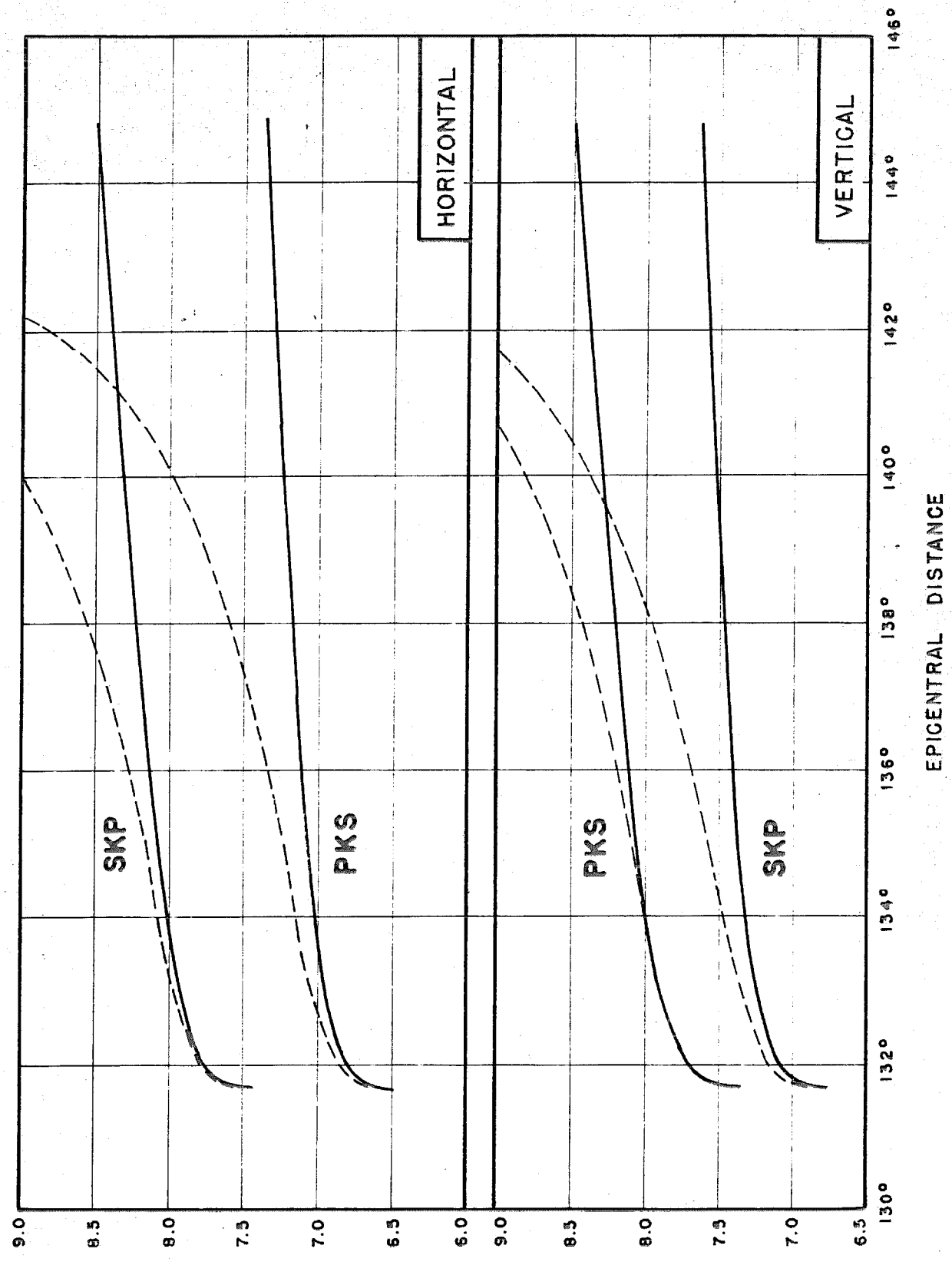
HORIZONTAL
VERTICAL
SKP
PKS
PKS
SKP
9.0
8.5
8.0
7.5
7.0
6.5
6.0
130°
132°
134°
136°
138°
140°
142°
144°
146°
EPICENTRAL DISTANCE
THEORETICAL ENERGY PARAMETER
A_1

Figure 61.

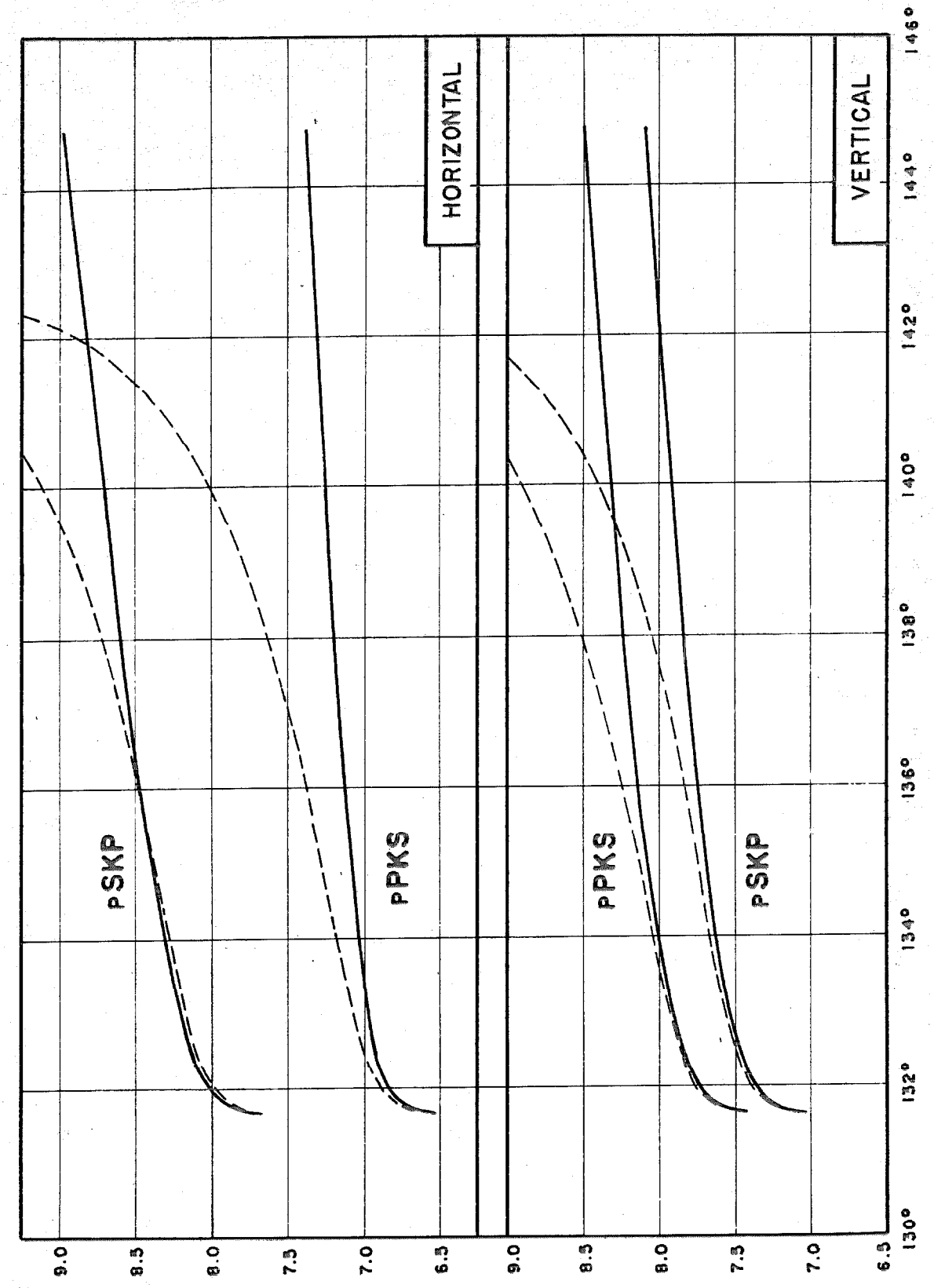
HORIZONTAL
VERTICAL
PSKP
PPKS
PPKS
PSKP
9.0
8.5
8.0
7.5
7.0
6.5
130°
132°
134°
136°
138°
140°
142°
144°
146°
EPICENTRAL DISTANCE
THEORETICAL ENERGY PARAMETER
A_1

Figure 62.

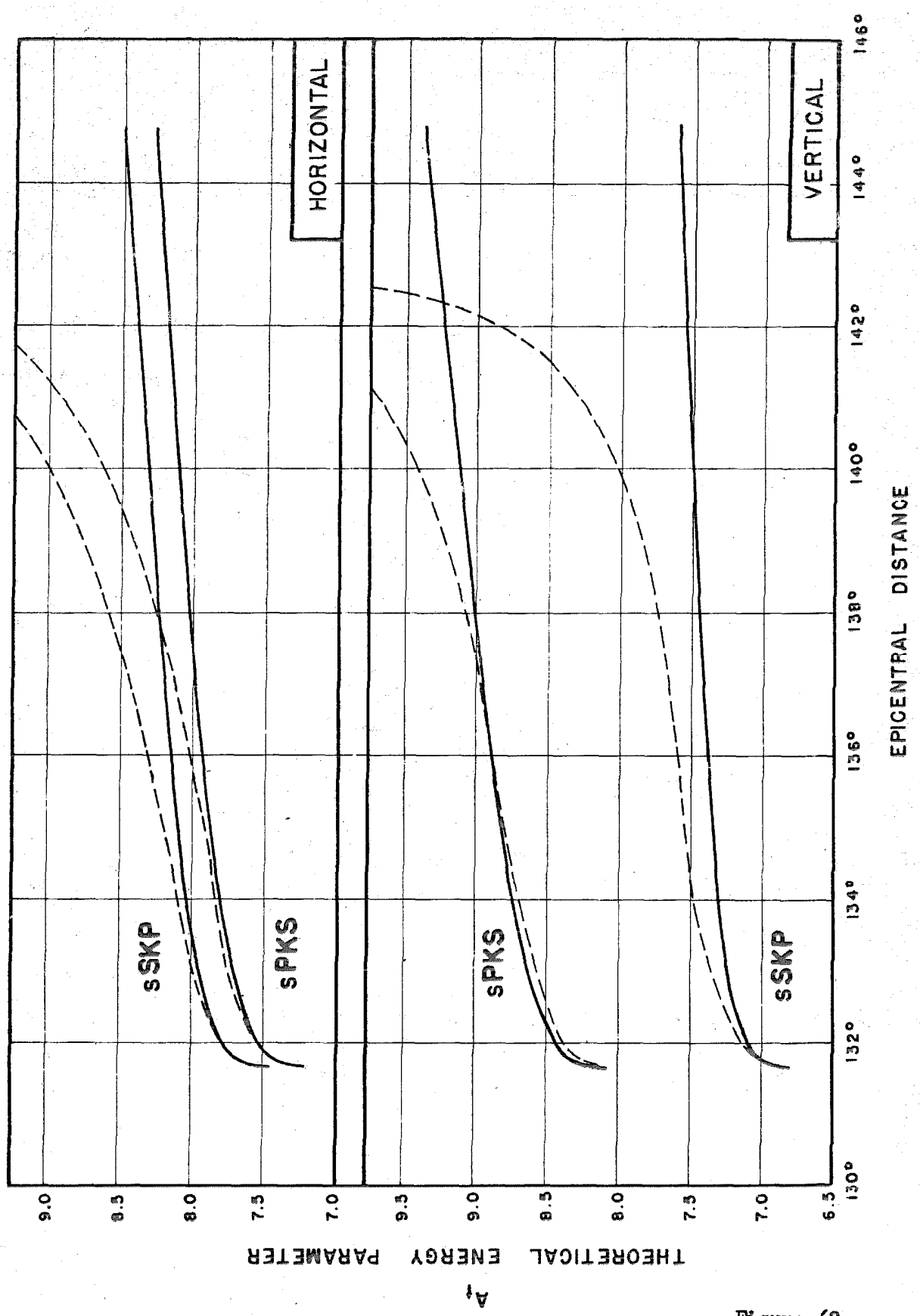
HORIZONTAL
VERTICAL
sSKP
sPKS
sPKS
sSKP
9.0
8.5
8.0
7.5
7.0
9.5
9.0
8.5
8.0
7.5
7.0
6.5
130°
132°
134°
136°
138°
140°
142°
144°
146°
EPICENTRAL DISTANCE
THEORETICAL ENERGY PARAMETER
A_i

Figure 63.

REFERENCES

Berlage, H. P.
1932. "Seismometer," Band 4, Abschnitt IV, Handbuch der Geophysik, pp. 299-506.

Dana, S. W.
1944. "The Partition of Energy Among Seismic Waves Reflected and Refracted at the Earth's Core," Vol. 34, No. 4, pp. 189-197.

Denson, M. E., Jr.
1950. "Longitudinal Waves through the Earth's Core," thesis for the Ph. D. Degree, Calif. Institute of Technology, Pasadena, Calif.
1952. "Longitudinal Waves through the Earth's Core," Bull. Seism. Soc. Am., Vol. 42, No. 2, pp. 119-134.

Dix, C. H.
1952. Seismic Prospecting for Oil, Harper and Bros.

Fu, C. Y.
1945. "On the Origin and Energy of Oscillatory Earthquake Waves," Bull. Seis. Soc. Am., Vol. 35, No. 1, pp. 37-42.
1947. "On Seismic Rays and Waves (Part One), "Bull. Seis. Soc. Am., Vol. 37, No. 4, pp. 331-346.

Gutenberg, B.
1944. "Energy Ratio of Reflected and Refracted Seismic Waves," Bull. Seism. Soc. Am., Vol. 34, No. 2, pp. 85-102.
1945a. "Amplitudes of P, PP, and S and Magnitudes of Shallow Earthquakes," Bull. Seism. Soc. Am., Vol. 35, No. 2, pp. 57-69.
1945b. "Magnitude Determination for Deep-focus Earthquakes," Bull. Seis. Soc. Am., Vol. 35, No. 3, pp. 117-130.
1948. "The Layer of Relatively Low Wave Velocity at a Depth of 80 Kilometers," Bull. Seis. Soc. Am., Vol. 38, pp. 121-128.
1951a. "PKKP, P'P', and the Earth's Core," Trans. Am. Geoph. Union, Vol, 32, No. 3, pp. 373-390.
1951b. Internal Constitution of the Earth, Dover Pub.

Gutenberg, B., and C. F. Richter
1934. "On Seismic Waves (First Paper)," Gerlands Beitr. z. Geophysik, Vol. 5, pp. 56-133.
1935. "On Seismic Waves (Second Paper)," Gerlands Beitr. z. Geophysik, Vol. 45, pp. 380-360.
1936. "Materials for the Study of Deep-focus Earthquakes," Bull. Seis. Soc. Am., Vol. 26, No. 4, pp. 341-390.
1938. "P' and the Earth's Core," Mon. Not. R. Acad. Sci., Geophy. Sup., Vol. 27, No. 3, pp. 156-183.
1939a. "On Seismic Waves (Fourth Paper)." Gerlands Beitr. z. Geophysik, Vol. 54, pp. 94-136.
1939b. "New Evidence for a Change in Physical Conditions at Depths near 100 Kilometers," Bull. Seis. Soc. Am., Vol. 29, No. 4, pp. 531-537.
1942. "Earthquake Magnitude, Intensity, Energy, and Acceleration," Bull. Seis. Soc. Am., Vol. 32, No. 3, pp. 163-191.
1949. Seismicity of the Earth and Associated Phenomena, Princeton Univ. Press.

Jeffreys, H.
1936. "The Structure of the Earth Down to the 20° Discontimuity," Mon. Not. Roy. Astron. Soc., Geophys. Suppl., Vol. 3, pp. 401-422.
1937. "The Structure of the Earth Down to the 20° Discontimuity (Second paper)", Mon. Not. Roy. Astron. Soc., Vol. 4, No. 1, pp. 13-39.
1939a. "The Times of PcP and ScS," Mon. Not. Roy. Astron. Soc., Vol. 4, No. 7, pp. 537-547.
1939b. "The Times of Core Waves," Mon. Not. Roy. Astron. Soc., Vol. 4, No. 7, pp. 548-561.
1939c. "The Times of Core Waves (Second Paper)," Mon. Not. Roy. Astron. Soc., Vol. 4, No. 8, pp. 594-615.

Lehmann, I.
1936. Pub. Bureau Central Seismol. Internat., Trav. Sci., Ser. A, Vol. 14, pp. 87-115.

Martner, S. T.
1950. "Observations on Seismic Waves Reflected at the Core Boundary of the Earth," Vol. 40., No. 2, pp. 95-109.

Mooney, H. M.
1951. "A Study of the Energy Content of the Seismic Waves P and $_pP$," Vol. 41, No. 1, pp. 13-30.

Slichter, L. B.
1932. "The Theory of the Interpretation of Seismic Travel-time Curves in Horizontal Structures," Physics, Vol. 3, pp. 273-295.

Wadati, K., and K. Masuda
1934. "On the Travel Time of Earthquake Waves, Part VI," Geophysical Magazine, Tokyo, Vol. 8, pp. 187-194.

Wenner, Frank
1929. "A New Seismometer Equipped for Electromagnetic and Optical Magnification," U. S. Bur. Stand., Jour. of Research, Vol. 2, p. 963.

Zoeppritz, K., L. Geiger, and B. Gutenberg
1912. "Ueber Erdbebenwellen. V." Nachr. Gesell. D. Wiss. Gottingen, Math.-phys. Kl., pp. 121-206.

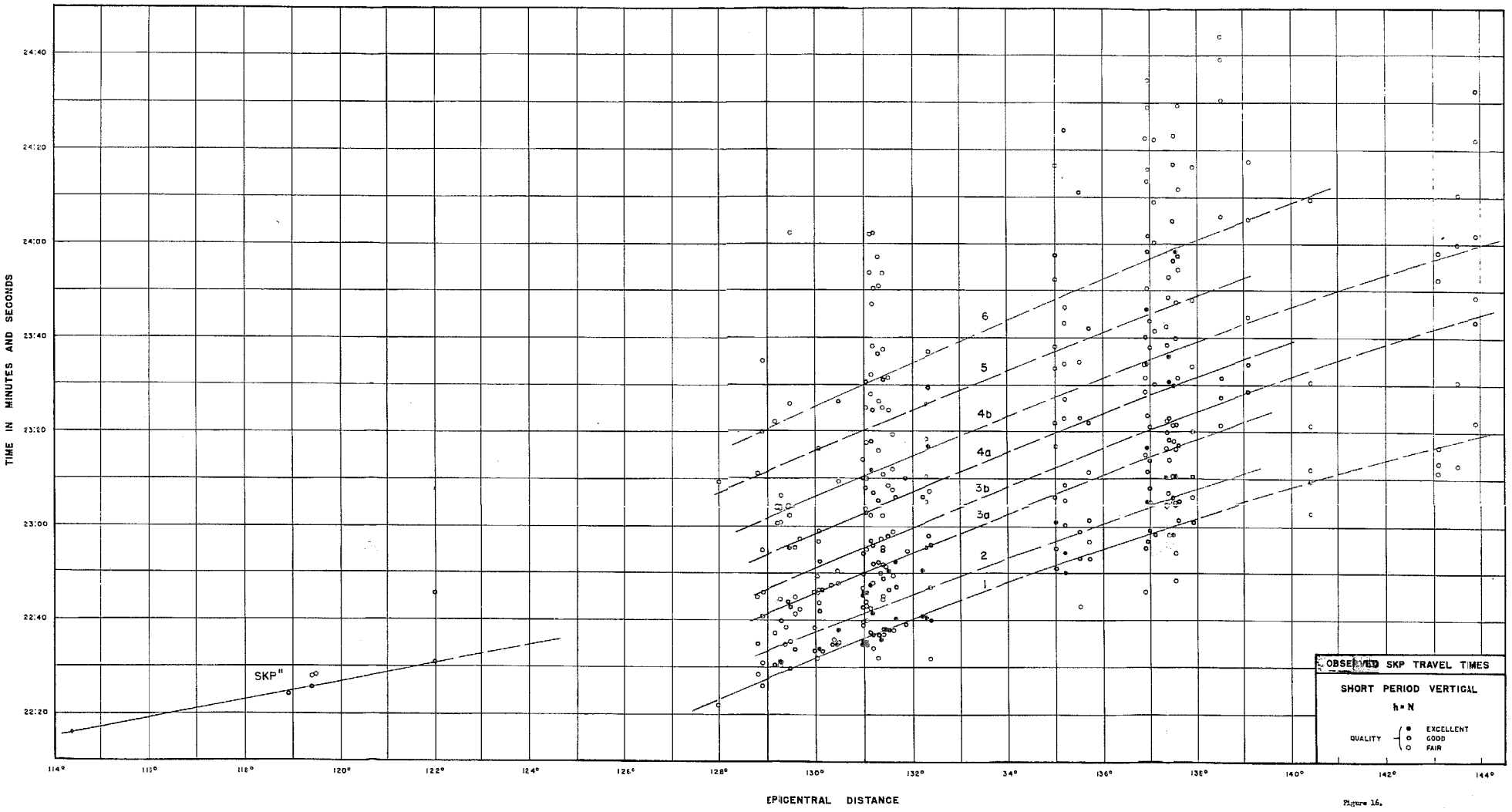
TIME IN MINUTES AND SECONDS
24:40
24:20
24:00
23:40
23:20
23:00
22:40
22:20
SKP
6
5
4b
4a
3b
3a
2
1
OBSERVED SKP TRAVEL TIMES
SHORT PERIOD VERTICAL
h = N
QUALITY
EXCELLENT
GOOD
FAIR
114°
116°
118°
120°
122°
124°
126°
128°
130°
132°
134°
136°
138°
140°
142°
144°
EPICENTRAL DISTANCE

Figure 16.

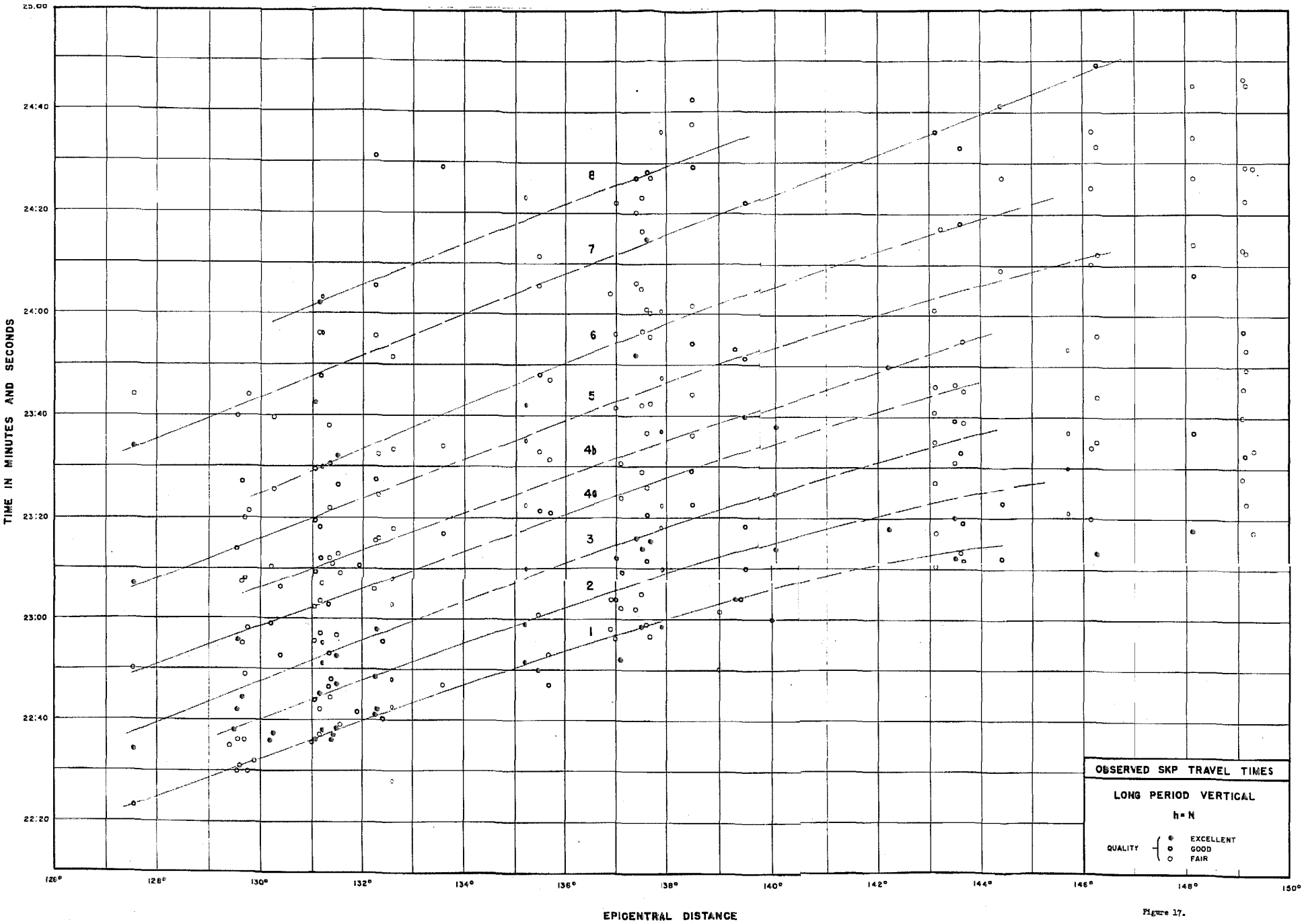
TIME IN MINUTES AND SECONDS
25:00
24:40
24:20
24:00
23:40
23:20
23:00
22:40
22:20
126°
128°
130°
132°
134°
136°
138°
140°
142°
144°
146°
148°
150°
EPICENTRAL DISTANCE
8
7
6
5
4b
4a
3
2
1
OBSERVED SKP TRAVEL TIMES
LONG PERIOD VERTICAL
h = N
QUALITY
EXCELLENT
GOOD
FAIR

Figure 17.

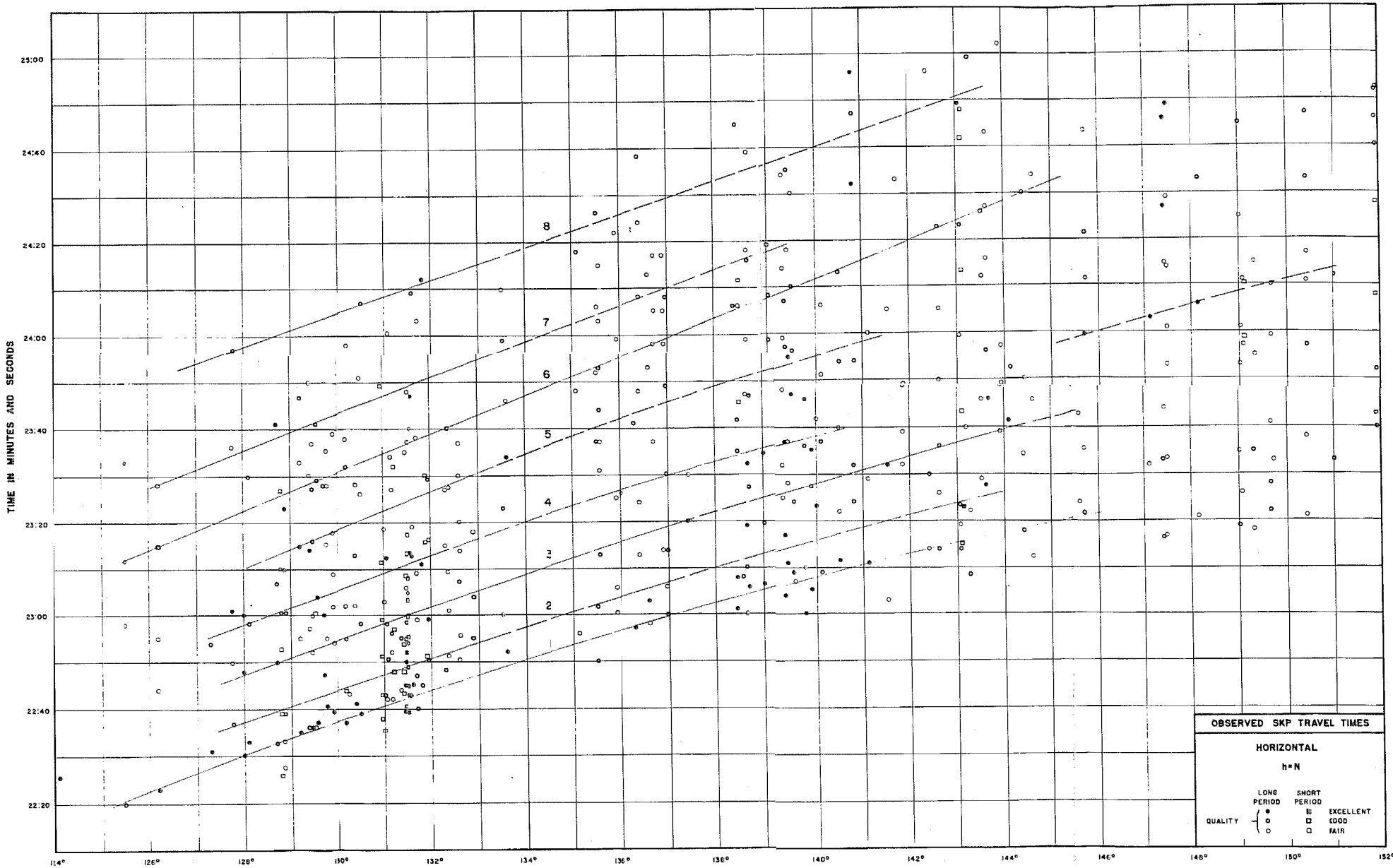
TIME IN MINUTES AND SECONDS
25:00
24:40
24:20
24:00
23:40
23:20
23:00
22:40
22:20
8
7
6
5
4
3
2
124°
126°
128°
130°
132°
134°
136°
138°
140°
142°
144°
146°
148°
150°
152°
OBSERVED SKP TRAVEL TIMES
HORIZONTAL
h=N
LONG PERIOD
SHORT PERIOD
QUALITY
EXCELLENT
GOOD
FAIR

Figure 16.